UNIVERSITY OF COPENHAGEN
FACULTY OF SCIENCE

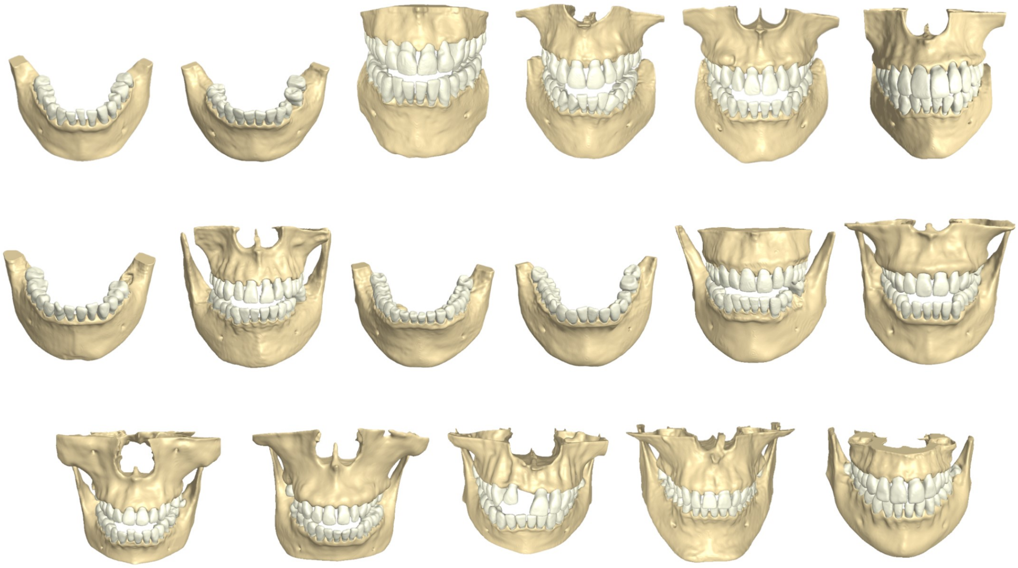

PhD Thesis

Torkan Gholamalizadeh

Computational Modeling and Analysis of Tooth Movement

Department of Computer Science

Supervisors: Kenny Erleben, Peter Lempel Søndergaard, Sune Darkner

Submitted on: 31August 2022

University of Copenhagen
Faculty of Science
Department of Computer Science

Computational modeling and analysis of tooth movement

Torkan Gholamalizadeh

Supervisors:	Kenny Erleben Peter Lempel Søndergaard Sune Darkner

This thesis has been submitted to the PhD School of The Faculty of Science,
University of Copenhagen, on August 31, 2022

To my beloved family

Abstract

Computational models obtained from medical data, such as finite-element (FE) methods, are numerical tools developed for predicting responses of different tissues under physical loads. Such models are beneficial, when measuring the desired phenomena directly in vivo is invasive, costly, difficult, or almost impossible to be performed. More specifically, these models can be used as pre-operative guides in different medical applications such as orthopedic surgery, orthodontic treatments, and cardiovascular surgeries by providing better insights into underlying geometries, answering clinical questions, or predicting specific behaviors under desired circumstances.

Developing an accurate computational model of the human jaw is challenging as the dimension of the involved tissues are almost on different scales, some of which has a thickness on edge with the commonly used resolution of medical imaging scans such as cone beam computed tomography (CBCT). For instance, in CBCT scans captured at a typical resolution of 0.3 mm or higher, the teeth and bone boundaries are separated by at most one voxel, making it challenging to accurately delineate the teeth/bone boundaries with relatively similar intensities. In addition, there are no publicly available high-resolution scans due to the known dangers of X-ray exposure. This leads to time-consuming and labor-intensive segmentation and meshing processes to prepare FE models of the human jaw. For instance, generating a detailed FE model of an entire human jaw can take up to several days to months, depending on the scan's resolution, the anatomical complexity, and the researchers' expertise.

As a result of these challenges and limitations, almost all studies in the field are limited to single-model analysis, which raises the question of the generalizability of their results to a larger population with significant geometrical variations. Besides, conducting a single-patient analysis can provide limited information about the potential correlations between geometrical variations and the simulation results. Hence, there is a need for population studies where FE models are developed for different patients, and inter-patient analyses are performed to investigate the effect of geometrical variations on the simulation results.

In this thesis, we first investigate the influence of geometrical variations on teeth movements of different patients by developing three models of human mandibles with the conventional FE model generation approach and conducting intra- and inter-patient analyses. Next, we develop a pipeline that nearly automates the model generation process, making it attainable to extend our dataset to 17 patient-specific, clinically-validated FE models. Finally, we evaluate and quantify the generated models in terms of mesh quality, geometry accuracy, and simulation stability in different scenarios and compare the results with the state-of-the-art.

Our results indicate that the developed computational models are precise, considering the low error/distance from input surface meshes. Moreover, the generated conformal volumetric meshes include quality elements suitable for various FE scenarios. Furthermore, studying the effects of geometrical variations on tooth movement shows that a combination of two clinical biomarkers, i.e., crown height and root volume, can affect tooth displacement. Therefore, these biomarkers, combined with the magnitude of the applied load, can be used to predict different patients' teeth displacements.

For the reproducibility of our work, we share our research materials, including unprocessed reconstructed geometries, quality conformal volumetric meshes, and the pipeline for generating them, as an open-access GitHub repository named as Open-Full-Jaw. We believe this unique repository, including a high-geometrical variation, will pave the way for future population studies focusing on human jaws by providing reproducible FE models and allowing researchers to easily produce simulation-ready models for their data without spending extensive time on conventional approaches.

Resumé

Beregningsmodeller skabt fra medicinske data, såsom finite-element (FE) modeller, er numeriske værktøjer udviklet til at forudsige reaktioner fra forskellige væv under forskellige fysiske belastninger. Sådanne modeller er gavnlige, når man ønsker forudsigelse af situationer der in vivo er invasive, dyre, vanskelige eller næsten umulige at udføre. Mere specifikt kan disse modeller bruges som præoperative guider i forskellige medicinske anvendelser såsom ortopædkirurgi, ortodontiske behandlinger og kardiovaskulære operationer. Modellerne kan give bedre indsigt i de underliggende geometrier, besvare kliniske spørgsmål eller forudsige specifik hændsler under specifikke omstændigheder.

Udviklingen af en nøjagtig beregningsmodel af den menneskelige kæbe er udfordrende. Dimensionerne af det involverede væv er på meget forskellige størrelses skalaer. Nogle vævstyper har en tykkelse på samme størrelse som den anvendte opløsning af de medicinske billedscanninger såsom cone beam computed tomography (CBCT). For eksempel, i CBCT-scanninger optaget med en typisk opløsning på 0,3 mm eller højere, er tænder og knogler adskilt af højst én voxel, hvilket gør det udfordrende at præcist se overfalden af tænder/knogler da de har næsten ens intensiteter. Derudover er der ingen offentligt tilgængelige højopløsningsscanninger på grund af strålingsfarer ved røntgeneksponering. Dette fører til tidskrævende og arbejdskrævende segmentering- og meshing-processer, der er nødvendige for at forberede FE-modeller af den menneskelige kæbe. For eksempel, som et resultat af disse udfordringer og begrænsninger er næsten alle undersøgelser på området begrænset til analyser af en enkelt kæbemodel, hvilket rejser spørgsmålet om analyse resultaterne generalisertil en større population med betydelige geometriske variationer. En enkeltpatientanalyse giver desuden begrænset information om de potentielle sammenhænge mellem geometriske variationer og simuleringsresultaterne. Der er derfor behov for befolkningsundersøgelser, hvor FE-modeller udvikles for forskellige patienter, og hvor der udføres inter-patientanalyser for at undersøge effekten af geometriske variationer på simuleringsresultaterne.

I denne afhandling undersøger vi først indflydelsen af geometriske variationer på tandbevægelser hos forskellige patienter ved at udvikle tre modeller af overkæber med en konventionel FE modelgenererings tilgang. Vi udfører både intra- og interpatientanalyser. Dernæst udvikler vi en pipeline, der næsten automatiserer model genereringsprocessen, hvilket gør det muligt at udvide vores datasæt til 17 patientspecifikke, klinisk validerede FE-modeller. Til sidst vurderer og kvantificerer vi de genererede modeller med hensyn til mesh-kvalitet, geometri-nøjagtighed og simuleringsstabilitet i forskellige scenarier og sammenligner resultaterne med state-of-the-art.

Vores resultater indikerer, at de udviklede beregningsmodeller er geometriske præcise med lave afstandsfejl fra segmenterings input maskerne. Desuden omfatter de genererede konforme volumetriske masker kvalitetselementer, der er egnede til forskellige

FE-scenarier. Vores undersøgelser af virkningerne af geometriske variationer på tandbevægelser viser at en kombination af to kliniske biomarkører, dvs. kronehøjde og rodvolumen, kan påvirke tandforskydning. Derfor kan disse biomarkører, kombineret med størrelsen af den påførte belastning, bruges til at forudsige forskellige patienters tandforskydninger.

Af hensyn til reproducerbarheden af vores arbejde deler vi hele vores forskningsproces og data. Herunder ubearbejdede rekonstruerede geometrier, kvalitetskonforme volumetriske meshes og pipelinen til at generere dem. Dette er tilgængelig som et GitHub-lager, Open-Full-Jaw, med åben adgang. Vi mener, at dette unikke lager, inklusive en højgeometrisk variation, vil bane vejen for fremtidige befolkningsundersøgelser med fokus på menneskelige kæber. Ved at levere reproducerbare FE-modeller giver vi forsker mulighed for nemt at producere simuleringsklare modeller til deres egne undersøgelser uden at skulle bruge lang tid på konventionelle tilgange.

Acknowledgements

This Ph.D. journey was a life-changing experience for me, both professionally and personally. I am grateful for working on an interdisciplinary project and developing my skills while collaborating with and learning from prominent researchers. This journey would not have been possible without all help I received from many people.

First and foremost, I would like to express my deepest appreciation to my advisors, Kenny, Peter, and Sune, for all their support, suggestions, and trust during this program. Those who were always open to discussions and patiently supported me to learn and work with insightful guidance, which is very much appreciated.

I thank the European Union's Horizon 2020 research and innovation program (Marie Sklodowska-Curie grant agreement No. 764644) for funding this project and providing an excellent opportunity for me to be part of the RAINBOW network and meet up and work with many talented young researchers, clinical experts, and other partners.

I especially thank 3Shape and DIKU for providing a friendly working and social environment. I am honored to be part of both departments. I thank to all my DIKU-3Shape colleagues and friends for always being there, even from far distances, during the challenging moments.

Finally, I would like to express my deepest gratitude to my parents and my beloved sister for their unwavering, unconditional love and encouragement during my whole life.

List of Publications

Chapter 2 **Torkan Gholamalizadeh**, Sune Darkner, Paolo Maria Cattaneo, Peter Søndergaard, and Kenny Erleben. "Mandibular Teeth Movement Variations in Tipping Scenario: A Finite Element Study on Several Patients." In Computational Biomechanics for Medicine, pp. 31-43. Springer, Cham, 2021.

Chapter 3 **Torkan Gholamalizadeh**, Sune Darkner, Peter Lempel Søndergaard, and Kenny Erleben. "A multi-patient analysis of the center of rotation trajectories using finite element models of the human mandible." Plos one 16, no. 11 (2021): e0259794.

Chapter 4 **Torkan Gholamalizadeh**, Faezeh Moshfeghifar, Zachary Ferguson, Teseo Schneider, Daniele Panozzo, Sune Darkner, Masrour Makaremi, François Chan, Peter Lempel Søndergaard, and Kenny Erleben. "Open-Full-Jaw: An open-access dataset and pipeline for finite element models of human jaw." published in Computer Methods and Programs in Biomedicine (2022): 107009.

Appendix A Peidi Xu, Faezeh Moshfeghifar, **Torkan Gholamalizadeh**, Kenny Erleben, and Sune Darkner. "Auto-segmentation of Hip Joints using MultiPlanar UNet with Transfer learning" in Medical Image Learning with Noisy and Limited Data, MICCAI workshop. 2022.

Appendix B Peidi Xu, **Torkan Gholamalizadeh**, Faezeh Moshfeghifar, Kenny Erleben, and Sune Darkner. "Individual Tooth and Bone Segmentation using MultiPlanar UNet with Transfer Learning and Watershed: Suitable for Simulation Studies" to be submitted to Medical Image Computing and Computer Assisted Intervention (MICCAI) 2023.

Appendix C Faezeh Moshfeghifar, **Torkan Gholamalizadeh**, Zachary Ferguson, Teseo Schneider, Michael Bachmann Nielsen, Daniele Panozzo, Sune Darkner, and Kenny Erleben. "LibHip: An Open-Access Hip Joint Model Repository suitable for Finite Element Method Simulation" submitted to Computer Methods and Programs in Biomedicine (2022).

Contents

Chapter 1

Introduction

This chapter provides a background on the tooth-supporting complex and further details on tooth movement modeling, discusses some critical challenges and criteria in generating large-scale FE models, and mentions our contribution to addressing the issues.

1.1 Background

1.1.1 Tooth supporting complex

Teeth are located in the jaw and supported by periodontium tissues. As shown in Figure 1.1, periodontium includes soft tissues such as periodontal ligament (PDL) and gingiva and hard tissues such as alveolar bone. In addition, a tooth is composed of four primary tissues: three hard tissues called enamel, dentine, and cementum, and one soft tissue called pulp at the center of the tooth containing blood vessels, nerves, and connective tissue. The alveolar bone is a mineralized tissue that mainly includes trabecular bone and a plate of compact bone (lamina dura) pierced to the PDL [63].

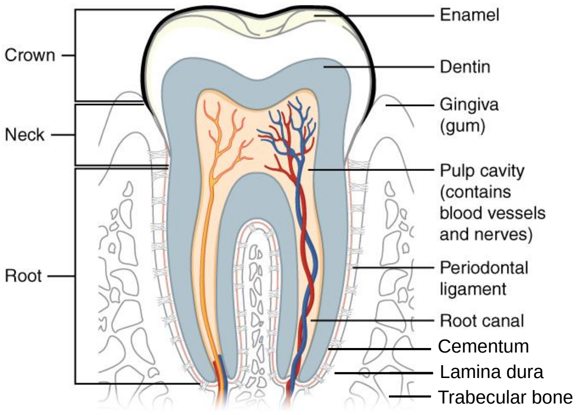

FIGURE 1.1: Tooth and its supporting complex, adapted from [88].

PDL is a dense fibrous tissue with an average width of 0.2 mm that attaches the teeth' cementum to the lamina dura of the surrounding alveolar bone. Its width can approximately be around 0.15 mm near the middle third of the root, and about 0.21 mm [12, 130] to 0.38 mm [63] near the root apex and cervical regions. Besides, its width progressively decreases over one's lifespan [83]. This connective tissue supports the tooth in its socket and enables it to bear chewing forces and act as a shock absorber [63].

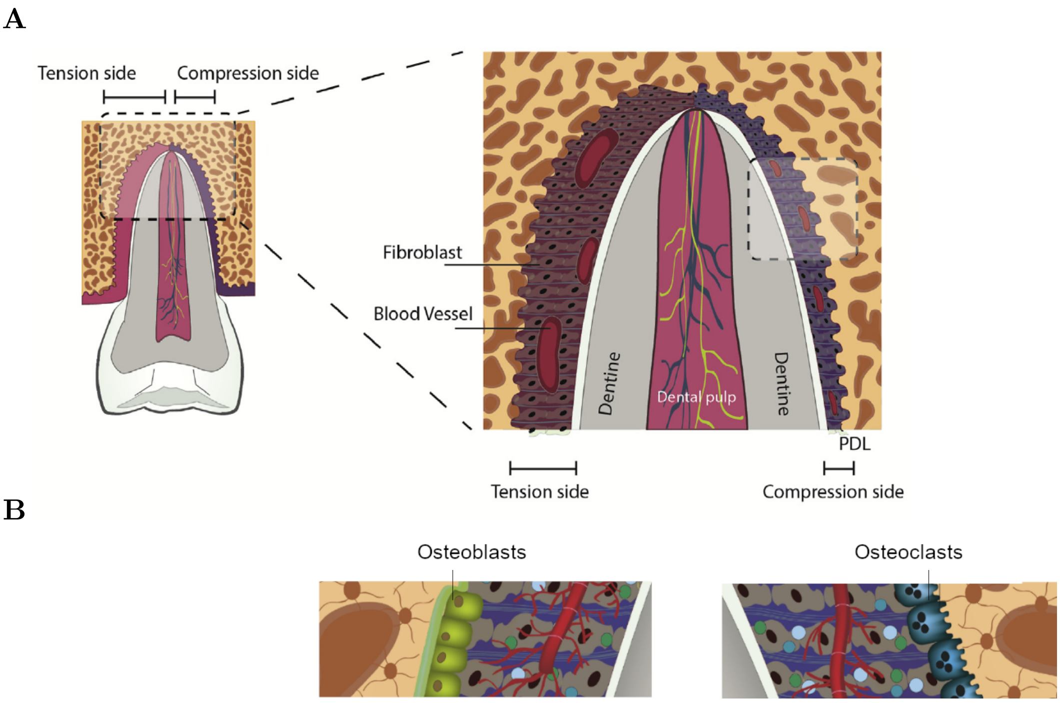

FIGURE 1.2: A schematic diagram of orthodontic tooth movement, adapted from [8]. **A (Initial tooth movement):** Applying an orthodontic force to a tooth causes the initial tooth movement, which is due to the compression of the PDL in the direction of the applied load and its tension on the other side. **B (Long-term tooth movement):** As a result of a continuous force, within a few days bone-remodeling process occurs. On the compression side, the osteoclast cells cause bone resorption, and the osteoblast cells, on the tension side, form new bone, resulting in bone and tooth socket deformation.

1.1.2 Tooth movement and bone remodeling

Orthodontic tooth movement results from alveolar bone remodeling caused by the applied forces and deformations in the periodontium. As can be seen in Figure 1.2, the tooth movement generally occurs in two phases [45]. In the first phase [25, 66, 105], which is the main focus of this thesis and called the "initial tooth movement", the tooth moves within the PDL space in a few seconds after applying the force [63]. This movement is due to the instantaneous deformation of the surrounding PDL tissue caused by the applied load. In the second phase [27, 45, 54] called "long-term tooth movement", the resulting stress-strain in the periodontium causes a bone remodeling process due to the applied load. More specifically, the bone-remodeling process occurs within a few days due to a continuous force, where the bone is resorbed and formed in the PDL's compressed and stretched regions. On the compression side, the osteoclast cells cause bone resorption, and the osteoblast cells, on the tension side, form new bone, resulting in bone deformation [8, 63, 66].

1.1.3 Finite element methods

The finite element method is a numerical analysis technique combined with computational modeling and continuum mechanics that models a physical phenomenon. It uses a similar concept to the ”divide-and-conquer” algorithm, where instead of solving the problem for the entire complex domain in a single operation, the domain is discretized into a finite number of smaller and simpler parts (elements), and the problem is formulated and solved for each element. Finally, the results are combined to approximate the solution for the entire discretized domain [70].

The FE method is widely used in medicine and dentistry when the clinical questions cannot be analyzed in vivo due to ethical issues or clinical challenges or when it is not feasible to analyze them experimentally due to extensive costs [10, 58]. Therefore, conducting FE analysis could be a non-invasive, time- and cost-efficient way to study the behavior of a phenomenon under the desired case.

Conducting an FE analysis requires a proper geometry reconstruction of the desired anatomies; by delineating the boundary and interior region of the studied regions from the medical scans. This is usually done by delineating the regions in different slices of a medical scan using semi-automatic segmentations and manual corrections. Next, the segmented regions are exported as a surface that covers the domain's boundary. This surface is first discretized with a finite number of surface elements, e.g., connected triangles comprised of points and the information of the connecting lines. Next, the surface mesh is converted to a volumetric mesh where the volumetric elements cover the shape's boundary and interior volume. After domain discretization, an FE problem is set up by defining the applied load information, boundary constraints, material properties, and degrees of freedom of different elements. Next, the FE problem is solved using FE solvers to find the unknowns.

1.2 Problem statement

Developing a patient-specific finite element model (FEM) of the human jaw begins with a (time-consuming) semi-automatic segmentation/annotation task to delineate the desired anatomies from the patient's medical scan. Next, the segmented regions are reconstructed as surface meshes, generally composed of irregular dense meshes with no guarantees of manifoldness, water-tightness, or absence of self-intersections. Such criteria are crucial for generating volumetric meshes to be used in simulations.

Besides, the reconstructed dense surface meshes are computationally expensive to be used directly in the simulations. Hence, they require additional geometry processing, mesh decimation, and re-meshing to provide FEMs with quality elements and a reasonable number of elements.

Most widely-used geometry processing and meshing tools in the field are designed based on the conventional one-by-one meshing approach, in which one domain is processed independently from the other domains at a time. Moreover, these approaches involve labor-intensive and time-consuming manual tasks. Thus, the current one-by-one meshing approach limits the possibility of automating the pipeline for generating a large number of FEMs.

Furthermore, performing the mentioned geometry and mesh manipulations on the surfaces with shared interfaces with other domains can produce undesired gaps/penetrations in the contacting interfaces, leading to instability in the contacting areas or causing convergence issues in the simulations.

All of the mentioned manual tasks and the meshing challenges hinder the researchers in the field from developing multi-patient FEMs and performing population studies, restricting almost all of the studies to single-patient analysis. Therefore, there is huge need for clinically validated multi-patient FEMs of the human jaw obtained using an automatic pipeline/framework to ensure reproducibility.

1.3 Challenges

1.3.1 Lack of high-resolution medical scans

The resolution of scans obtained from different parts of the human body, typically using Computed Tomography (CT) and Magnetic Resonance Imaging (MRI), are not comparable to those captured from fine-detailed areas like teeth. For example, the public dataset of The Cancer Imaging Archive (TCIA) [30] provides CT/MRI scans of different human body parts with a minimum resolution of 0.3 mm, or the commercial dataset of Virtual Population (ViP) [4, 44] provides MRI scans of whole-body human anatomies with an isotropic resolution of 0.5 mm. Unfortunately, these resolutions are not high enough for a detailed reconstruction of teeth and jaw anatomies and make it almost impossible to perform population studies on tooth movement, for instance.

1.3.2 Accurate automatic geometry reconstruction

The initial requirement of a reliable FEM is to obtain an accurate segmentation for the desired anatomies from the medical scans. In the case of developing FEMs of the human jaw, three main structures need to be modeled: teeth, PDL layers, and bone geometries. However, segmenting the PDL layers' boundaries directly from the CBCT scans is not feasible, as the generally-used resolutions for the CBCT scans,ranging from 0.2 mm to 0.5 mm [23], are not fine enough to capture the thin structure of PDL with an average thickness of 0.2 mm. Besides, the PDL's adjacent hard tissues, i.e., the tooth cementum and lamina dura, have relatively similar intensities in the CBCT scans due to their material properties and compact structures. This means these hard tissues with relatively similar intensities are separated with at most one voxel where the PDL resides. Because of these anatomical features and the lack of high-resolution scans, an accurate tooth-bone segmentation process is highly time-consuming and challenging [134], especially when using the existing semi-automatic segmentation approaches that require excessive manual refinements. Based on our experience, the segmentation of a CBCT scan can take up to several days per scan, depending on the scan's resolution, the existence of metal filling artifacts, and the desired accuracy of the delineations.

In addition to the common semi-automatic approaches, the deep-learning-based segmentation approaches could be used for teeth-bone segmentations. However, due to the lack of publicly available CBCT scans with teeth-bone delineations, we first segmented seven scans semi-automatically and then trained a deep learning method. Next, for any new scans, the teeth-bone predictions of the trained network are used as the initial segmentation. Later, we refine and improve the delineations until it reaches our accuracy criteria. Finally, the improved label maps are fed to the network to enhance the tooth-bone segmentation result for the new scans. Our automatic-segmentation method is designed based on a multi-planar U-Net architecture [95] and uses a transfer learning strategy to improve poor segmentations and fine-tune the network with a dedicated loss function for precise segmentation of the CBCT scans considering the anatomical information. The results are presented in Appendix B.

Likewise, we use the network to segment the bones in the human hip joint and pelvic area by enforcing gaps in segmented bone regions where the soft tissues reside. First, the network is trained based on 10 CT scans from a publicly available dataset with an inferior/coarse segmentation of the hip area [31, 129] having no gaps between the bones. The model is then fine-tuned in an interactive learning step using two anatomically accurate segmentations and two corrected segmentations to improve the segmentation accuracy while having the gap between the bones where the cartilage resides, as presented in Appendix A.

1.3.3 Domain discretization and contacting interfaces

The second step in the FE model generation pipeline is to discretize the delineated domains into a finite number of elements, first on the surface mesh level and next on the volumetric level. Unfortunately, volumetric discretization algorithms usually require a set of closed, self-intersection-free surface meshes as input, which is difficult to guarantee when working with reconstructed geometries acquired from medical images. Hence, it is required to perform an additional "cleanup process" that involves manual tasks for removing self-intersections, holes, or other imperfections commonly appearing when working with data-driven geometries.

Besides, the conventional one-by-one domain discretization includes mesh reduction and quality meshing processes that may generate undesired gaps or penetrations between two contacting surfaces, making it challenging to achieve congruent surfaces with conformal meshes. These gaps/penetrations mainly affect the numerical stability of the computational models when soft structures, e.g., PDL, contact hard tissues like bone or teeth. Moreover, a coarse or poor-quality discretization of the domains can cause a locking effect and influence the accuracy of the predicted stress/strain values and concentrations compared to the values measured in vivo.

In Chapter 2 and 3, we utilized the commonly used one-by-one meshing approaches to develop FEMs. First, we clean up the surface meshes to provide perfect surface meshes as input to a volumetric meshing algorithm. However, this approach demands manual modifications; hence, in Chapter 4, we propose a very different approach, where we accept the imperfect meshes and develop a multi-domain meshing pipeline, mainly based on the method recently introduced in [47, 49]. More specifically, instead of meshing one domain at a time, we mesh the entire volume of the bounding box containing all input surface meshes. This avoids any numerical errors caused by non-congruent contacting meshes and results in multi-domain conformal meshes, leading to stable and accurate computational models.

1.3.4 Lack of publicly available research data

Due to the mentioned challenges, developing several patient-specific FEMs may not be feasible for many researchers. In addition, there are currently no publicly available datasets of 3D models of full dentition human jaw, except for one study [128] that shares detailed geometries of one mandible obtained from a dried male skull. However, the detailed geometries obtained from a single mandible cannot cover geometrical variations across different patients in the population.

In other words, in almost all of the studies focusing on full dentition or single/multiple tooth analysis, the utilized geometries, volumetric meshes, and FEMs have not been made publicly available [16,16,19,32,61,86,90,102,104,113]. Therefore, extending the dataset or a quantitative comparison is not attainable due to the used unreproducible manual procedures and the use of commercial tools that are not available for everyone.

In this thesis, we use free and open-source meshing tools and libraries to reproduce our work. In Chapter 3, we share adaptive meshes of three mandibles involving the teeth, PDLs, and the bone. Note that these models are developed using the conventional FEM generation approach that involves manual geometry and mesh editing.

In Chapter 4, we provide the largest open-access dataset of the human jaw, including 29 mandibles and maxillae, with a high geometrical variation obtained from 17 patients' CBCT scans. We produce all of these models using a nearly-automated pipeline for the reproducibility of our work and avoiding time-consuming manual procedures. We share the pipeline code as well as the mentioned dataset. The pipeline is intentionally developed based on free open-access geometry processing libraries [52] and meshing algorithm [48], which generates simulation-ready meshes with minimal human intervention and error in the model generation procedure.

1.3.5 Parameter tweaking and simulation setup

One of the essential steps of FE analysis is properly setting up an FE problem to mimic the desired scenario. This can involve setting various parameters and conditions for choosing proper material models and properties, defining contacts between different domains, and specifying boundary conditions. Next, the defined FE problem is solved using an FE solver of choice. Various commercial and open-source FE solver software and libraries are used to solve FE problems and post-processing the obtained results. However, modeling complex scenarios involving many parameters using commercial software in the field can make it challenging for others by limiting access to that software to reproduce the results and quantitative comparison.

Some of the assigned parameters in the FE problem setup, like contact parameters, can significantly affect the simulation results and stability. Hence, one needs to tune the parameters to assign proper values for them and avoid convergence issues. This implies that the parameters must be chosen in a trial and error approach. This, in turn, requires a proper understanding of how each involved parameter affects the simulation results. Besides, this trial and error process can be challenging when adjusting the parameters of contact can influence the behavior of other contacts. Furthermore, the obtained parameters for the FEM of one patient may not always result in proper convergence of another patient's model, which is mainly due to the anatomical and geometry variations and errors caused by one-by-one discretization methods.

To this end, we opt for free and open-access FE frameworks and libraries to address the reproducibility problem. In Chapter 2 and 3 we use FEBio software packages [3] which is open-source software for nonlinear FE analysis in biomechanics. Defining contacts in FEBio requires specifying contacting surfaces and ensuring one of the involved surfaces is denser than the other. Even though FEBio provides a user-friendly user interface for setting up FE problems, the implemented contact formulations still require parameter adjustments for a new model. This can make it challenging for the users to perform large-scale population studies because of the involved human intervention and parameter adjustments. Therefore, in Chapter 4, we utilize PolyFEM for solving the FE problems. It is an FE simulation toolkit that supports elastodynamic deformations with linear and nonlinear material models. In addition, it uses the incremental potential contact formulation [62] for contact response and friction, which ensures inversion- and penetration-free meshes under large deformations during the entire simulation. Moreover, the contacting surfaces are automatically detected; hence, there is no need to specify contact surfaces, significantly simplifying the scene setup.

1.3.6 Multi-patient analysis

Because of the mentioned challenges, studies in the field are limited to single-patient analysis, which raises the question of the generalizability of their conclusions to a larger population. Although patient-specific FEMs are powerful tools for pre-operative uses, implant, and treatment designing for a patient, the observed behavior and deduced hypothesis based on a single-patient model may not be generalized for a larger population with large geometry variations [35]. To be more specific, one needs to consider inter-patient variations for answering clinical and biomechanical questions of a larger population. Hence, a population study involves two main steps: first, generating a large number of patient-specific FEMs and performing identical scenarios across all patients; second, investigating the validity of a pre-defined hypothesis across the population and examining the influence of the patient-specific features on the simulation results. The second step plays a crucial role as it can result in generalizable results for a larger population and decrease the uncertainties of the predictions.

In Chapter 2, we provide a computational analysis tool for investigating the influence of tooth geometry on the movement of different patients' teeth. We perform the first full dentition intra- and inter-patient analysis of tooth movement and propose nonlinear functions for predicting tooth translation and rotation of different teeth considering the applied load and two clinical biomarkers, i.e., crown height and root volume. Proposing such functions allows for the generalizability of the tooth movement predictions across different patients. However, in Chapter 3, we employ the registration methods to define loading conditions for different patients' teeth and analyze the simulation results, i.e., trajectories of the teeth center of rotations under varying loading conditions. Using the registration approaches, we aimed to eliminate the geometrical variation and analyze different simulation results in the same space.

1.4 Contributions

Our main contributions in analyzing the effects of geometrical variations on tooth movement [41] can be summarized as follows:

1. We generate patient-specific FEMs for three patients by segmenting the CBCT scans of the patients. To the best of our knowledge, this is the first computational model in orthodontics applied to three different patients.
2. We estimate tooth movements (i.e., rotation and translation) as nonlinear functions of both load and the ratio of crown height to root volume to show that variations in the teeth anatomy of different patients and the load magnitudes can affect the resulting tooth displacement.
3. We show that a combination of two clinical biomarkers, i.e., crown height and root volume, can affect tooth displacement. These biomarkers can be used to predict the translation and rotation of different patients' teeth for applied load magnitudes.

4. We consider teeth motions under an identical scenario, both in intra-patient and inter-patient analyses. This helps us obtain a general pattern for the movement of different teeth using patient-specific teeth and bone geometries.

Our main contributions in trajectory analysis of the center of rotations (CRots) of the teeth [42] can be summarized as follows:

1. We consider patient-specific full dentition computational models of three human mandibles to investigate the position of the CRots in different patients' teeth.
2. We represent the effect of geometrical variations on the position of the CRot under the same boundary and loading conditions for different patients.
3. We model the clinical forces with no specific limitation in the force magnitudes by using a hyperelastic material model for PDL tissue and investigate the position of the CRot in a 3D space to better represent the resulting rotation.
4. We assess the influence of the couple directions on the positions of the CRots of a specific tooth and show that equally rotating the direction of the couple about the three principal axes results in different patterns for the CRot positions, especially in labiolingual direction. Modeling different types of tooth movements using a more realistic force system on the crown, and investigating the effect of these couple forces on the CRots can help us to better estimate the force systems needed to achieve the desired tooth movement.
5. We introduce a repository containing adaptive surface meshes of the bones, teeth, and PDL layers that can be used in FE simulations.

Our main contributions in Open-Full-Jaw [43] can be summarized as follows:

1. We provide an open-access dataset of different patient-specific models of the human jaw, including the maxilla, mandible, full dentition, and the PDL geometries obtained from CBCT scans of 17 patients. It is the largest publicly available dataset with validated segmented geometries and quality volumetric meshes that can directly be used in FEM studies.
2. We introduce a repository containing (1) clinically-validated segmented geometries and the resulting dense irregular surface meshes; (2) the quality and adaptive volumetric/surface meshes to be used in FE simulations; (3) the automatically generated FEM files for tipping and biting scenarios used for the FE analysis of this work.
3. For reproducibility, we share our pipeline developed based on open-source meshing tools [48, 52] to generate the models of this study. This python-based library automates the FE model generation process, including geometry processing and re-meshing tasks with minimal human intervention, by setting a few required parameters.

4. Our pipeline ensures conformal meshes in the contacting interfaces without any undesired gaps or penetrations and provides adaptive meshes that are vital for reducing the total number of elements while using finer meshes in specific regions, e.g., teeth sockets, alveolar crest, and alveolar process.

1.5 Thesis outline

The rest of this thesis is organized as follows. Chapter 2 focuses on the effects of geometrical variations on the movement of different patients' teeth. Chapter 3 describes the analysis performed on the trajectories of the center of rotations of different patients' teeth movements. In Chapter 4, we introduce the details of the largest open-access dataset of human jaws and the framework for automating the model generation processes. Chapter 5 summarizes the thesis based on the published studies and describes possible future directions for the research carried out during this Ph.D. project.

This thesis also involves three appendices with different studies presenting examples of the author's contribution in different yet relevant areas with similar challenges. Appendices A and B show the study about a deep learning method applied to automate the hip area segmentation from CTs and tooth-bone segmentation from CBCTs, respectively. Appendix C presents an open-access dataset of patient-specific human hip joint models adapting similar concepts from the study mentioned in Chapter 4 but using complete geometries for the pelvic girdles and hip joints.

Chapter 2

Effect of Geometrical Variations on Tooth Movement

This chapter is based on our work presented in [41] focusing on the effects of geometrical variations on different patients' teeth movements. It shows our first attempt to develop quality FEMs of several patients' mandibles using free and open-source geometry processing, meshing tools, and an FE solver. This work particularly benefited from our collaboration with the clinical experts from Aarhus University. In addition, it addresses the common challenges related to multi-patient analysis (Section 1.3.6) by introducing the first computational tool applied to different patients' teeth to provide more generalized tooth movement predictions by considering teeth' anatomical features and loading conditions.

Previous studies on computational modeling of tooth movement in orthodontic treatments are limited to a single model and fail in generalizing the simulation results to other patients. To this end, we consider multiple patients and focus on tooth movement variations under the identical load and boundary conditions both for intra- and inter-patient analyses. We introduce a novel computational analysis tool based on finite element models (FEMs) addressing how to assess initial tooth displacement in the mandibular dentition across different patients for uncontrolled tipping scenarios with different load magnitudes applied to the mandibular dentition. This is done by modeling the movement of each patient's tooth as a nonlinear function of both load and tooth size. As the size of tooth can affect the resulting tooth displacement, a combination of two clinical biomarkers obtained from the tooth anatomy, i.e., crown height and root volume, is considered to make the proposed model generalizable to different patients and teeth.

2.1 Introduction

Orthodontic tooth movement is the result of alveolar bone remodeling caused by the applied forces and deformations in the periodontium. Finite element models (FEMs) is widely used to assess stress/strain in the alveolar bone and periodontal ligament (PDL), the fibrous connective tissue between tooth and

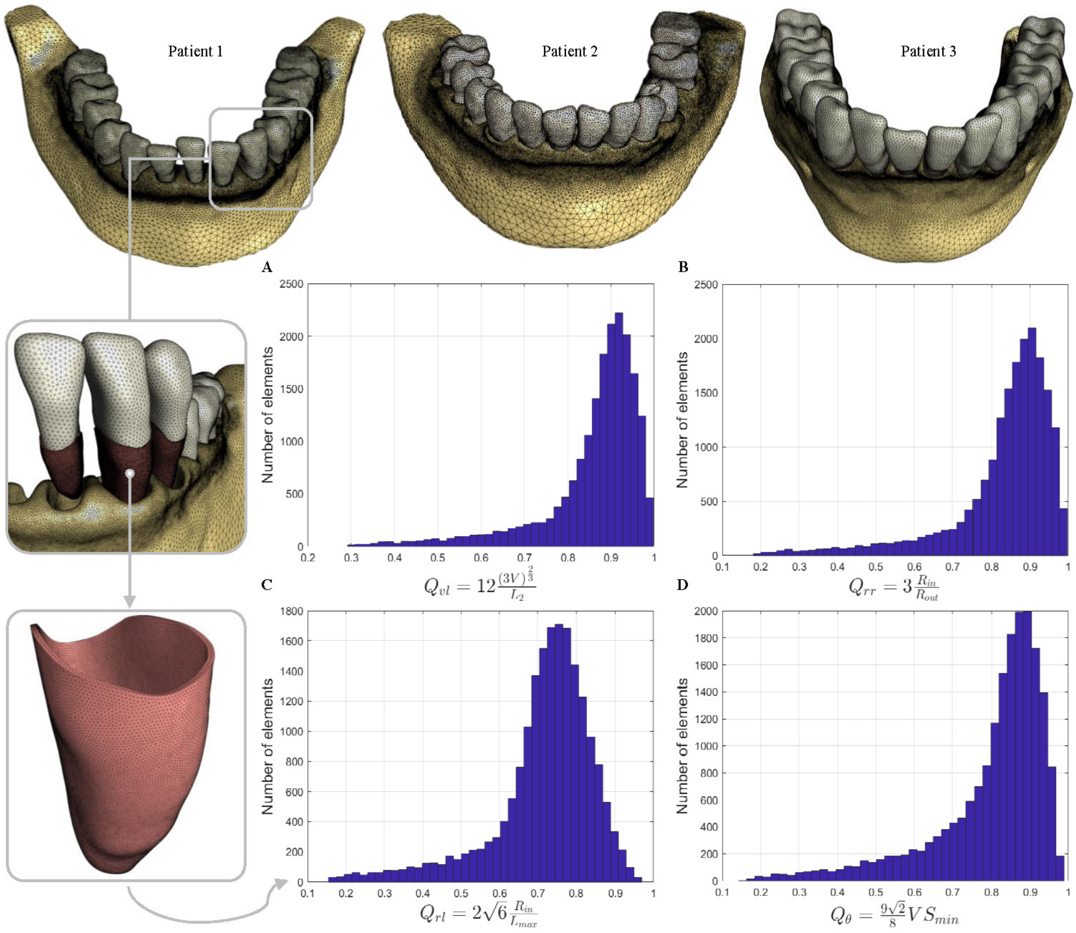

FIGURE 2.1: FEMs and meshes for three patients, and mesh quality histograms for the PDL of the left canine. **A:** The volume-edge ratio, **B:** The radius ratio, **C:** The radius-edge ratio, **D:** A metric introduced in [40].

bone, in the orthodontic treatments [25,27,45,54,68,105]. Moreover, the initial and long-term tooth movements can be investigated using these models. In this work, we use an FEM to provide a biomechanical model of the full mandibular dentition focusing on initial teeth displacements caused by the applied load on the teeth (see Figure 2.1 and Figure 2.2). We generate patient-specific FEMs for three patients by segmenting the cone-beam computed tomography (CBCT) scans of the patients. The models are provided by using the same boundary conditions under the same scenarios. In each scenario, an identical force magnitude is applied perpendicular to the surface of each tooth to mimic an uncontrolled tipping movement. Besides, the load magnitude can change from 0.3 N to 1 N with 0.1 N increments, and teeth transformations are recorded for all teeth of each patient. Finally, the results are compared with the corresponding teeth of other patients.

Our hypothesis is that variations in the teeth anatomy of different patients and the load magnitudes can affect the resulting tooth displacement. Therefore, in this study, tooth movements (i.e., rotation and translation) are estimated as nonlinear functions of both load and the ratio of crown height to root volume using the obtained biomechanical models.

2.2 Related Work

The performance of the orthodontic treatments can be improved if the movement of the teeth could be predicted in a reliable way. Therefore, many studies have focused on predicting tooth movements in orthodontic treatments using FEMs. In general, the tooth movement occurs in two phases [45]. In the first phase [24,25,66,105], which is the main focus of this study, tooth moves within the PDL space in few seconds after applying a force [63]. This movement is substantially due to the deformation of the PDL tissue caused by the applied load. In the second phase [27,45,54,68,68], the resulting stress in the PDL and bone tissue causes a bone remodeling process, where the bone is resorbed and formed in the compressed and stretched regions of the PDL, respectively.

In the context of FE-based modeling of the initial tooth movement, some studies [24, 105] have investigated different types of movements individually including bodily movement, controlled tipping, and uncontrolled tipping. Some others have explored the teeth mesialization, distalization, or retraction scenarios [54, 66,68,93]. These studies have considered the effect of the force direction [54,105], moment-to-force [24,105], and force magnitude [24,76] on tooth transformation [24, 54, 93] or location of the center of rotation [24, 105]. However, the jaw model, force system, and number of teeth used in the analyses are not consistent. For example, [24, 105] used a small portion of jaw, while [50] worked on a fully segmented jaw model. Likewise, different studies have examined different number of teeth, e.g., using a single tooth [105], two [24, 66] or more [54, 93]. The force and/or moments have also been applied to different parts including the surface of tooth [24, 66], center of the resistance [105], and orthodontic appliances [54, 68].

The abovementioned biomechanical models, however, might not be applicable for analyzing different teeth motions obtained from multiple patients. In other words, the obtained tooth displacement results represented only by visualizing the displacement fields [66, 93], measuring the displacement of the selected landmarks [24, 93], or acquiring the translations/rotations using some predefined measurement points [54] lack useful information about different tooth motion tendencies for full dentition of multiple patients and, hence, are less interpretable when it comes to the across patients modeling analyses.

Moreover, existing FEMs applied in computational orthodontics are mostly limited to a single patient [24, 50, 54, 66, 93, 105]. Although Likitmongkolsakul et al. [68] propose a stress-movement function of a canine for two orthodontic patients under an identical scenario, to the best of our knowledge, there are no other studies considering multiple patients for tooth movement modeling.

In this work, by considering the biomechanical models of human mandible acquired from CBCT scans of three patients, we investigate the tooth movement variations in multiple patients using rigid body transformations under different load magnitudes. To the best of our knowledge, this is the first computational model in orthodontics applied to three different patients. Our experiments consist of both intra- and inter-patient analyses. Considering teeth motions under an identical scenario, both in intra-patient and inter-patient analyses, helps us to obtain a general pattern for the movement of different teeth using patient-specific teeth and bone geometries.

2.3 Setting up the Finite Element Model

This section describes different consecutive steps that are conducted to generate a patient-specific FEM of the human mandible. First, the geometry reconstruction takes place by segmenting the CBCT scan of the patient. Second, the surface mesh of the obtained geometries are re-meshed and a volumetric mesh is generated for each geometry. Next, the resulting volumetric meshes are imported into a finite element (FE) framework to set up the FE problem. The details of the biomechanical model, e.g., boundary conditions, contact definitions, and utilized material models are presented in this section. Finally, the model is numerically verified by using mesh convergence study and parameter sensitivity analysis. Segmentation is performed using 3D Slicer [37] based on a semi-automatic watershed algorithm applied to the bone and teeth. Next, the wrongly segmented regions are modified to obtain the final segmentation result. Since the resolution of the orthodontic scans with a voxel size of $0.3 \times 0.3 \times 0.3$ mm^3 is not high enough for segmenting the thin PDL tissue (≈ 0.2 mm width) from the scans, the PDL layer is generated with a uniform width of 0.2 mm around each tooth root as shown in Figure 2.1. We select three patients' scans of various crown height, root length, and teeth sizes, to ensure having enough geometrical variations. Each segmentation result is later verified by an orthodontic expert.

The segmented geometries are exported as surface meshes in STL files. These meshes are decimated and re-meshed using Meshmixer [2] to provide high-quality surface meshes. Uniform meshes are used for teeth and PDL geometries. Table 2.1 presents the edge length of the triangular meshes for each component. For bone geometry, an adaptive mesh is generated in which the edge length of the surface mesh triangles varies between 0.4 mm and 2 mm from the neighboring regions to the PDL and the bottom region of the mandible. Utilizing an adaptive mesh helps us to obtain a finer mesh in the regions of interest, and consequently, an accurate result in the FE analysis, yet reducing the total number of elements.

High quality volumetric meshes are generated for each surface mesh using TetGen [5], by defining an upper limit for the radius-edge ratio of to-be-generated tetrahedra. This mesh quality constraint controls the ratio between the radius of the circumscribed sphere and the shortest edge of each tetrahedron, which prevents the production of low-quality (badly shaped) tetrahedra. Later, four different mesh quality measurements presented in [114], i.e., the volume-edge ratio [69, 78], the radius-edge ratio [11], and the radius ratio [22, 40] are chosen to verify the quality of the generated 4-noded tetrahedral meshes (TET4) (see the quality histograms in Figure 2.1). Finally, the obtained meshes are used to set up and solve the FE problem. For reproducibility, we generate and solve the computational biomechanical models in FEBio software package [3] which

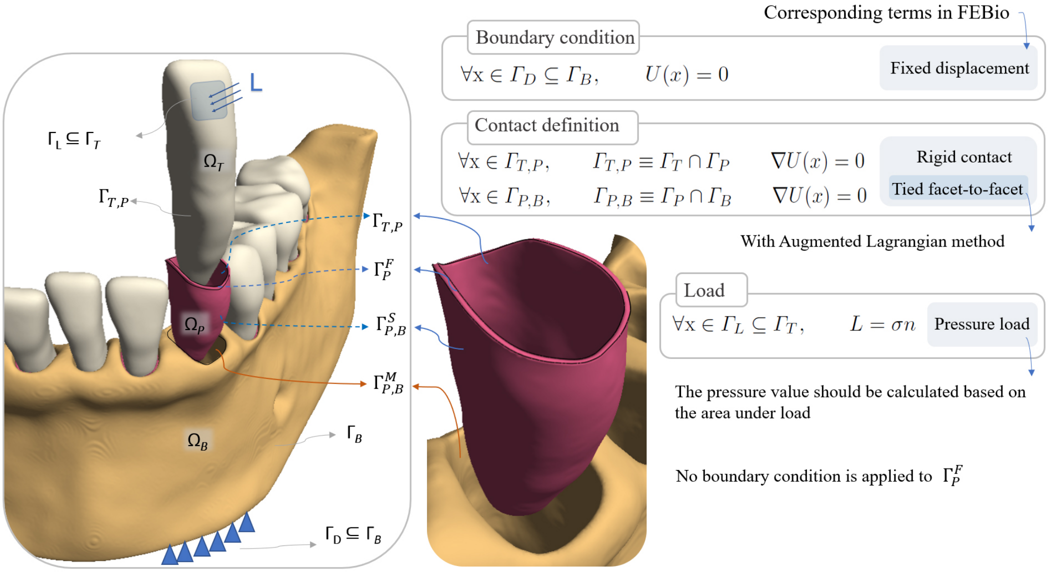

FIGURE 2.2: A closeup view of the tooth supporting complex. The contacts between different domains and boundary conditions are presented. Tooth (Ω_T), Periodontal ligament (Ω_P), Alveolar bone (Ω_B), Tooth-PDL contact ($\Gamma_{T,P}$), PDL-Bone contact ($\Gamma_{P,B}$) and a Dirichlet boundary condition (Γ_D) are shown.

is an open-source software for nonlinear FEA in biomechanics. A nonlinear quasi-static simulation is performed to analyze the teeth displacements in each FE model.

The different domains of the FEM, material properties, contact types, boundary conditions and the applied load are summarized in Figure 2.2. To simplify the proposed model, the tooth domain is assumed as rigid-body with 6 degrees of freedom. The center of mass for each tooth is calculated automatically using FEBio based on a predefined density parameter [72]. Furthermore, since the deformation of the bone tissue is negligible under the orthodontic forces, no distinction is made for the cortical and trabecular bone [98,135], and an isotropic elastic material model is used for the homogeneous bone geometry.

The importance of the PDL tissue in transferring loads from the tooth to the

TABLE 2.1: Summary of the materials and mesh properties.

Domain	Material model	Material properties		Mesh properties	
		Young's modulus (MPa)	Poisson's ratio (−)	Surface mesh Edge length (mm)	Volumetric mesh Number of elements †
Tooth	Rigid body	–	–	0.4	14±5 K
Bone	Isotropic elastic	1.5×10^3	0.3	Adaptive mesh (from 0.4 to 2)	3,261±329 K
		C_1 (MPa)	C_2 (MPa)		
PDL	Mooney-Rivlin *	0.011875	0	0.1	127±41 K

* $C_2 = 0$ reduces the Mooney-Rivlin material to uncoupled Neo-hookean. The values assigned for C_1 and C_2 correspond to the Young's modulus and Poisson's ratio of 0.0689 MPa and 0.45, respectively.
† The values are shown as the mean ± standard deviation of the number of elements across all cases.

Table 2.2: Summary of parameter sensitivity analysis conducted on the model.

	PDL		Bone		PDL-Bone Tied Contact	
	Young's Modulus	Poisson's Ratio	Young's Modulus	Poisson's Ratio	Augmented Lagrangian	Penalty Factor
Interval of parameter change	0.044 - 0.0938	0.45 - 0.49	1200 - 13700	0.2 - 0.4	0.2 - 0.1	0.25 - 1.75
Relative difference in Von Mises stress (%)	2.127	2.127	0.709	3.900	1.418	3.900

alveolar bone has been shown in the literature [25,74,89]. Accordingly, the PDL tissue is included in our model as a thin layer of finite elements [25, 46, 89, 105]. This allows for investigating the stress/strain field in the PDL, e.g., using data-driven models, that can later be used in the bone remodeling process [27]. Moreover, several studies have characterized the biomechanical behavior of the PDL tissue [33, 98, 123], some of which have suggested the Mooney-Rivlin Hyperelastic (MRH) model for the PDL [98, 123]. In this study, an MRH material model is used for the PDL domain based on the parameter values reported in Table 2.1.

The Tooth-PDL interface and PDL-Bone interface are fixed in both normal and tangent directions using a Neuman condition (see Figure 2.2). In addition, all elements at the bottom surface of the bone (Γ_D) are fixed in all directions by applying a Dirichlet boundary condition.

To mimic the uncontrolled tipping scenario, a pressure load is applied perpendicular to the labial/buccal surface of the tooth crown, as shown in Figure 2.2. The area under the load, which represents the area under the orthodontic bracket, is set to the center of the teeth crowns. To ensure that the same force magnitude is applied to the teeth, the area under the load is measured separately for each tooth. Next, the corresponding pressure value for the desired force magnitude is calculated and used as the *pressure load* in FEBio. An identical force magnitude is exerted to all teeth simultaneously in order to investigate the tooth movement variations of the mandibular teeth across the three patients.

The model is then verified by studying the mesh convergence and parameters sensitivities. The final resolution of the mesh is defined in the mesh convergence study process where the total number of elements, except for the rigid body teeth, is iteratively increased by a factor of 2 until the relative error is less than 4% of the maximum stress (see Figure 2.3). The number of tetrahedra in the refined mesh is presented in Table 2.1. The parameter sensitivity study, summarized in Table 2.2, is done on the material parameters of different tissues and the parameters used for the tied contact in the PDL-bone interface.

2.4 Experiments and Results

This section describes the experimental setup under the uncontrolled tipping scenario among the three patients. First, the obtained results are presented and discussed. Next, we propose two functions that describe the translation

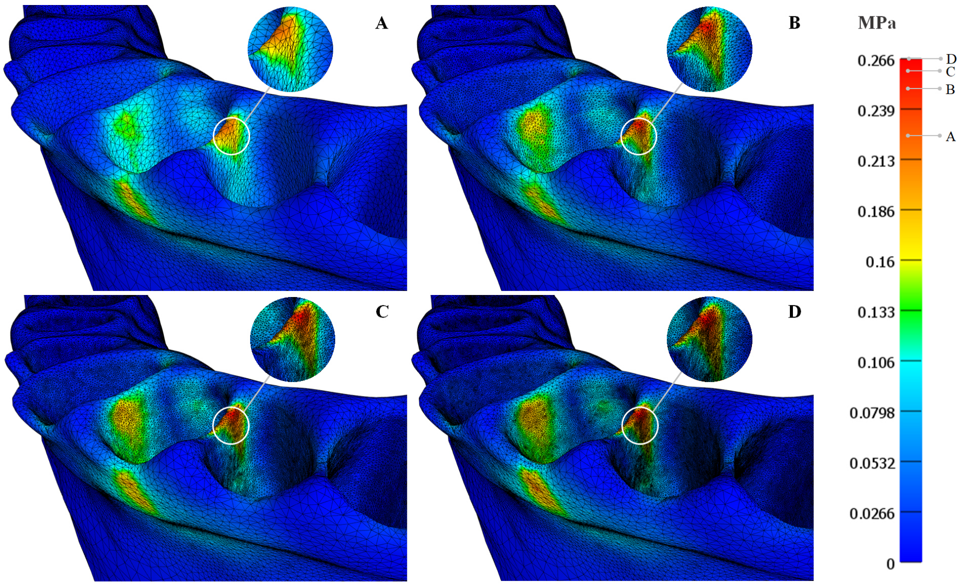

FIGURE 2.3: Mesh convergence study showing the Von Mises stress in the bone geometry under the same boundary conditions. **A to D:** The model with N (coarse), $2N$, $4N$, and $8N$ elements. The stress fields are consistent in the finer models.

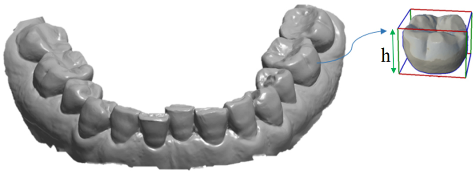

FIGURE 2.4: An intraoral scan of a patient and the obtained crown height for a tooth.

and rotation of different tooth types of the patients based on tooth IDs and selected clinical biomarkers, i.e., crown height and root volume.

In order to have a comprehensive inter-patient analysis, we select the patients with roughly the same number of teeth. We use the intraoral scan of each patient, captured by the 3Shape Trios scanner [1], to obtain the crown height of each tooth. Therefore, we ensure that the intraoral optical scans are available for all patients, and the CBCT scans have sufficient quality for performing the segmentation. Figure 2.4 shows an intraoral scan of a patient and illustrates how the crown height is obtained for a tooth.

In each scenario, an identical force magnitude is applied perpendicular to the surface of each tooth. The load magnitude (l) varies from 0.3 N to 1 N with 0.1 N intervals. The displacement of each tooth is measured as the translation of center of the mass ($\vec{t}$) and rotation of the rigid body teeth (with angle θ and axis $\vec{n}$). Besides, in each simulation, we record the tooth ID (k), load magnitude, and the relevant biomarkers. *Universal Numbering (UNN)* system is used for the tooth ID, where k changes between 17 and 32 from the left third molar to the right third molar, respectively. Figure 2.5 illustrates relation between the translation/rotation and applied load for different teeth of each patient. As can

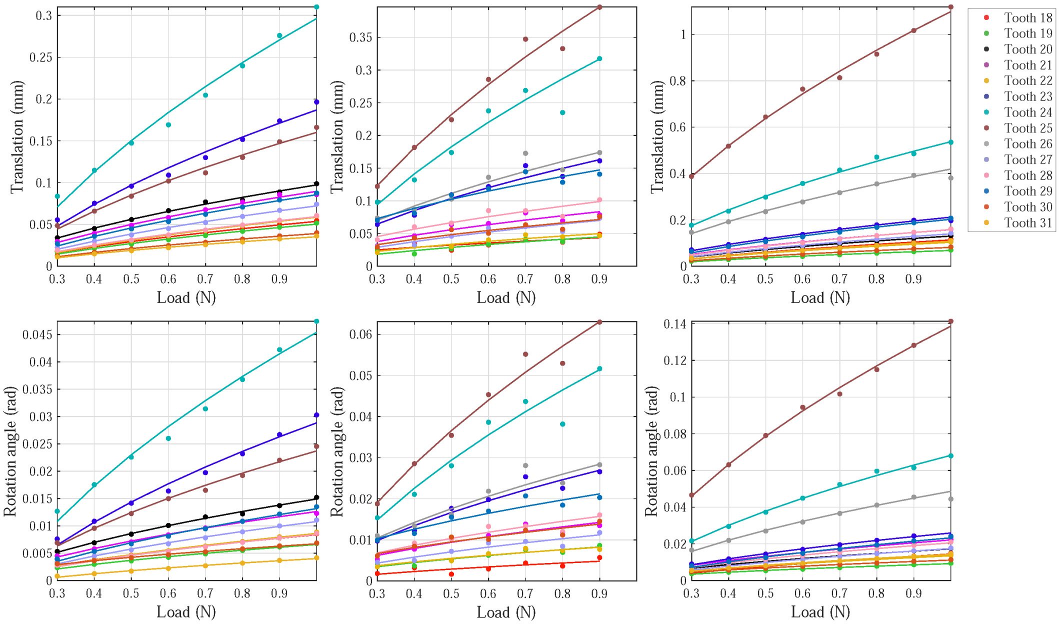

FIGURE 2.5: The diagrams of translation magnitudes and rotation angles versus the applied load. Each data point represents the displacement of a tooth under the applied load. We use a nonlinear square root regression model to fit the data from each patient's tooth. **Top-row:** Translation magnitude, **Bottom-row:** Rotation angle, **Left to Right:** Patient 1 through 3.

be seen, the translation magnitude of the mandibular incisors for an applied load of 0.4Nchanges from 0.07 mm to 0.11 mm, 0.13 mm to 0.18 mm, and 0.24 mm to 0.51 mm, for patient 1 through 3, respectively. These values are similar to the results of the clinical study done by Jones et al. [53], where the obtained initial tooth movements ranged from 0.012 mm to 0.133 mm for maxillary incisors of ten patients under a constant load of 0.39 Nover one-minute cycles.

The translation magnitude and rotation angle of the teeth can be described as the square root functions of the applied load, i.e., $t_{j,k} = \alpha_{t_{j,k}}\sqrt{l} + \beta_{t_{j,k}}$ and $\theta_{j,k} = \alpha_{\theta_{j,k}}\sqrt{l} + \beta_{\theta_{j,k}}$, where $\alpha_{t_{j,k}}$ and $\alpha_{\theta_{j,k}}$ are the translation/rotation function coefficients for the k-th tooth of the j-th patient, and $\beta_{t_{j,k}}$ and $\beta_{\theta_{j,k}}$ are the corresponding function intercepts which are nearly zero. This nonlinear relation between the displacement and load is in line with the experimental findings of the clinical study of [29] and numerical results of the biomechanical model of [24]. However, the function coefficients vary across different patients' teeth, i.e., the values increase when moving from the molars to central incisors.

It can be deduced from Figure 2.5 that the estimated coefficients of the nonlinear functions vary across different patients for the same tooth types. This finding is due to the fact that the initial tooth movement can be influenced by different factors such as tooth anatomical variations and surrounding alveolar bone and PDL layer. Additionally, the root length of tooth and its surrounding alveolar bone can affect the initial tooth movement, center of rotation, and center of the resistance [120]. The same behavior applies for the crown height. In other words, a specific tooth with a longer crown (or a shorter root) would experience more displacements than the same tooth with a shorter crown (or a longer

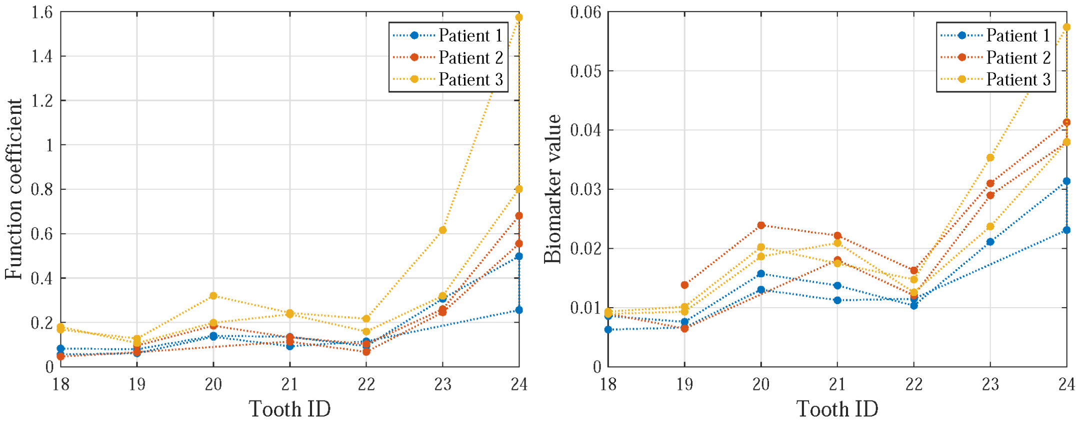

FIGURE 2.6: Teeth movement variations of the three patients. **Left:** The coefficients of the functions fitted to the translation-load data. **Right:** The proposed biomarker values estimated for each patient's teeth. The right teeth IDs are reflected using the corresponding left teeth IDs, which results in two curves per patient.

root). However, the exact relationship between the crown/root size and tooth displacement is missing. Our hypothesis is that the intra- and inter-patient variations in crown and root size can influence the teeth movements of different patients. Therefore, we propose the ratio of crown height to root volume as the biomarker causing tooth movement variations together with the applied load.

To investigate the abovementioned assumption, first, we analyze the estimated coefficients of the fit functions ($\alpha_{t_{j,k}}$ and $\alpha_{\theta_{j,k}}$) for each tooth type. We observe that the teeth on the right side of the mandible show the same movement patterns as the corresponding teeth on the left side, where the UNN of the left side teeth can be calculated by subtracting the UNN of the corresponding teeth on the right side from 49. This provides us with more data points for the fitting purpose. The estimated coefficients of the nonlinear translation-load functions of the different patients are shown per tooth ID in Figure 2.6. Note that the right teeth IDs are reflected in the same plot using the corresponding left teeth IDs.

Second, the crown heights of teeth are extracted from the intraoral scan of each patient. These measured values are then divided by the root volumes of the corresponding teeth, in which the root volumes are calculated using the associated bounding boxes of the PDL geometries. Figure 2.6 illustrates the estimated biomarker values for each patient's tooth. The obtained ratios needs to be considered as a patient's tooth biomarker in the tooth displacement models of translation and rotation. Therefore, we investigate the relationship between the coefficients of the displacement functions and the proposed biomarker values. Figure 2.7 shows the biomarker values versus coefficients of the teeth displacement functions (translation magnitude and rotation angle) for all patients' teeth. As it can be seen, the biomarker values and coefficients are in line with each other. For example, lower biomarker values and coefficients are associated with the molars while higher biomarker values and coefficients belongs to the incisors.

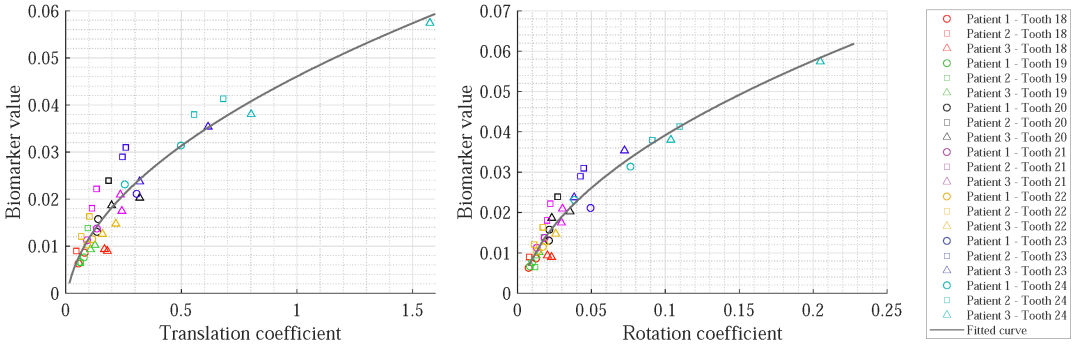

FIGURE 2.7: The biomarker values versus coefficients of the displacement functions (translation and rotation). In each case, the behavior of the data is explained by a square root function.

The relation between the biomarker values and coefficients of the teeth displacements can also be described by the square root functions, i.e., $b_t = \lambda_t\sqrt{\alpha_t} + \gamma_t$ and $b_\theta = \lambda_\theta\sqrt{\alpha_\theta}+\gamma_\theta$, where b_t and b_θ are the biomarker functions associated with the translation/rotation function coefficients α_t and α_θ, respectively. Hence, the tooth displacements (translation/rotation) will be seen as a nonlinear function of both load (l) and the proposed biomarker (b), wherein the displacement-load function coefficients are replaced with the biomarker values. In other words, to obtain a patient's tooth displacements $t_{j,k}$ and $\theta_{j,k}$ for an applied load, one only needs to obtain the function coefficients $\alpha_{t_{j,k}}$ and $\alpha_{\theta_{j,k}}$ based on the biomarker value of the specific tooth using the fits shown in Figure 2.7.

2.5 Summary and Conclusion

The main goal of this work was to introduce a computational analysis tool for investigating the influence of the teeth geometry of different patients on the resulting teeth movements. Three biomechanical models were generated for studying the tooth movement variations of three patients. Our study showed that a combination of two clinical biomarkers, i.e., crown height and root volume could affect the tooth displacement. Therefore, we proposed two nonlinear functions for predicting translation and rotation of different patients' teeth for any applied load magnitudes. Proposing such functions not only allows for generalizability of the model across different patients but also provides a way to avoid having multiple values for different teeth IDs. To the best of our knowledge, this is the first time a full dentition intra-patient and inter-patient tooth movement analyses have been considered. This study focused on modeling the movement of teeth under an uncontrolled tipping scenario applied to three patients. The work still can benefit from investigating different tooth movement types such as the crown tipping, root tipping, and pure translation applied to some more patients.

Chapter 3

Trajectory Analysis of the Center of Rotations of the Teeth

This chapter is based on our work presented in [42], focusing on analyzing the trajectories of the center of rotations for different patients' teeth movements. This work was done based on the three obtained FEMs from the first study to get a better insight into the movement patterns/trajectories of teeth using their centers of rotations. In addition, it addresses the common challenges related to multi-patient analysis (Section 1.3.6). We employed the registration methods to define loading conditions for different patients' teeth and analyze the simulation results under varying loading conditions, eliminating the geometrical variation by analyzing the simulation results in the same space.

Studying different types of tooth movements can help us to better understand the force systems used for tooth position correction in orthodontic treatments. This study considers a more realistic force system in tooth movement modeling across different patients and investigates the effect of the couple force direction on the position of the center of rotation (CRot). The finite-element (FE) models of human mandibles from three patients are used to investigate the position of the CRots for different patients' teeth in 3D space. The CRot is considered a single point in a 3D coordinate system and is obtained by choosing the closest point on the axis of rotation to the center of resistance (CRes). A force system, consisting of a constant load and a couple (pair of forces), is applied to each tooth, and the corresponding CRot trajectories are examined across different patients. To perform a consistent inter-patient analysis, different patients' teeth are registered to the corresponding reference teeth using an affine transformation. The selected directions and applied points of force on the reference teeth are then transformed into the registered teeth domains. The effect of the direction of the couple on the location of the CRot is also studied by rotating the couples about the three principal axes of a patient's premolar. Our results indicate that similar patterns can be obtained for the CRot positions of different patients and teeth if the same load conditions are used. Moreover, equally rotating the direction of the couple about the three principal axes results in different patterns for the CRot positions, especially in labiolingual direction.

The CRot trajectories follow similar patterns in the corresponding teeth, but any changes in the direction of the force and couple cause misalignment of the CRot trajectories, seen as rotations about the long axis of the tooth.

3.1 Introduction

Finite element (FE) modeling is a widely used computational method for the analysis of the reactions to real-world physical effects such as forces and biomechanical responses occurring during treatments in medicine and dentistry [103] that attempts to solve partial differential equations numerically, based on reconstructing the desired geometry and discretizing the domain into a finite mesh, with minimum need for clinical trials of patients [26]. One of the main goals in FE-based modeling of the tooth and its supporting complex, i.e., periodontal ligament and adjacent alveolar bone, is to improve tooth movement prediction performance in orthodontic treatments. Compared to clinical studies that aim, among other things, to assess the accuracy of digital planning in dentistry [60] or investigate anatomical characteristics for optimal occlusions [100] using different patient scans, computational modeling allows for more efficient plannings in orthodontic treatment for correcting dentofacial anomalies using more generic solutions.

Tooth movement modeling in an uncontrolled tipping scenario using a perpendicular loading system has been widely used for initial tooth movement simulations due to its simplicity [41]. However, in addition to the uncontrolled tipping movements, different tooth movements such as the pure translation, crown/root tipping, intrusion/extrusion, or a combination of them are typically required for tooth position correction in orthodontic treatments. Each of these movements can be described based on the position of the center of resistance (CRes) and center of rotation (CRot) with respect to the tooth geometry [77, 85]. For example, a pure translation, root tipping, and crown tipping can result in CRots located at infinity, crown, and root apex, respectively. The CRes of a tooth within its supporting complex can be seen as the center of the mass of a free rigid body [126]. To be more specific, the tooth CRes is a point at which applying any forces would always result in a pure translation of the tooth [85]. Although the location of the CRes has been investigated in the literature either experimentally in vivo [116, 117, 132], analytically [97, 125], or computationally using finite-element (FE) models [77, 87, 126], estimating the exact position of the CRes is challenging as it depends on the root shape, the anatomy and mechanical properties of the supporting complex [77,108], the direction of the tooth movement and force [67, 76, 77, 85, 106]. More specifically, since the CRes may not exist as a single point in 3D space [126] due to the asymmetric geometries, it is proposed to use a volume of CRes instead [87].

The CRot is another important concept in tooth movement analysis and is a point at which the movement of the tooth can be defined as pure rotation. Different approaches can be used for determining the position of the CRes and CRot. One simple approach for determining the tooth CRes is exerting a couple in different directions. A couple consists of a pair of forces with the same magnitude and parallel line of action, but in opposite directions where they are not collinear [118]. Therefore, utilizing only a couple results in a pure rotation in the tooth where the position of the CRot coincides with the position of the CRes.

The CRot position depends on the load system applied to the tooth. The loading system can result in some moments and forces in different directions, and due to its complexity in a 3D coordinate system, it can be decomposed into three planes of the tooth. Hence, tooth movement can be analyzed by decomposing each moment-to-force ratio ($M : F$) on each principal plane of a tooth, where each $M : F$ on a plane can be defined based on the force vectors located on the plane and moments perpendicular to the studied plane [105].

A classical theory on the relation between the applied load and the type of the tooth movement is *Burstone's formula* [21]. In this theory, the effect of the various moment-to-force ratios ($M : F$) is studied on the position of the CRot for a canine with a parabolic root, while the force is applied perpendicular to the long axis of the tooth at the bracket level. The study introduces the following formula

$$M : F = \frac{0.068 \times h^2}{D},$$

where h is the distance from the alveolar crest to apex, and D is the perpendicular distance between the CRes and CRot. Note that $M : F$ has a unit of millimeters where F corresponds to the magnitude of the applied force and M denotes the moment of the couple m_c exerted to the tooth in order to counteract the moment caused by the applied force m_f [118]. According to this theory, specific values of $M : F$ ratios always correspond to specific types of tooth movement. That is, the location of the CRot for a specific tooth is only dependent on the moment-to-force ratio of that tooth.

The classical theory has been widely studied by using FE models [24, 76, 105]. Cattaneo et al. [24] study the influence of $M : F$ on the same force magnitude and analyze the effect of applying various load magnitudes on a mandibular premolar and canine teeth with a constant $M : F$. The study reports that a constant $M : F$ with different force magnitudes can result in different types of tooth movements. However, this finding does not follow Burstone's formula, and this is due to considering a nonlinear material model for the PDL layer where the location of the CRot is dependent on both the $M : F$ and the magnitude of the applied load to the teeth.

Different studies have utilized different $M : F$ ratios for the pure translation of various teeth. For example, unlike the generally accepted $M : F$ of 10 and 12 for pure translation of the premolar and canine, Cattaneo et al. [24] suggest $M : F$ of 9 and 11, respectively, for a mandibular premolar and a canine. Also, it is recommended [67] to avoid using a universal $M : F$ and CRes due to the patient-specific geometries, reporting $M : F$ of approximately 8.8, 9.7, and 10.2, to simulate the pure translation of maxillary first premolar, lateral incisor, and canine.

Unlike the abovementioned studies that are limited to single-plane analysis, Savignano et al. [105] investigate the effect of the force system directions on the tooth movement of a maxillary first premolar by performing analysis on principal planes of the tooth. More specifically, the mesiodistal, buccolingual, and occlusal planes are used to study the location of the CRot using the projected axis of rotation on these planes for various $M : F$ and directions. This study suggests a nonlinear relation between the direction of the force system and the projected CRots. However, the mentioned study is limited to a single tooth analysis with a limited load magnitude range applied to the CRes due to using a linear elastic material model for the PDL layer. Although two patients are considered in a recent work [104], an inter-patient analysis is missing in general.

The existing studies do not represent the effect of geometrical variations on the $M : F$ ratios and the position of the CRot under the same analysis setup, boundary conditions, and loading system for different patients. To this end, in this work, we consider patient-specific full dentition computational models of three human mandibles to investigate the position of the CRots in different patients' teeth. For a comprehensive and consistent inter-patient analysis, we register different patients' teeth to a corresponding reference tooth of the first patient using an affine transformation and use this transformation to map the selected force directions and force application points on the reference teeth into the registered teeth domain. Moreover, we model the clinical forces with no specific limitation in the force magnitudes by using a hyperelastic material model for PDL tissue and investigate the position of the CRot in a 3D space to better represent the resulting rotation. Finally, we assess the influence of the couple directions on the positions of the CRots of a specific tooth and show that equally rotating the direction of the couple about the three principal axes results in different patterns for the CRot positions, especially in labiolingual direction. Modeling different types of tooth movements using a more realistic force system, i.e., tipping and couple forces applied to the tooth crown, and investigating the effect of these couple forces on the CRots can help us to better estimate the force systems needed to achieve the desired tooth movement.

3.2 Materials and methods

This section first reviews the details of the FE models used in this study including the geometry reconstruction, mesh generation, boundary conditions, contact definitions, and material models. Next, it focuses on describing an approach for setting up a consistent loading condition for different patients' teeth, both for intra- and inter-patient analysis. Finally, it briefly specifies how the CRot is computed and illustrated in 3D.

3.2.1 Geometry reconstruction

In this work, we consider three patient-specific and anatomically accurate FE models of the human mandible composed of mandibular teeth, corresponding PDLs, and bone. To have enough geometrical variations in the dataset, the

Table 3.1: Detail of the utilized scans.

Patient	Dimensions			Slice thickness (mm)	
ID	Scan size	ROI size	Resampled ROI size	Original	Resampled ROI
Patient 1	400 × 400 × 280	338 × 265 × 140	776 × 530 × 280	0.3	0.15
Patient 2	400 × 400 × 280	335 × 220 × 172	670 × 440 × 344	0.3	0.15
Patient 3	532 × 532 × 540	534 × 435 × 338	534 × 435 × 338	0.15	0.15

three patients' scans are chosen of various crown heights, root lengths, and teeth sizes. The scans are used from the 3Shape A/S private dataset collected from different clinics by orthodontists as a part of treatment. More specifically, the anonymized Cone-Beam Computed Tomography (CBCT) scans of patients stored in Digital Imaging and Communications in Medicine (DICOM) format used in this study contain no sensitive personal information including gender and age or details of the scanner device utilized for image acquisition.

The utilized patient scans labeled as *Patient 1*, *Patient 2*, and *Patient 3* have an isotropic voxel size of 0.3 mm, 0.3 mm, and 0.15 mm, respectively. For a consistent and detailed geometry reconstruction, a cropped region of interest (ROI) of every patient scan including full dentition and mandible is upsampled to an isotropic voxel size of 0.15 mm. Further details of the utilized scans can be found in Table 3.1. Note that the patient-specific geometries are reconstructed by importing DICOM files to 3DSlicer [37], resampling the ROIs, and segmenting the teeth and bone geometries in CBCT scans using a semi-automatic watershed algorithm.

The accuracy of the annotated scans is verified by a clinical expert and any required modifications are applied to the segmented regions accordingly. A general criterion for the verification is precise segmentation of roots, crowns, and bone cervical regions including the teeth sockets, and the miss-annotated regions indicated by the expert are revised until reaching the criterion. The segmented geometries are then exported as surface meshes in STL file format. Since the resolutions of the original scans are not high enough to properly represent the thin layer of the PDL, annotating the PDL layer using the available CBCT scans is not feasible. The width of the PDL layer is a tooth root dependent factor which can vary between 0.15 mm and 0.38 mm with an average suggested as 0.2 mm [63]. This average thickness is used in the literature [13, 63, 113] to generate the PDL geometries by uniformly extruding the teeth roots in Meshmixer [107]. Therefore, we first re-mesh the teeth and bone geometries using a uniform and adaptive mesh, respectively. Next, the obtained bone surface is offset by 0.2 mm in the reverse direction of the surface normals to create the required space for the PDL layers in between the teeth roots and the regenerated bone. Finally, the PDL geometries are produced by extruding the teeth roots, filling the generated gap in between the teeth and bone. It should be noted that the generated surface mesh for each PDL geometry includes a uniform mesh with two elements in the PDL thickness. The reconstructed geometries have been made publicly available and can be obtained from Electronic Research Data Archive at the University of Copenhagen under the OpenJaw Dataset (`https:`

TABLE 3.2: Summary of the materials and mesh properties.

Domain	Material model	Material properties		Mesh properties	
		Young's modulus (MPa)	Poisson's ratio (−)	Surface mesh Edge length (mm)	Volumetric mesh Number of elements †
Tooth	Rigid body	–	–	0.4	14±5 K
Bone	Isotropic elastic	1.5×10^3	0.3	Adaptive mesh (from 0.4 to 2)	3,261±329 K
		C_1 (MPa)	C_2 (MPa)		
PDL	Mooney-Rivlin *	0.011875	0	0.1	127±41 K

* $C_2 = 0$ reduces the Mooney-Rivlin material to uncoupled Neo-hookean. The values assigned for C_1 and C_2 correspond to the Young's modulus and Poisson's ratio of 0.0689 MPa and 0.45, respectively.
† The values are shown as the mean ± standard deviation of the number of elements across all cases.

//doi.org/10.17894/ucph.04e91c97-5c5d-45d7-afd3-c5e0b5953f58).

After preparing the surface meshes, high-quality tetrahedral meshes are generated by preserving the surface meshes using TetGen [115]. The mesh quality required for an FE analysis can vary depending on the application and utilized numerical methods [114]. In general, a regular tetrahedron has the highest mesh quality, and the main guideline is to avoid using low-quality tetrahedra with small or large dihedral angles, as they can affect the accuracy of the numerical methods [114]. Therefore, we use an upper limit constraint of 1.2 for the radius-edge ratio, as the ratio of the circumscribed sphere's radius and the shortest edge of the linear tetrahedral meshes. Additionally, the quality of the generated volumetric meshes are assessed using four different quality measurements, i.e., the volume-edge ratio [69, 78], radius-edge ratio [11], radius ratio [22, 40], and volume-area ratio [40]. The volumetric meshes are then imported into the FEBio software package [73], which is open-source software for nonlinear FE analysis in biomechanics, to set up a reproducible FE model for each patient. A summary of the utilized mesh properties is provided in Table 3.2.

A mesh convergence study is performed to obtain an optimal mesh size for the FE models [41] by iteratively increasing the number of elements per step with a factor of 2. We continue the process until the relative stress error does not exceed 4% of maximum von Mises stress. This study is concerned with smooth bone meshes where there are no sharp elements on the meshes. Therefore, the model does not experience extreme local stresses in a single node or element. However, in nonsmooth geometries with sharp edges, more robust methods can be applied to avoid any extreme local stresses as outliers [99, 136]. Also, note that using more elements in the PDL thickness would exponentially increase the total mesh size of the full jaw models and the required computational time. Besides, based on our experience, using smaller elements would result in extreme element distortion, causing problems in FE model convergence especially for higher load values. Similar behavior is also seen in [89] for hexahedral elements.

3.2.2 Material properties

We assume teeth as rigid bodies with six degrees of freedom to simplify the proposed model. Also, we assume the center of mass as the CRes for each tooth which can automatically be calculated using FEBio user-defined options [72]. Since the deformation of the bone tissue is negligible under the orthodontic forces used in this study, no distinction is made for the cortical and trabecular bone [98, 135], and isotropic elastic material model is used for the homogeneous bone geometry. Due to the importance of the PDL tissue in transferring loads from the tooth to the alveolar bone [25, 89], a Mooney-Rivlin Hyperelastic (MRH) material model is used to simulate its nonlinear behavior [98, 123]. Furthermore, for the simplicity of the model and following the literature [87, 89, 104, 105], the gingival tissue is discarded from our computational model due to its extremely low elasticity modulus compared to that of the other tissues, i.e., PDL, bone, and tooth.

3.2.3 Boundary condition and contact definition

A *rigid contact* is defined between rigid teeth and PDLs, and a tied *facet-on-facet* contact with an augmented Lagrangian method is used in PDL-bone interfaces to model adhesion in these two interfaces, as their corresponding surfaces do not have any sliding or separation. Other parameters, such as boundary conditions, edge length of the elements, and material properties are chosen as mentioned in Table 3.2. Also, a Dirichlet boundary condition is applied to all nodes at the bottom surface of the bone in all directions to fix the jaw model.

3.2.4 Loading conditions for different scenarios

Three different scenarios with varying loading conditions are studied in this work, as shown in Fig 3.1. In the first scenario, various $M : F$ values are examined for different patients' teeth using a consistent loading system. In the second scenario, the influence of the direction of the couple is studied on a specific tooth. As our third scenario, the loading conditions are applied to the CRes, which makes us able to compare our simulation results with those obtained by Savignano et al. [104, 105].

Scenario 1: Consistent loading conditions for intra- and inter-patient analysis

In the first scenario, to perform a systematic intra- and inter-patient analysis and to avoid potential errors caused by the selection of the load points and force directions, different teeth of each patient are registered to a reference tooth of the same type. To do so, the left teeth of one of the patients (here, *Patient 1*), with the *Universal Numbering (UNN)* ID of 18 through 24, are selected as the reference teeth. Next, the mandibular teeth of all other patients on both sides, as well as the right mandibular teeth of *Patient 1*, are all registered to the corresponding reference teeth. This allows us to analyze more tooth models of the same type and study the position of the CRots for different teeth of different patients.

Before any tooth registration, the jaw models of different patients are aligned based on rigid body transformation using the Iterative Closest Point (ICP)

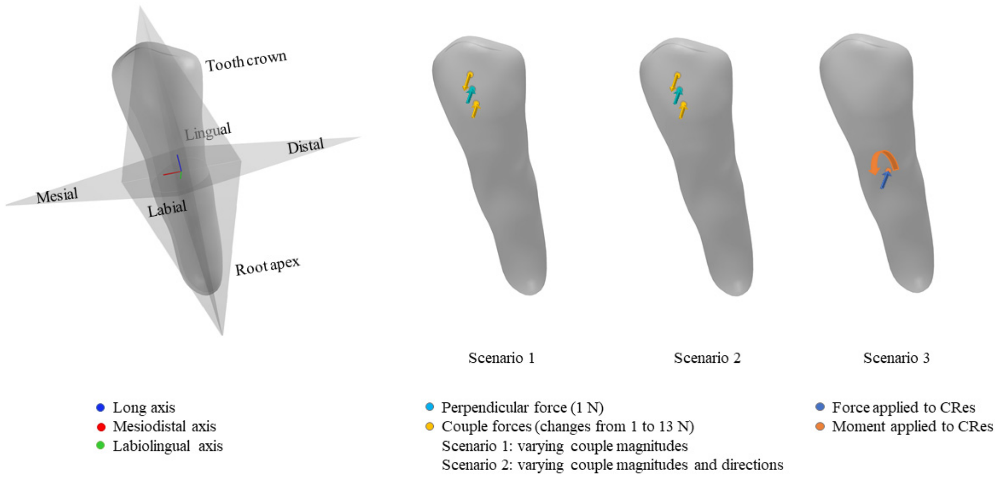

FIGURE 3.1: **The studied scenarios.** An illustration of the principal axes and planes of premolar and loading conditions used in three different scenarios.

algorithm [18, 28]. Moreover, the Coherent Point Drift (CPD) algorithm [82] is used for teeth alignment based on an affine transformation of the corresponding left/right teeth of different patients. The registration processes are all performed in MATLAB by considering vertices of each surface mesh as a set of a point cloud. Compared to the ICP algorithm, CPD is computationally intensive, yet it is more robust to noise and outliers. Therefore, we prefer using CPD for teeth registration which includes fewer data points than jaw models. It should also be noted that all teeth on the right side of the mandibles, with the UNN of 25 through 31, are horizontally flipped with respect to the sagittal plane of each patient's jaw before applying the affine transformation using the CPD method. This is to ensure that the labial surfaces of the registered teeth are properly aligned to the labial surfaces of the reference teeth.

After registering all patients' teeth to the reference teeth, three points, at which the force and couple are applied, are selected on each reference tooth. One point is set for tipping force, and two points are used for the couple. The center of the middle third of the crown is set for the tipping load, and two points are selected with a 0.5 mm distance below and top of the tipping load point for the labiolingual and linguolabial couple, respectively. The normal vector of the reference mesh at the tipping point is used for both directions of the force and the couple. More specifically, the direction of the computed normal vector is used for the linguolabial couple force on top, and the opposite direction is used for both the tipping force and the labiolingual couple. *Nodal loads* are utilized to simulate the mentioned forces in the FEBio framework.

The corresponding three load points are then obtained based on finding the closest mesh points in each registered tooth mesh. These points, as well as the direction of the forces, are finally transformed back to the original coordinates of each patient's tooth. This would ensure unbiased loading conditions for the intra- and inter-patient analysis. Fig 3.2 displays how registration is employed for defining consistent loading conditions and calculating the CRots using FE models of mandibles from three patients.

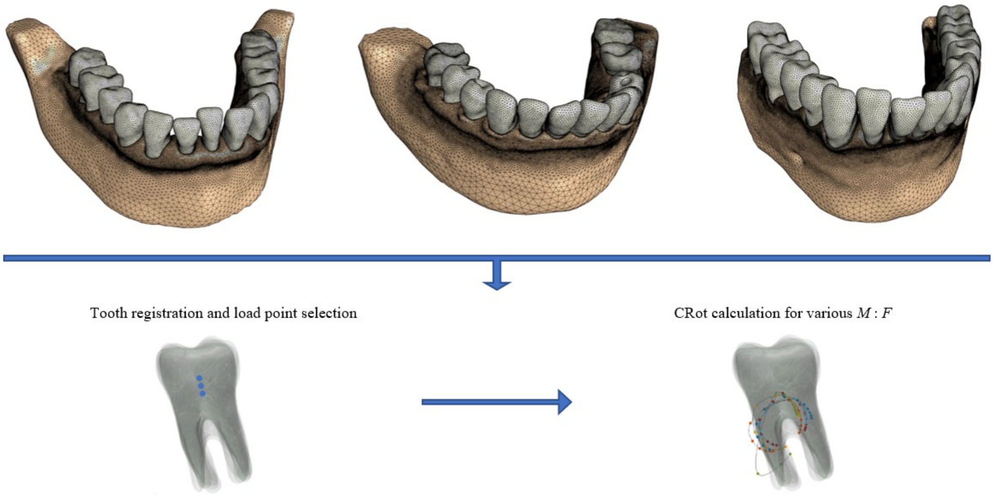

FIGURE 3.2: **Tooth registration and CRot calculations pipeline.** An illustration of the utilized method for calculating the CRots using finite-element models of mandibles from three patients under consistent loading conditions.

Multi-patient analyses are conducted on different teeth to evaluate the effect of the couple's magnitude on counteracting the moment produced by the tipping load. In this scenario, the simulations are performed with a constant tipping force of 1 N and varying couple magnitudes of 1 N to 13 N with 1 N intervals. Note that the applied force points are fixed for both the couple and the tipping load. Hence, increasing the load magnitude of the couple will increase the resulting moment on the tooth according to the force-moment relation $M = F \times d$, where d is the distance between the applied force point and the CRes of the tooth. Finally, the corresponding CRots are computed for each patient's teeth and the same transformations are used to align different teeth of the same type and their CRots.

Scenario 2: The effect of the couple's direction on the position of the center of rotation

In the second scenario, as an example, the left premolar of *Patient 1* is selected to study the influence of the couple's direction on the position of the CRot. The three load points, the initial load directions, and the direction and magnitude of the tipping load remain the same as in the first scenario. The couple's directions are rotated about the mesiodistal, the labiolingual, and the long axis of the tooth with different degrees varying from 0 to 90 degrees with 10-degree increments. To investigate the trajectories of the CRots in 3D space, for each direction, we conduct experiments with incremental couple magnitudes of 1 N to 13 N with intervals of 0.0625 N. This generates a dense representation of the CRot trajectories in 3D space.

Scenario 3: The effect of the force's direction on tooth movement

As our third scenario, we investigate the influence of the force's direction on tooth movement and the position of the CRot, and compare our results with those obtained by Savignano et al. [104, 105]. More specifically, the effect of the force direction is investigated at the CRes of the left premolar of *Patient 1*, while the load direction changes in one of the three principal planes of the tooth, and a perpendicular moment is applied to the studied plane. Additionally, instead of using the couple for generating the moments on the tooth crown, we follow the same scenarios of the aforementioned study and use a load and a moment applied to the CRes, using *prescribed rigid force constraint* and *prescribed rigid torque constraint*, respectively, in FEBio framework. The direction of the load changes with 10-degree increments, and the $M : F$ changes from -12 to 12 with 2 mm intervals.

3.2.5 Computing the center of rotation

The axis of rotation is computed for each tooth by considering displacement vectors of two nodes arbitrarily selected on the tooth crown. To this end, the intersection line of the perpendicular bisector planes of the displacement vectors is obtained. Any point on the intersection axis can be assumed as the CRot in 3D space, and to find a unique CRot in 3D, the point with the closest distance to the CRes of the tooth is selected on the rotation axis. This allows for representing the axis of the rotation in 3D as a single point and for better analyzing the influence of the couple directions on the location of the CRot with respect to the CRes.

3.3 Results

We conduct our experiments on a 3.4 GHz processor with 64 GB of RAM, which takes about an hour to solve the FE model. First, we focus on the analysis of the position of the CRots for various couple magnitudes of all patients' teeth. Second, the influence of the couple directions is studied on the position of the computed CRot of the left premolar of *Patient 1*. Third, we assess the influence of the force direction with fixed moment direction on the position of the CRots. In all the experiments, the position of the closest point to the CRes on the rotation axis is considered as a single point CRot in 3D coordinate system for each tooth. Fig 3.3 illustrates the position of the CRots of each tooth for varying magnitudes of the couple from 1 N to 13 N with 1 N increments. As can be seen, the CRots follow parabolic shapes with varying slopes from one tooth type to another.

To better represent the inter-patient results, the utilized patients' teeth and their CRots were registered to the corresponding reference teeth. Fig 3.4 shows the registered teeth geometries, with transparent shapes located on either left or right side of the mandible, and their CRots for the utilized patients. Note that the third molars were missing in all cases. Hence, the different teeth types

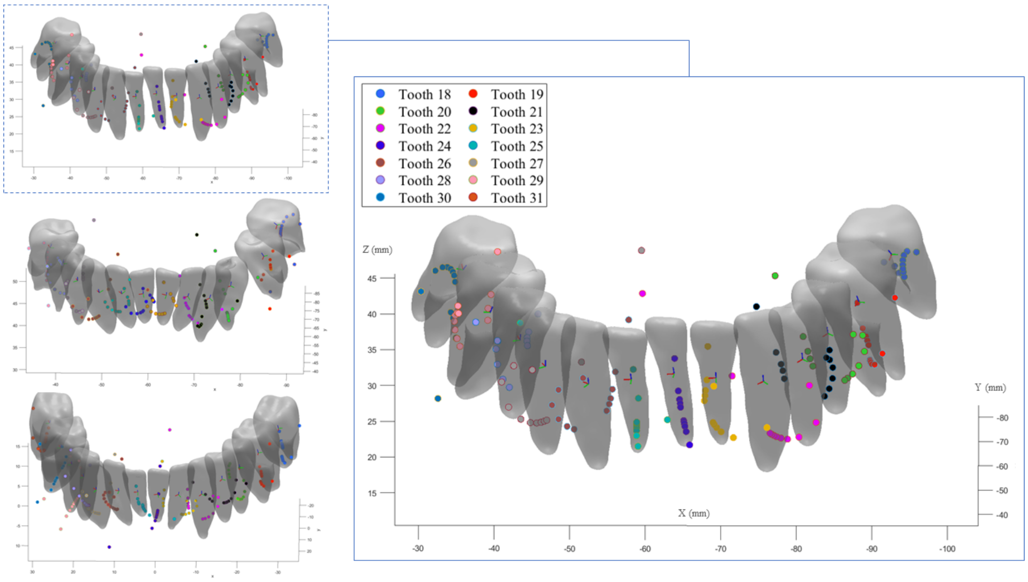

FIGURE 3.3: **Calculated CRots.** Calculated CRots for different couple magnitudes changing from 1 N to 13 N with 1 N intervals shown in 3D space for all teeth with transparent teeth geometries, **Left:** Results of the three different patients. **Right:** A closeup view of the results for *Patient 1*.

are represented from the second molars to the central incisors. As can be noted, the CRot trajectories experience similar patterns in each tooth type.

In practice, more CRot data points are required for a better illustration of the trajectory curves in 3D space. This in turn requires sampling more data points by using smaller intervals of the couple magnitudes. As mentioned before, we conduct this experiment using the left premolar of *Patient 1* and investigate the CRot trajectories influenced by the couple's directions based on smaller increments in the magnitude of the couple. More specifically, the directions of the couple are rotated about the mesiodistal, labiolingual, and long axes of the tooth from 0 to 90 degrees with 10-degree increments. Fig 3.5 illustrates the CRot trajectories for different directions of the couple rotated about the principal axes of the tooth.

As our third analysis, we examine the effect of the force direction on the position of the CRot by considering three principal planes of the tooth. We use the same scenarios followed by Savignano et al. [105], where the force and moment are applied to the CRes with a force of 1N magnitude. Fig 3.6, shows the effect of the load's direction on the position of the CRot, where the rotation range of the direction of the force system can vary from one axis of the tooth to another with 10-degree increments. As it can be seen in both subfigures, the distance between the CRots of the same direction changes nonlinearly with linear increments of the $M : F$. The nonlinear variation increases when the force direction is rotated from the mesiodistal or labiolingual axis direction towards the long axis direction. Additionally, the distance of the CRots associated with the same $M : F$ ratios changes nonlinearly for linear increments of the rotation

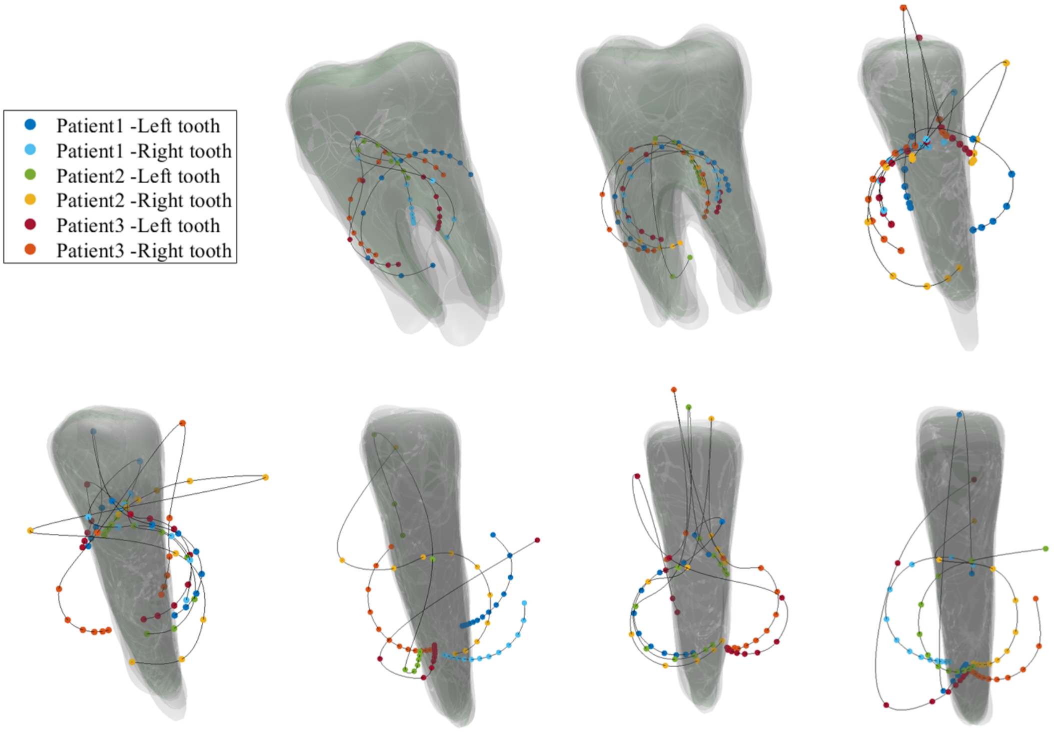

FIGURE 3.4: **CRots trajectories of registered teeth in scenario 1.** Trajectories of the obtained CRots for the different patients' teeth registered to the reference teeth of the same types and shown as transparent teeth. **Top-row:** The second molars, the first molars, the second premolars. **Bottom-row:** The first premolars, the canines, the lateral incisors, and the central incisors. A consistent loading condition is applied to all teeth of the same types, and the magnitude of the couple changes from 1N to 13N. Note that a few extreme outliers are discarded for a better illustration purpose.

degree in 3D space. This pattern is also shown by Savignano et al. [105] on 2D planes.

3.4 Discussion

3.4.1 Scenario 1

As illustrated in Fig 3.4, the computed CRots for different patients follow similar trajectories for the teeth of the same types. It can also be seen that linear increments in the magnitude of the couples nonlinearly increases the distance between the neighboring CRots of each tooth. The same behavior was reported by Savignano et al. [104, 105]. Moreover, the CRot trajectories begin from the CRes of the tooth, and by increasing the $M : F$, the trajectories move towards the crowns of the teeth, and then, they change their directions to the back of the teeth. A schematic curve of the aforementioned path can be seen in part A of Fig 3.5.

The turning points can be found as outlying points on the top of each tooth with the highest distance from their neighboring CRots. These points are associated

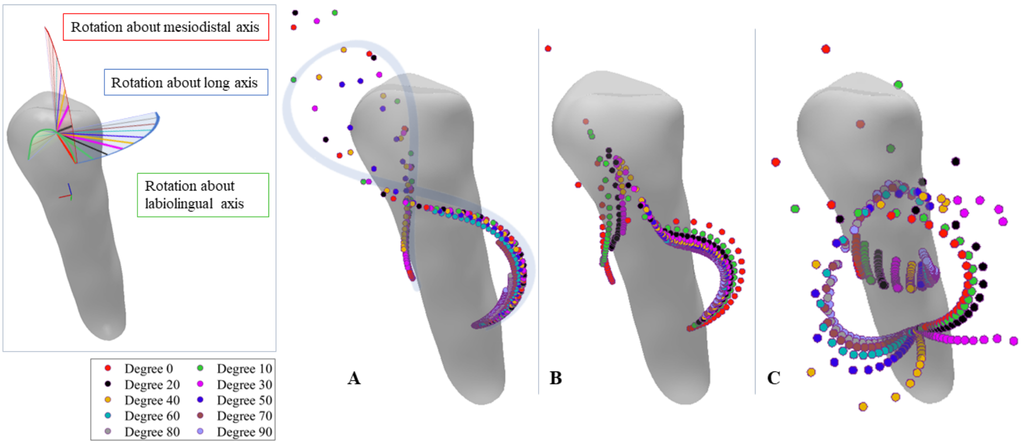

FIGURE 3.5: **Effects of the couple's directions on the CRots trajectories in scenario 2.** Directions of the couple rotated about the tooth principal axes with various angles and the corresponding CRots for different couple magnitudes. **Left:** An illustration of how the couple forces are rotated about mesiodistal, long axis, and labiolingual of the tooth. **Right(A to C):** The corresponding CRots for the rotated couple about mesiodistal, long axis, and labiolingual of the left premolar of *Patient 1*, respectively. Note that the initial direction of the couple and tipping load are set based on the surface normal direction.

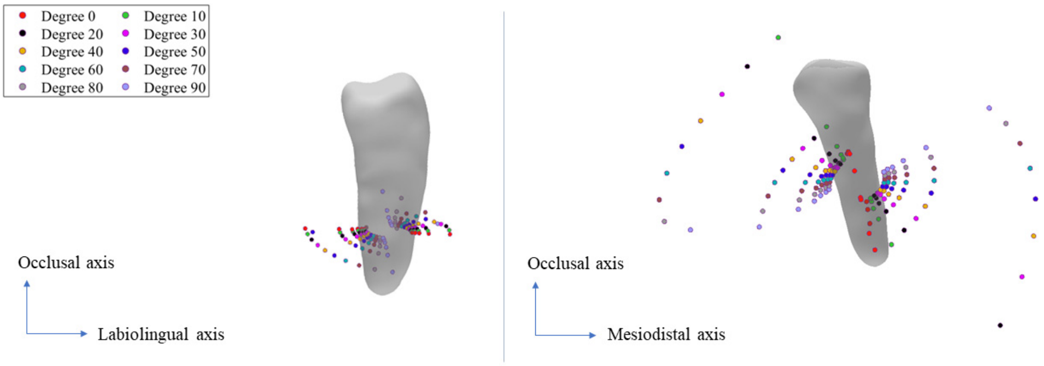

FIGURE 3.6: **The influence of the force direction on the position of the CRots in scenario 3.** The force and moments are applied directly to the CRes of the left premolar of *Patient 1*. **Left:** The CRots of the forces rotating from long axis towards the labiolingual direction of the tooth. **Right:** The CRots of the forces rotating from the mesiodistal axis towards the long axis of the tooth. Note that each color corresponds to a different force direction, the $M:F$ changes from $-12\,\mathrm{N}$ to $12\,\mathrm{N}$, and the distance between the CRots of the same color changes nonlinearly while the $M:F$ values increment linearly.

with specific $M:F$ values where the direction of the tooth movement changes in the opposite direction. In other words, in the turning point, the generated moment by the couple counteracts the generated moment caused by the tipping load. In addition, it can be observed that, in some cases, the CRot trajectories are not well aligned, i.e., they seem to be rotated about the long axis of the tooth. This could be due to the registration errors in matching the teeth models of different patients to each other, most likely caused by the size and high geometry variations of teeth.

3.4.2 Scenario 2

The investigation of the effects of the direction of the loading conditions on the CRot trajectories in Fig 3.5 reveals that although rotating the couples about each axis results in similar CRot trajectories for different rotation angles, equally rotating the direction of the couple about the three principal axes results in different patterns for the CRot positions, especially in labiolingual direction. Besides, by increasing the magnitude of the couples in a specific direction, the distances between two neighboring CRots changes nonlinearly which is in line with the results of the state-of-the-art [104, 105], indicating that changing the $M : F$ nonlinearly affects the position of the CRots.

As it can be observed in Fig 3.5, the CRot trajectories almost follow the same ∞-shaped curve by the rotation of the couple direction about the mesiodistal and long axes of the tooth with different angles (subfigure A and B). However, the sequence of the CRot points stops earlier when increasing the rotation angle. The situation in rotating the couple's direction about the labiolingual axis of the tooth looks a bit different. That is to say, the CRot trajectories follow different ∞-shaped curves which are seemed to be rotated about the long axis.

Considering the obtained results in Fig 3.4 and subfigure C of Fig 3.5, one can deduce that any changes in the direction of force and couple can result in the misalignment of the CRot trajectories, and specifically, rotation of the CRots trajectories about the long axis of the tooth. In fact, the latter case shows how such systematic changes can affect the trajectory of the CRots, from which we can infer the reason for the misalignments that occurred in the former case. This behavior is somehow seen in a related work [105] where the CRot points scatter in the mesiodistal-long axes plane seems more incoherent than the other cases.

In this study, the direction of the load and couples are determined based on the normal of the tooth surface at the underlying region. As a result, the normal direction is not necessarily parallel to the labiolingual direction of the tooth. Therefore, in contrast to the literature where the force system is simplified in 2D planes by assuming force and couple directions parallel to the labiolingual direction, we investigate a more realistic clinical force system and study the influence of the couple's direction in the tooth movement.

3.4.3 Scenario 3

This work benefits from using more realistic material models and scenarios, such as applying the forces on the tooth crown, for better modeling of the forces in clinical environments. A hyperelastic material model is used here to model the nonlinear behavior of the PDL tissue under orthodontic forces which allows us to model different scenarios without any prior assumptions for the range of the applied load. Furthermore, we propose using 3D space for representing the position of the CRot for the exerted force and moment to help with better analysis and understanding of the results in real-world applications. In contrast, Savignano et al. [104, 105] have represented the results in 2D planes and applied the loads and moments on the CRes, which is difficult to precisely be determined for different teeth. Besides, they have utilized a linear material model to the PDL tissue which confines the range of the applied load [56].

3.4.4 Future directions

Although an accurate geometry of the PDL can be obtained in vitro using micro-computed tomographies, these methods are known to be highly invasive and can only be applied to dead specimens. In contrast, reconstructing the PDL layer using CBCT scans obtained in vivo is a challenging process [46] due to the small width of the PDL layer compared to the commonly-used voxel size of the scans [34, 103]. Therefore, for a consistent analysis of different patients and following the literature, the PDL layers of this study are generated by extruding the teeth roots with a uniform thickness of 0.2 mm. Still, further investigation on the PDL is required to study, for example, the effect of nonuniform PDL geometry on the position of the computed CRots since different factors such as the patient's age and the presence of periodontal disease can influence the shape and thickness of the PDL geometry [63], and consequently, the local stress maxima and tooth displacements [46]. In addition, the same material parameters are used in this study for the teeth, PDLs, and bones of different patients. It should however be noted that the initial and long-term teeth movements can vary from an individual to another based on differences in material properties, the density of the surrounding bone, and the rate of the bone remodeling process, apart from the geometrical differences.

In addition to an accurate geometry reconstruction, utilizing appropriate material models and parameters is important for accurately describing the mechanical behavior of the PDL. Although experimental studies investigating the biomechanical behavior of the PDL in vitro [101] and vivo [57, 132, 133] have indicated an anisotropic nonlinear viscoelastic behavior of the fibrous PDL [98], computational studies mostly consider simpler material models such as linear elastic, bilinear, and piecewise linear [25] models. The linear assumption confines the range of the applied load [56], preventing the simulation of realistic load systems in clinical environments. More complex material models such as hyperplastic and viscoelastic have been used in the literature [84, 98], and few studies [89] have considered collagen fibers in the PDL layer to simulate an anisotropic behavior of the PDL layer, allowing it to absorb more energy in compression than in tension and shear [38, 59]. However, more investigations are required to see the effectiveness of such complex material models applied to tooth movement modeling using full dentition data in terms of computational complexity and accuracy.

3.5 Conclusion

In this work, three patient-specific computational models of human mandibles, composed of full dentition, PDL layers, and jawbone, were utilized to assess the position of the CRots in different patients' teeth against varying $M : F$ ratios. The patients' teeth were aligned for a consistent inter-patient analysis and FE simulations were performed under identical scenarios and boundary conditions for different teeth of each patient to obtain the CRots.

This work benefitted from using more realistic material models and scenarios for better modeling of the forces in clinical environments. A hyperelastic material model was used for the PDL tissue under orthodontic forces which allows for modeling different scenarios without any force constraints. The 3D space was used for representing the positions of the CRots for the exerted force and moment for better analysis and understanding of the results in real-world applications.

The influence of the couple's magnitudes and directions on the positions of the CRots of the patients' teeth were examined. The results show that the CRot trajectories could follow similar patterns in the corresponding teeth, but any changes in the direction of the force and couple could cause misalignments of the CRot trajectories that could be seen as rotations about the long axis of the tooth.

This work considered a more realistic force system in multi-patient tooth movement modeling by studying the CRot positions. The measured CRot position in relation to the tooth geometry can be used to infer the type of tooth movement, e.g., pure translation, uncontrolled tipping, and crown or root tipping. This, in turn, can be used in treatment planning software to assist clinicians to identify optimal forces required for achieving a desired patient-specific tooth movement.

Chapter 4

Open-Full-Jaw: Open Dataset and Model Generation Pipeline

This chapter is based on our work presented in [43], focusing on developing an open-access dataset of human jaws and a framework that automates model generation processes. It particularly benefited from our collaboration with the researchers from New York University and clinical experts from the University of Bordeaux. This work addresses most of the critical problems for developing many FEMs of human jaws. These challenges involve the lack of clinically-validated and publicly available research data and reproducibility (Section 1.3.4), geometry discretization in the contacting surfaces (Section 1.3.3), and parameter tweaking for contact modeling (Section 1.3.5).

State-of-the-art finite element studies on human jaws are mostly limited to the geometry of a single patient. In general, developing accurate patient-specific computational models of the human jaw acquired from cone-beam computed tomography (CBCT) scans is labor-intensive and non-trivial, which involves time-consuming human-in-the-loop procedures, such as segmentation, geometry reconstruction, and re-meshing tasks. Therefore, with the current practice, researchers need to spend considerable time and effort to produce finite element models (FEMs) to get to the point where they can use the models to answer clinically-interesting questions. Besides, any manual task involved in the process makes it difficult for the researchers to reproduce identical models generated in the literature. Hence, a quantitative comparison is not attainable due to the lack of surface/volumetric meshes and FEMs.

We share an open-access repository composed of 17 patient-specific computational models of human jaws and the utilized pipeline for generating them for reproducibility of our work. The used pipeline minimizes the required time for processing and any potential biases in the model generation process caused by human intervention. It gets the segmented geometries with irregular and dense surface meshes and provides reduced, adaptive, watertight, and conformal surface/volumetric meshes, which can directly be used in finite element

(FE) analysis. We have quantified the variability of our 17 models and assessed the accuracy of the developed models from three different aspects; (1) the maximum deviations from the input meshes using the Hausdorff distance as an error measurement, (2) the quality of the developed volumetric meshes, and (3) the stability of the FE models under two different scenarios of tipping and biting. The obtained results indicate that the developed computational models are precise, and they consist of quality meshes suitable for various FE scenarios. We believe the provided dataset of models including a high geometrical variation obtained from 17 different models will pave the way for population studies focusing on the biomechanical behavior of human jaws.

4.1 Introduction

Finite element modeling (FEM) is a numerical approach for predicting responses of different tissues under physical loads, which can be difficult or impossible to measure directly in vivo [10]. It is a widely used tool as a pre-operative protocol in different medical applications such as orthopedic surgery, orthodontic treatments, and cardiovascular surgeries [16]. More specifically, in the orthodontic and dental fields of studies, FEM is utilized to predict teeth movements, stress/strain distribution in different tissues (e.g., periodontal ligament, gingiva, and alveolar bone) or orthodontic appliances [23]. Except for a few recent studies [41,42,104], almost all of the previous studies in the field are limited to single-patient analysis [16,19,32,90,113,128], in which the results might not be generalized to a larger population with high geometrical variations in the teeth, periodontal ligament (PDL), and bone anatomies [41,104].

The main reason for using a single model in the literature is that developing accurate computational models of the human jaw is challenging and involves time-consuming and labor-intensive processes such as segmentation, geometry reconstruction, geometry processing, re-meshing, and mesh simplification tasks. For instance, generating a complex and highly detailed finite element (FE) model of the entire human jaw can take up to several months per scan [128]. Therefore, developing several patient-specific FE models may not be feasible for many researchers. In addition, currently, there are no publicly available datasets of full dentition human jaw to be used by researchers, except for two studies [6,128] with a limited number of studied subjects.

In other words, in almost all of the studies focusing on full dentition or single/multiple tooth analysis [16, 16, 19, 32, 61, 86, 90, 102, 104, 113], the utilized geometries, volumetric meshes, and FE models have not been made publicly available, which makes it difficult to reproduce and compare the results. Table 4.1 presents an overview of the related studies in the literature by providing details on the studied cohort, discretization type, and availability of the models.

As one of the few studies with public data, the OpenMandible [128] provides detailed geometries of one mandible structure and all teeth obtained from a dried male skull. The study scans the mandible in two different steps to provide detailed teeth structures, i.e., pulp and enamel. First, the mandible was scanned using a CBCT scanner with a voxel size of 0.133 mm. Second, all mandibular teeth were removed from the bone before being scanned by the micro-computed tomography (micro-CT or μCT). Micro-CTs are high-resolution CT scans that are normally acquired from dead specimens or cadavers due to high x-ray exposures. However, the detailed geometries obtained from a single mandible cannot cover geometrical variations across different patients in the population.

The recently introduced OpenJaw Dataset [6] provides open-access reconstructed geometries of three patients' mandibles acquired from CBCT scans. Each patient's data includes surface meshes of the reconstructed mandible, teeth, and PDL geometries. In the geometry reconstruction step, the utilized scans in the study (one with 0.15 mm and two with 0.3 mm voxel sizes) were upsampled to the same resolution of 0.15 mm [42]. Although this study provides more public samples, generalizability to the population remains a problem. Moreover, both of the abovementioned studies include manual tasks in different geometry-processing or meshing tools making it difficult for other researchers to reproduce their meshes using the unprocessed reconstructed meshes.

Our main contributions in the Open-Full-Jaw study can be summarized as,

1. We provide an open-access dataset of different patient-specific models of the human jaw, including the maxilla, mandible, full dentition, and the PDL geometries obtained from CBCT scans of 17 patients. It is the largest publicly available dataset with validated segmented geometries and quality volumetric meshes that can directly be used in FEM studies. Furthermore, to the best of our knowledge, it is the first repository containing the maxillary jaws of different patients.

2. We introduce a repository called "Open-Full-Jaw" and containing (1) clinically validated segmented geometries and the resulting dense irregular surface meshes; (2) the quality and adaptive volumetric/surface meshes to be used in FE simulations; (3) the automatically generated FEM files for tipping and biting scenarios used for the FE analysis of this work; (4) the principal axes of every patient's tooth providing great information for the users to automatically set up different loading conditions.

3. For reproducibility, we share our pipeline developed based on open-source meshing tools [48, 52] to generate the models of this study. This python-based library automates the FE model generation process, including geometry processing and re-meshing tasks with minimal human intervention, by setting a few required parameters.

4. This pipeline allows other researchers in the field to generate quality volumetric meshes and FE models directly from dense and uncleaned meshes with minimal human intervention. This will help other researchers to easily extend their datasets without spending much time and effort on manually cleaning up the meshes and non-trivially producing conformal meshes.

5. Our pipeline ensures conformal meshes in the contacting interfaces without any undesired gaps or penetrations and provides adaptive meshes

that are vital for reducing the total number of elements while using finer meshes in specific regions, e.g., teeth sockets, alveolar crest, and alveolar process.

All in all, we believe the Open-Full-Jaw dataset can be used for various intra- and inter-patient analyses [41, 104] such as intact tooth movement modeling, bite force estimation, restorative procedures modeling including cavity fillings and dental implants, just to name a few. Besides, it can greatly impact the reproducibility of future studies. For the reproducibility of this study, we use open-source meshing tools. Still, the reconstructed geometries provided in our dataset can be imported into any desired open-source or commercial meshing tools or FE frameworks to re-mesh and generate computational models.

4.2 Important traits required for a successful FEM

Developing a patient-specific FE model begins with segmenting/annotating the desired regions of the medical scan obtained from the patients. Next, the segmented regions are reconstructed as surface meshes generally composed of irregular dense meshes with no guarantees of manifoldness, watertightness, or absence of self-intersection, which are crucial for developing stable and accurate computational models. Hence, one needs to generate quality meshes from the exported dense and irregular meshes that are not necessarily guaranteed to have the mentioned criteria.

Moreover, different preprocessing steps such as geometry processing, mesh reduction, and re-meshing are essential for developing FE models from image-based reconstructed geometries. When modeling geometries with shared contacting interfaces, each of the mentioned processes can produce errors on the contacting surfaces and result in undesired gaps/penetrations between them. In the cases where two adjacent segments are watertight, it is still challenging to discretize the segmented domains such that they agree on the same discretization on the shared contacting interfaces. Therefore, the focus of this section is on essential aspects needed to be considered for the discretization of the computational domains with shared contacting interfaces; we also discuss potential options for developing a proper FE model of the human jaw.

4.2.1 Congruent contacting interfaces

The discretization of the computational domain is an essential step for developing computational models considering the biomechanical behavior of tissues having sliding or bilateral contact with other domains/tissues. It mainly affects the numerical stability of the computational models when soft structures, e.g., PDL, contact hard tissues like bone or teeth. Besides, a coarse or poor-quality discretization can itself cause a locking effect and influence the accuracy of the stress/strain concentrations compared to that of the values measured in vivo.

TABLE 4.1: Related studies in the literature and their details on the data availability and mesh conformity. The few studies with public models are listed below the dashed line. Note that there are empty cells in some studies, as it was difficult to evaluate the meshes.

Study/Dataset	Cohort Info		Scan Info	Geometry and Discretization Info			Interface info		Availability		
	#Patient	#Jaws	Scan Modality	Tooth Type	PDL Type	Bone Type	Interface Congruency	Mesh Conformity	Surface Meshes	Volumetric Meshes	FE model file
Seo et al. (2021) [113]	1	Half-arch	CBCT	H, Uniform	H, Uniform	CC, Uniform	CG	CM	No	No	No
Ding et al. (2014) [32]	1	1 Mandible	CBCT + MRI	EDP, Adaptive	H, Uniform	CC, Semi-Adaptive			No	No	No
Savignano et al. (2020) [104]	2	4 Jaws	CBCT	H, Uniform	H, Uniform	H, Uniform	CG	Non-CM	No	No	No
Ortun et al. (2020) [90]	1	2 Jaws	CBCT + μCT	EDP, Uniform	H, Uniform	CC, Uniform	CG	Non-CM	No	No	No
Benaissa et al. (2020) [16]	1	Single Tooth	CT	H, Adaptive	H, Uniform	CC, Adaptive		Non-CM	No	No	No
Kawamura et al. (2019) [54]	DM	1 Mandible	N/A	H, Uniform	H, Uniform	N/A	CG †	CM	No	No	No
Kawamura et al. (2022) [55]	DM	1 Maxilla	N/A	H, Uniform	H, Uniform	N/A	CG †	CM	No	No	No
Oenning et al. (2018) [86]	1	Half-arch	CBCT	EDP, Uniform	H, Uniform	CC	Non-CG		No	No	No
Sarrafpour et al. (2013) [102]	1*	1 Mandible	CBCT	EDP, Uniform	H, Uniform	CC, Adaptive	Non-CG †	Non-CM	No	No	No
Lee et al. (2018) [61]	1	2 jaws	CBCT	EDP	H	CC, Uniform	CG	Non-CM	No	No	No
Boryor et al. (2009) [19]	1*	Single Tooth	μCT	EDP, Adaptive	H, Uniform	CC, Adaptive	CG	Non-CM	Yes	Yes	No
OpenMandible (2021) [128]	1*	1 Mandible	CBCT + μCT	EDP	H, Uniform	O, Adaptive	CG	Non-CM	Yes	Yes	Yes
OpenJaw (2021) [6, 42]	3	3 Mandibles	CBCT	H, Uniform	H, Uniform	H, Adaptive	Non-CG	Non-CM	Yes	No	No
Open-Full-Jaw (our study)	17 *	29 Jaws *	CBCT	H, Adaptive	H, Uniform	H, Adaptive	CG	CM	Yes	Yes	Yes

N/A: Not Applicable; **DM**: Dental Model; **H**: Homogeneous; **EDP**: Enamel, Dentine, and Pulp; **CC**: Cortical and Cancellous bone; **O**: Orthotropic bone, further details can be found in [128]; **CG**: Congruent interface (no gap/penetration in the contacting interfaces); **Non-CG**: Non-congruent interface; **CM**: Conformal Mesh; **Non-CM**: Non-Cnformal Mesh.
$\star$ Obtained from cadaver or dried skull. * See Table 4.2 for further details., † Non-smooth top surface of PDL, see [54, 55, 102] for illustrations.

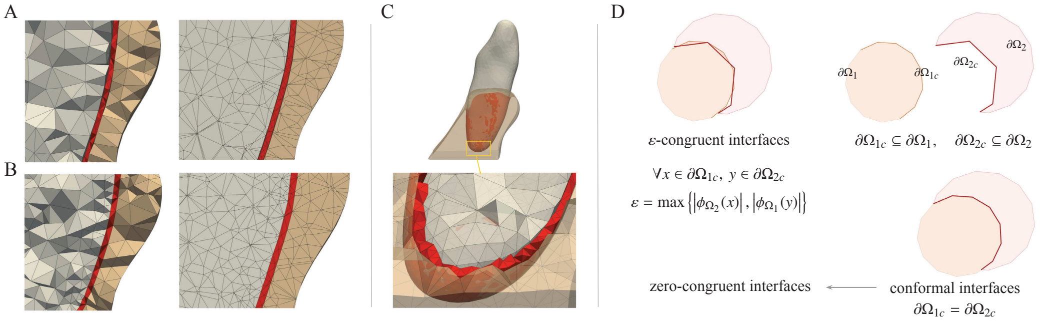

FIGURE 4.1: A visualized comparison between the ε-congruent and conformal meshes. **A**: the ε-congruent contacting surfaces with gaps/penetrations in the contacting interfaces. **B**: the same structure with the multi-domain discretization resulting in conformal meshes. **C**: a close-up cross-section view of the gaps/penetrations at the root level. **D**: a schematic illustration of the ε-congruent and conformal meshes.

When two contacting domains are reconstructed, discretized, or re-meshed independently, undesired gaps/penetrations are inevitable, causing two different boundary definitions for an identical contacting interface between the two adjacent/contacting domains. The agreement of the two contacting geometries on the contacting boundary or shared interface can be analyzed in two different levels; first, on the geometry level and based on the curvature of the contacting surfaces; second, on the mesh-based level focusing on the agreement on the identical discretization of the contacting interface in terms of the position of vertices, edges, and faces. The former is called here the "interface congruency". In the biomechanical field of study, different theoretical and computational studies analyze the effect of the "ball-and-socket" joint congruencies such as in shoulder, hip, and temporomandibular joints to analyze their instabilities and dislocations under different circumstances [15,36]. It should be noted that the current study only focuses on developing computational models of human mandible and maxilla for tooth movements and the mesh congruency of the contacting surfaces instead of congruency of the "ball-and-socket" joints, and the utilized "congruency" term needs to be distinguished from those in biomechanical studies for analyzing the joint congruencies [15,36].

As mentioned before, by using the conventional one-by-one domain discretization, mesh reduction, or quality meshing processes, it is challenging to achieve congruent surfaces due to the generation of gaps/penetrations between two contacting surfaces (see Figure 4.1). We propose using signed distance fields in the contacting surfaces to quantitatively evaluate the error between two contacting regions. The signed distance function, $\phi_\Omega(x)$, for a domain $\Omega \subset R^3$ and an arbitrary point $x \in R^3$ is defined as

$$\phi_\Omega(x) = \begin{cases} -d(x, \partial\Omega), & \text{if } x \ \in \Omega, \\ 0, & \text{if } x \ \in \partial\Omega, \\ d(x, \partial\Omega), & \text{if } x \ \in \Omega^c, \end{cases} \tag{4.1}$$

where $\partial\Omega$ denotes the boundary of the domain Ω, Ω^c represents the complement of Ω, and $d(x, \partial\Omega)$ indicates the Euclidean distance between the point x and the boundary of the domain $\partial\Omega$. We measure the congruency of the surfaces by calculating the signed distance field of each contacting surface with respect to the other domain as

$$\begin{aligned} \varepsilon = \max\left\{\left|\phi_{\Omega_2}(x)\right|, \left|\phi_{\Omega_1}(y)\right|\right\}, \\ \forall x \in \partial\Omega_{1c},\ y \in \partial\Omega_{2c}, \\ \partial\Omega_{1c} \subseteq \partial\Omega_1,\ \partial\Omega_{2c} \subseteq \partial\Omega_2, \end{aligned} \tag{4.2}$$

where $\partial\Omega_1$ and $\partial\Omega_2$ denote the boundaries of the domains Ω_1 and Ω_2, respectively, and $\partial\Omega_{1c}$ and $\partial\Omega_{2c}$ refer to the contacting surfaces of the domains. The computed ε values for two contacting domains are then called epsilon-congruent surfaces. The epsilon value indicates the measurement error, where the values close to zero refer to completely congruent surfaces.

4.2.2 Conformal mesh interfaces

A special case for the congruent surfaces is “conformal meshes” or “mesh conformity” and can be described as the identical discretization of the contacting interfaces. That is to say, for two contacting domains/geometries like Ω_1 and Ω_2, the contacting surfaces $\partial\Omega_{1c}$ and $\partial\Omega_{2c}$ are assumed identical. More specifically, they share identical vertices, edges, and elements on the contacting interfaces. In general, applying the conformal mesh criterion on multi-domains with contacting surfaces is a challenging process, as most of the geometry and mesh processing algorithms used in different free software produce the quality meshes per domain independently. Therefore, the contacting surfaces should be identified and combined as a different step to create identical contacting interfaces on the mesh of each domain.

Finally, the volumetric meshes can be generated by enforcing the meshing algorithm to fully preserve the input surface mesh. This raises questions about the final mesh quality, as the additional surface preservation constraint affects the mesh generation and the optimization algorithms. Hence, the best approach for generating conformal meshes is to consider all contacting domains simultaneously while generating the volumetric meshes.

Generating multi-domain volumetric meshes would generate zero-congruent and conformal meshes that omit any numerical errors caused by non-congruent contacting meshes. Therefore, it is essential to utilize a meshing algorithm that generates volumetric meshes considering multi-domain boundaries and performing boolean operations on the input surface meshes by using an implicit representation of the input meshes. In this study, we use fTetWild [48] that supports all aspects mentioned above for multi-domain volumetric meshes. This provides a volumetric mesh of teeth-PDL-bone geometries in which there are shared points in the teeth-PDL and PDL-bone contacting surfaces.

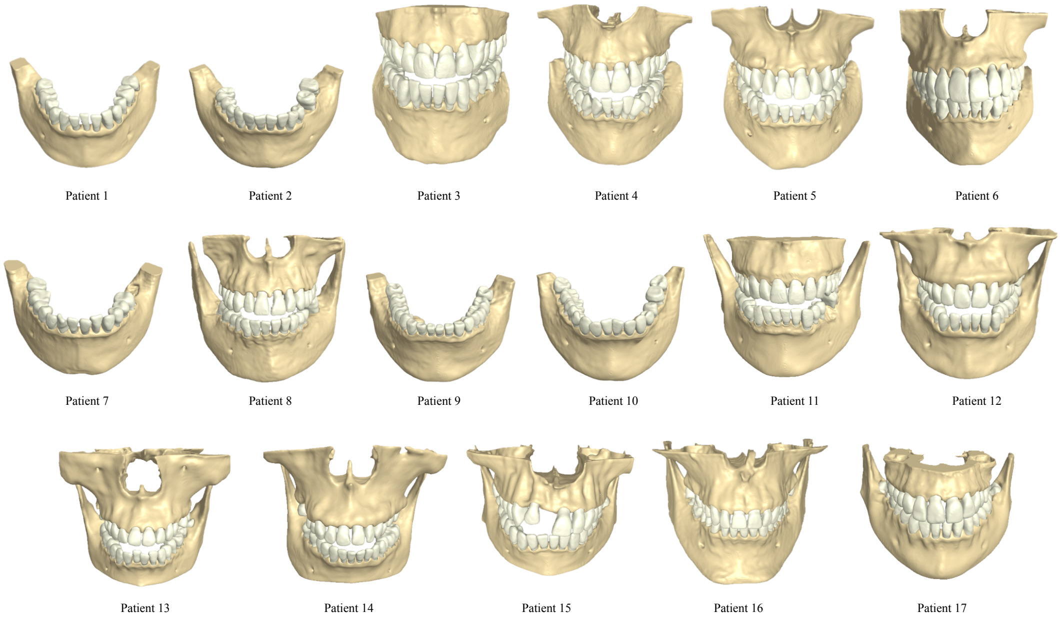

FIGURE 4.2: Reconstructed 3D geometries from 17 CBCT scans. Note that the maxillary jaw is removed in some scans due to having several metal artifacts and/or missing teeth. The anatomical variations in different jaws and teeth of our dataset indicate the necessity for introducing such a model repository for assessing the generalizability of the FEM results in the related clinical/population studies.

4.2.3 Proper modeling of the PDL layer

PDL is a thin structure that connects alveolar bone to the teeth cementum and acts as a shock absorber in the chewing or biting process. It also plays an important role in transferring load from teeth to the bone in orthodontic treatments; when triggered with enough orthodontic forces, it results in a bone remodeling process. As this thin and soft structure shares interfaces with two hard tissues of the teeth and bone geometries, the computational model may become unstable if the PDL geometry does not have congruent surfaces with teeth and bone in the contacting interfaces.

4.2.4 Quality mesh generation

Tetrahedralization algorithms usually require a set of closed, self-intersection free surface meshes as input, which is a requirement that is challenging to guarantee in our setting without manual interaction. In fact, traditional medical imaging pipeline require the large majority of the manual processing in this cleanup phase, as self-intersection, holes, or other imperfections normally appear when processing real-world data, and are especially common (and time consuming) when dealing with thin layers, like the PDL layer.

We propose a very different approach, where we accept that these imperfection exist, and design a meshing pipeline that tolerates and automatically heals them. We base our approach on the method recently introduced in [47, 49]: instead of meshing one domain at a time, TetWild meshes the entire volume of the bounding box containing the soup of triangles of all surfaces of interest. The triangles are approximated with faces of the tetrahedral mesh. This procedure does not require clean input geometry, it can tolerate degenerate input triangles, self-intersections, and holes [49]. In the original TetWild algorithms, the final mesh is extracted using a robust filtering procedure based on either flood fill or the generalized winding number [51], in both cases assuming that the user is interested in a single material mesh. We propose a novel filtering procedure for the filtering of multi-material tetrahedral meshes common in medical imaging in Section 4.3.5, and we show that our extension of TetWild is ideal for constructing our dataset, as it removes the expensive and tedious manual cleanup of the input surface meshes.

4.3 Controlling shared interfaces using volume mesh generation

This section reviews the entire process for developing the FE models of 17 jaws presented in Figure 4.2. To be more specific, Section 4.3.1 describes the utilized criteria for the cohort selection process; Sections 4.3.2 and 4.3.3 provide a detailed description for the CBCT segmentation and clinical validation; the geometrical variations of the reconstructed mandibles and maxillae are investigated in Section 4.3.4 based on widely used clinical landmarks; and finally, the different steps of the used pipeline for developing high-quality volumetric meshes of human jaws are studied in Section 4.3.5.

4.3.1 Cohort selection

We use CBCT scans of 17 different patients with different voxel resolutions from 3Shape A/S in-house dataset. Various criteria including the original voxel size of the scan, minimal metal filling artifacts, and the absence of implants and severe periodontal diseases are considered in selecting the mentioned cohort. Also, the selected cohort has no evidence of maxillofacial surgery or skeletal diseases. Sensitive information of the patients such as name, age, and gender are stripped due to the General Data Protection Regulation (GDPR) rules. The utilized scans were acquired from the patients by their associated doctors/orthodontists as a part of treatment plans, and the authors had no roles in the acquisition process.

4.3.2 Data specifications and geometry reconstruction

To reconstruct the patient-specific geometries, first, the scans are imported in 3DSlicer [37] in the standard Digital Imaging and Communications in Medicine (DICOM) format. Table 4.2 provides details of the scans utilized in this study. Next, according to the pre-evaluation criteria (metal fillings or implant artifacts), we decide on which jaws are suitable to be segmented from the scan.

The resolution of the selected CBCT scans is at most 0.3 mm since based on our experience, accurate tooth-bone segmentation of the scans with slice thicknesses above 0.3 mm is very challenging. Besides, applying smoothing functions with identical kernel sizes results in smoother segments for coarse

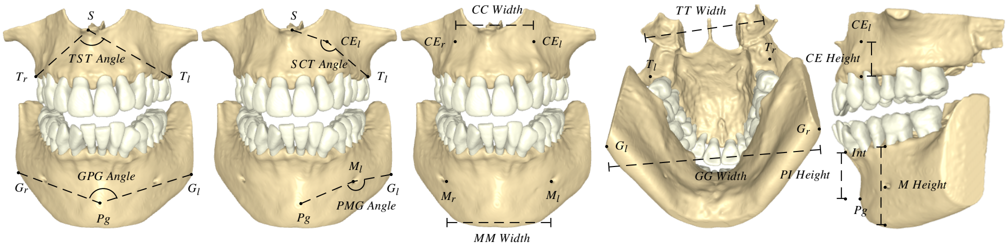

FIGURE 4.3: The utilized morphological landmarks for analyzing and quantification of the geometrical variation of the reconstructed mandibles and maxillae in different models.

voxel sizes, making it difficult to remove the segmentation noise (e.g., rugged surfaces) while preserving the fine details in desired regions (e.g., the alveolar crests of teeth sockets and root apexes). As a result, to avoid biases in the geometry reconstruction process, we convert all scans to an identical resolution of 0.15 mm, as summarized in Table 4.2, by oversampling a cropped region of interest (ROI) containing the jaws using linear interpolation.

The tooth-bone segmentation is performed based on the semi-automatic watershed algorithm [119] provided in 3DSlicer's SegmentEditorExtraEffects extension. The result of the watershed algorithm is then refined to correct the misclassified teeth and bone. Later, the geometries are smoothened using the 3DSlicer's standard *median* and *joint smoothing* modules [96, 121]. The joint smoothing method [121] smooths the adjacent segments simultaneously and enforces watertight interfaces between them. The tooth-bone segmentation procedure proceeds until the segmentation accuracy meets our clinical validation criteria (see Section 4.3.3). Finally, the segmented regions are exported as surface meshes in the Object file format (OBJ).

4.3.3 Clinical validation of the teeth-bone segmentation

The segmented teeth-bone geometries of all patients are validated by clinical experts. This is done by identifying the existence of any periodontal diseases and categorizing each patient into one of the no, mild, or moderate periodontal disease categories. The patients with severe periodontal diseases are excluded from the analyses based on the cohort selection criteria mentioned in Section 4.3.1. Moreover, we assess the accuracy of segmentation in areas close to teeth/bone borders, cervical regions of bone around teeth sockets, tooth-bone interfaces, and roots.

4.3.4 Geometrical variations of the dataset

We evaluate the geometrical variation of the reconstructed geometries using 3D morphological and cephalometric landmarks and measurements adapted or inspired from the literature [14, 20, 122, 124, 127], as illustrated in Figure 4.3 and described in Table 4.3. Accordingly, the measured values per patient and the mean and standard deviation of each morphological measurement across all

Table 4.2: Specifications of the utilized CBCT scans. Different scans with various filed-of-views and slice thicknesses are used in this study. All scans are converted to an identical slice thickness of 0.15 mm to avoid biases in the geometry reconstruction process, especially when applying smoothing filters to eliminate noises on the segmented teeth and bone geometries. Note that the maxillary jaws of the patients with many metal artifacts and/or missing teeth are removed.

Patient's	Original scan		Final resampled ROI		Jaws		Periodontal disease	
ID	Dimension	Slice thickness (mm)	Dimension	Slice thickness (mm)	Mandible	Maxilla	Mandible	Maxilla
Patient 1	400 × 400 × 280	0.3	676 × 530 × 280	0.15	Yes	-	No	Missing teeth
Patient 2	400 × 400 × 280	0.3	670 × 440 × 344	0.15	Yes	-	No	Missing teeth
Patient 3	532 × 532 × 540	0.15	534 × 435 × 338	0.15	Yes	Yes	Moderate	Moderate
Patient 4	532 × 532 × 540	0.15	534 × 435 × 338	0.15	Yes	Yes	Mild	Mild bone loss
Patient 5	532 × 532 × 540	0.15	525 × 425 × 290	0.15	Yes	Yes	No	No
Patient 6	534 × 534 × 430	0.15	534 × 534 × 430	0.15	Yes	Yes	No	No
Patient 7	400 × 400 × 280	0.3	614 × 470 × 270	0.15	Yes	-	No	-
Patient 8	400 × 400 × 280	0.3	800 × 800 × 560	0.15	Yes	Yes	Moderate	Moderate
Patient 9	400 × 400 × 280	0.3	525 × 425 × 290	0.15	Yes	-	No	-
Patient 10	400 × 400 × 280	0.3	525 × 425 × 290	0.15	Yes	-	No	-
Patient 11	400 × 400 × 280	0.3	525 × 425 × 290	0.15	Yes	Yes	No	No
Patient 12	400 × 400 × 280	0.3	525 × 425 × 290	0.15	Yes	Yes	Moderate	Moderate
Patient 13	400 × 400 × 280	0.3	525 × 425 × 290	0.15	Yes	Yes	No†	No*
Patient 14	400 × 400 × 280	0.3	525 × 425 × 290	0.15	Yes	Yes	No	No
Patient 15	750 × 750 × 400	0.2	525 × 425 × 290	0.15	Yes	Yes	No†	No*
Patient 16 ⋆	520 × 406 × 340	0.25	866 × 636 × 566	0.15	Yes	Yes	No	No
Patient 17	500 × 500 × 500	0.2	668 × 530 × 364	0.15	Yes	Yes	No†	No

⋆ The scan obtained from 3DSlicer's "Sample Data" module, titled "CBCT-MRI Head".
† The mandible includes partially erupted wisdom tooth/teeth.
* The maxilla includes an impacted wisdom tooth.

patients are listed in Table 4.4. Note that even though the standard deviation of each measurement may seem rather small, such small changes can lead to significant variations in the overall shape of the jaw, indicating the availability of high geometrical variations among different jaws under the study.

4.3.5 The pipeline for generating FE model of a human jaw

The flexibility of the FE method allows it to use a wide range of spatial discretizations [9]. We opt for an unstructured tetrahedral mesh as can be robustly generated using automatic meshing tools [48] and can lead to similar accuracy and running time when using high order elements as structured meshes [112].

To eliminate the manual geometry processing, quality meshing, or mesh decimation steps, we propose to directly use the exported surface meshes as an input to our pipeline. Figure 4.4 shows a comparison between the conventional labor-intensive approach and our method for developing FE models of a human jaw. For the reproducibility purpose, the pipeline is implemented based on the free open-access geometry processing library libigl [52] and the meshing algorithm fTetWild [48]. The pipeline generates conformal volumetric meshes using imperfect meshes exported from the segmentation software with minimal human intervention. Figure 4.5 shows the flowchart of the utilized pipeline and the characteristics of the meshes at different steps.

TABLE 4.3: Description of the utilized morphological landmarks obtained based on the literature [14, 20, 122, 124, 127], as illustrated in Figure 4.3.

Jaw type	Landmark	Landmark's description
Mandible	MM Width	Maximum breadth of mandibular body at the mental foramen [20]
	MF Height	Body height: the height of the mandible at the mental foramen (M_l) [122]
	PMG Angle	Mandibular body angle: the angle between the lines connecting the left mental foramen (M_l) to pogonion (Pg) and left gonion, inspired from [14]
	GPG Angle	Pogonion angle: the angle between the lines connecting pogonion (Pg) to the left and right gonia (G_l, G_r), inspired from [20, 127]
	GG Width	Intergonial distance: direct distance between the left and right gonia [124]
	PI Height	The perpendicular distance between the anterior interdental (Int) and pogonion (Pg) [124]
Maxilla	CC Width	Anterior maxillary basal width: the length of the line connecting the left and right canine eminences (CE_l, CE_r) [14]
	CE Height	The perpendicular distance from the left canine eminence (CE_l) to the alveolar crest
	SCT Angle	The angle between the lines connecting the left canine eminence (CE_l) to the anterior nasal spine (S) and the left maxillary tuberosity (T_l)
	TST Angle	Anterior nasal spine angle: the angle between the lines connecting the anterior nasal spine (S) to the left and right maxillary tuberosity (T_l, T_r)
	TT Width	Posterior maxillary width; the distance between the left and right maxillary tuberosity (T_l, T_r), inspired from [14]

TABLE 4.4: Assessment of the geometrical variations of the mandibles and maxillae based on the computed measurements illustrated in Figure 4.3. Note that even small changes in the values can change the overall shape of the jaw considerably, indicating that high geometrical variations are available within our models.

Patient's ID	Mandibular jaw						Maxillary jaw				
	MM Width (mm)	MF Height (mm)	PMG Angle (deg)	GPG Angle (deg)	GG Width (mm)	PI Height (mm)	CC Width (mm)	CE Height (mm)	SCT Angle (deg)	TST Angle (deg)	TT Width (mm)
Patient 1	49.30	28.94	147.20	77.50	95.32	21.70	-	-	-	-	-
Patient 2	46.54	27.31	142.30	79.00	83.54	21.45	-	-	-	-	-
Patient 3	46.89	33.31	131.70	86.60	69.80	26.43	40.84	15.62	141.60	68.40	63.66
Patient 4	41.61	32.73	141.40	81.20	73.02	19.94	30.21	12.24	146.90	61.10	52.62
Patient 5	42.51	25.57	158.70	96.50	78.20	16.41	29.92	12.88	154.50	67.80	59.87
Patient 6	38.42	26.72	151.80	85.80	71.61	19.71	30.09	16.09	143.50	66.70	55.36
Patient 7	47.18	27.39	140.20	71.90	82.10	21.07	-	-	-	-	-
Patient 8	41.19	29.48	146.10	75.30	88.88	21.63	27.68	13.04	148.60	68.30	54.78
Patient 9	50.31	32.33	142.40	81.70	94.29	26.53	-	-	-	-	-
Patient 10	48.34	33.14	150.80	77.60	86.19	23.02	-	-	-	-	-
Patient 11	51.29	32.36	151.40	80.50	97.08	27.21	37.13	17.08	129.20	69.90	61.01
Patient 12	46.34	33.96	154.00	81.30	97.10	26.21	35.83	14.70	133.20	69.90	68.12
Patient 13	45.62	19.24	147.00	77.90	89.11	17.86	33.46	12.49	132.40	80.30	61.51
Patient 14	49.39	23.02	145.00	91.90	89.42	17.68	34.65	13.30	147.60	77.30	72.85
Patient 15	45.15	20.01	147.80	75.80	91.21	18.83	25.90	17.43	131.70	63.70	58.99
Patient 16	46.76	36.57	151.40	71.70	104.70	26.88	35.94	17.00	140.20	74.60	71.66
Patient 17	40.21	24.76	148.20	70.20	91.76	19.16	27.61	11.70	137.50	67.70	53.33
Mean	45.71	28.64	146.91	80.14	87.25	21.87	32.44	14.46	140.58	69.64	61.15
± STD	± 3.73	± 5.03	± 6.24	± 7.00	± 9.79	± 3.58	± 4.55	± 2.10	± 7.96	± 5.43	± 6.85

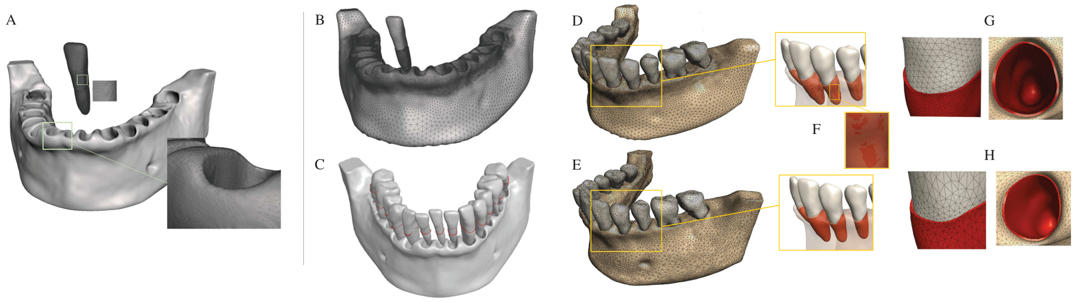

FIGURE 4.4: Finite element models created based on irregular dense meshes (**left subfigure, A**) exported from the segmentation step. **Right subfigure:** A comparison between the results of the conventional meshing approach (**top-row**) and utilized pipeline **(bottom-row)**. The conventional approach involves time-consuming and labor-intensive geometry and mesh processing tasks **(B)**; this results in non-congruent contacting interfaces **(F)**, and non-conformal meshes **(G)**. Note that the spotted marks in **F** indicate the undesired gaps/penetrations in the contacting interfaces. In contrast, the utilized method generates multi-domain volumetric meshes directly using the input irregular meshes from the generated PDL rims (shown in red in **C**) and guarantees the interface congruency as well as the mesh conformity as depicted in **H**.

Preprocessing

As can be seen in Figure 4.5, the input meshes to the pipeline are dense irregular meshes, which are not necessarily guaranteed to be watertight, manifold, and self-intersection-free, referred to as "triangle soup" in the computer graphics [47, 49, 131]. Hence, we apply a preprocessing step to both reduce the mesh sizes and produce meshes that are manifold, watertight, and self-intersection-free. These mesh characteristics assure meaningful values for the utilized signed distance functions in the next geometry processing steps of the used pipeline, i.e., the gap and PDL rim generation steps [131]. We use fTetWild [48] as a robust meshing tool to decimate and "clean up" the imperfect meshes. To be more specific, the teeth and bone geometries are tetrahedralized separately, and the boundary faces of the resulting tetrahedral meshes are then extracted as the cleaned-up reduced surface meshes to be used as the input meshes to the gap generation step. Further details on the surface mesh extraction process can be found in Section 4.3.5.

Gap generation for the PDL tissue

PDL has an average width of 0.2 mm [63]; its width can approximately be 0.15 mm around the middle third of the root and about 0.21 mm [12, 130] to 0.38 mm [63] near the root apex and cervical regions.

Reconstructing the PDL layer using CBCT scans obtained in vivo from patients in clinics is a challenging process [46] as the commonly used voxel dimensions for the CBCT scans, ranging from 0.2 mm to 0.5 mm [23], are not fine enough to capture such a thin structure (roughly 0.2 mm) [34, 103]. Although the geometry of the PDL layer can be reconstructed by segmenting it from the

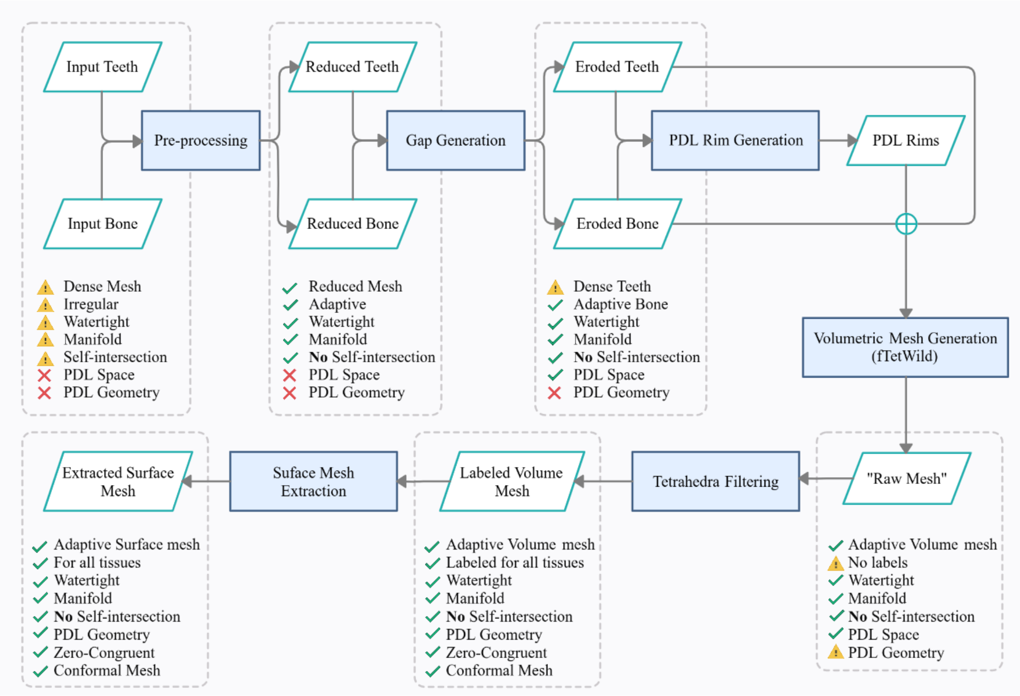

FIGURE 4.5: Flowchart of the utilized pipeline and the characteristic of the meshes at each step. The pipeline consists of five main consecutive steps, as further described in Section 4.3.5.

micro-CTs acquired in vitro, the x-ray exposure in such scans is extremely high and harmful for the human body, and it is usually obtained from dead specimens. Therefore, we first conduct the teeth-bone segmentation from the CBCT scans and then apply geometry processing techniques to create a gap between the teeth and bone geometries where the PDL can reside with an average thickness of 0.2 mm.

Ideally, to generate the required gaps for PDL geometries, we shrink the bone and teeth, each by 0.1 mm. First, we shrink the bone geometry by 0.1 mm, by moving its mesh points in the reverse direction of per-vertex normal with a magnitude of 0.1 mm, which we call it *explicit shrinking approach*. Before performing any *explicit shrinking process*, the radius curvature is locally computed for bone vertices to identify the sharp and thin structures. This is done by calculating the radius r of the mean curvature h at point t based on $r(t) = 1/h(t)$, as the reciprocal of the curvature at that point. The radius of the curvature provides useful information about the maximum magnitude that the surface vertices can be moved in the opposite direction of the normals of the surface before a singularity occurs. This means that the movement of the nodes with larger values would cause self-intersection issues and artifacts on the surface mesh. For this reason, evaluating the shrinking limits prior to the bone shrinking process is important. In the case where the shrinking limit is less than 0.1 mm, the pipeline shrinks the bone to its maximum shrinking limit, while more shrinking the teeth to compensate for the total desired gap.

To shrink the teeth, we use an *implicit shrinking approach* based on signed distance functions presented in Equation (4.1). The signed distance field contains the boundary of the geometry, i.e., zero iso-surface [91] and the information from different offset surfaces with positive and negative values. The positive offsets/iso-surfaces represent a dilated version of the geometry, while the negative values represent the eroded geometry. Consequently, we use an iso-contour of $\phi_\Omega(x) = -0.1$ to shrink the tooth with a magnitude of 0.1 mm. Since the iso-contour is still an implicit representation of the shrunk tooth, we use a contouring method based on a marching cubes algorithm [71] to convert it to an explicit representation including the vertices and connectivity matrix. As a result, wherever the radius curvature might be less than the desired offset value, the *implicit shrinking approach* can prevent any singularities at the root apexes. It can therefore be used as a more robust shrinking approach, especially for thin and sharp geometries with lower radius curvature values (here, the root apex of incisors). Note that the applied approach to the teeth creates a slightly wider space than the desired gap in the root apexes, which is in line with the clinical studies [79, 130].

Boundary representation of PDL

Instead of an explicit representation of PDL which uses closed surface meshes, we use a boundary representation (B-Rep) approach using triangle meshes to describe the PDL domain. This needs to be distinguished from the basis spline (B-Spline) representation. we use B-Rep for describing the PDL domain for three main reasons. First, fTetwild uses the winding number information together with the input surface mesh to generate a volumetric mesh with no prior assumptions such as watertight or closed surfaces. Therefore, a shell surface can be used as a part of the input mesh to represent the domain boundary. Second, since fTetwild uses an implicit algorithm, it enables us to use B-Rep and perform boolean operations on different components to describe the domain boundary [48]. This is while it is not trivial to correctly define the B-Rep models for complex geometries using the Delaunay-based algorithms such as TetGen [115]. Third, B-Rep models help us to achieve zero-congruent contacting interfaces and avoid numerically small values for ε produced due to machine/floating-point precision. This, in turn, assures congruency and mesh conformity at the contacting interfaces for modeling the PDL layer as mentioned in Section 4.2.3.

The PDL geometry can be described using three main surfaces: the top surface of PDL, tooth-PDL, and PDL-bone interfaces, in which the two last interfaces can be replaced with the teeth and bone geometries. To represent the free surface of the PDLs that are not in contact with the teeth and bone geometries, we generate only the top surface of each PDL, called the PDL rim in this study. B-Rep model using PDL rim and teeth-bone geometries as inputs to fTetWild helps to generate multi-domain volumetric mesh using boolean operations to guarantee geometry congruency and mesh conformity in the contacting interfaces.

We utilize a gap filling method [81] to generate the rims that connect the bone to shrunk teeth. This method detects an initial surface on the bone within

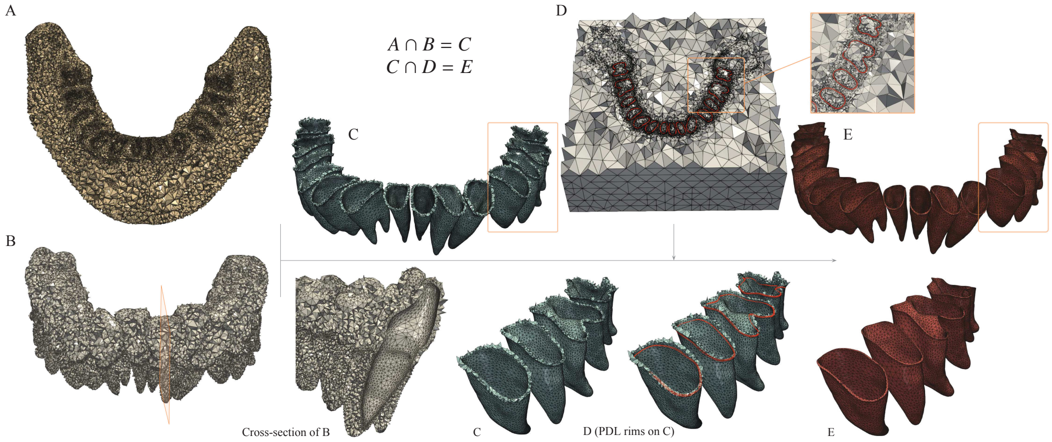

FIGURE 4.6: The proposed tetrahedra-filtering method and its close-up view (bottom row) for proper labeling of the PDL from the raw mesh. Thetrahedra around teeth (**A**) and bone (**B**) are used to obtain the conformal tooth-PDL and PDL-bone interfaces (**C**). The obtained mesh includes jagged top surfaces which can be removed by using the positive winding numbers with respect to the PDL rims (**D**), resulting in smooth and clean top surfaces for the generated PDLs (**E**).

the desired distance like 0.3 mm. Next, the boundary nodes of the detected surface are smoothened using a Laplacian smoothing approach to provide a base surface on the tooth socket with a smooth boundary on the bone. The smoothened boundary points are then snapped to the bone surface to assure the smoothened boundary is on the bone. Afterward, the base function with smoothened boundary is extruded with the desired thickness (0.2 mm), and the extruded surface is snapped to the tooth surface to assure the points are located on the tooth surface. Finally, the PDL rim is constructed by connecting the boundary points of the base and extruded surfaces. We only use the PDL rims without the base/extruded surface to avoid any redundant representations of tooth-PDL and PDL-bone interfaces having potential numerical errors. These errors can cause issues in the volumetric mesh generation process of fTetwild, when the value of the user-defined maximum deviation parameter called envelope is less than or equal to the produced error in the duplicated surfaces.

Volumetric mesh generation

A unified volumetric mesh is generated using the surface meshes of the teeth, bone, and produced PDL rims, It is obtained by applying a union operation on the provided input surface meshes using fTetWild [48] with optimal *envelope* (ϵ) and *ideal edge length* values of 2×10^{-4} and 0.01, respectively. Applying a union operation using fTetWild generates a single volumetric mesh for the bounding box surrounding all input surface meshes called the *raw mesh* [48]. Note that the default filtering method in fTetWild exports a labeled version of the raw mesh that assigns the tetrahedra outside the closed input surfaces as the background elements.

Proposed tetrahedra filtering method

The default tetrahedra filtering/labeling method in fTetWild can only be used when all input meshes are closed surface meshes, which is not the case for the PDL rims. Hence, a specific filtering approach is used for assigning each tetrahedron a label associated with one of the input domains, i.e., the teeth, PDL, or bone. The remained tetrahedra are labeled as background. We use a distance field-based labeling method for teeth and bone. To do so, the barycenter of each tetrahedron is used as an average point of tetrahedron vertices to decide whether the element is positioned inside or outside a surface considering the distance field of each barycenter with respect to each of the teeth and bone geometries. The negative distance values indicate the points are located inside the surface mesh.

We propose using a signed distance-based method combined with the winding number information to obtain the PDL geometries. The PDL is expected to reside in the gap between the teeth and bone; hence, as shown in Figure 4.6, we first select all tetrahedra with positive distance values below 0.3 mm around teeth (A) and bone (B) based on the intersection of these two sets of tetrahedra (C). Next, the intersection of the obtained tetrahedra (C) and the tetrahedra with positive winding numbers with respect to the PDL rims (D) is utilized to produce a smooth boundary (E) for the top-free surface of each PDL. The winding numbers, as also used in fTetWild for implicit meshing, are applied to eliminate all meshing artifacts introduced by the intersection operation (C). As can be seen, applying the proposed filtering method considering the information of the winding numbers to the raw mesh provides smooth PDL top surfaces as well as conformal meshes in the tooth-PDL and PDL-bone interfaces, which include shared nodes in the contacting interfaces and provide perfect adhesions in the contacting interfaces.

Surface mesh extraction

After labeling all tetrahedra in the raw mesh, we select boundary faces of each domain, i.e., the shared faces between the domain and background tetrahedra, and save them as reduced adaptive surface meshes. Note that the extracted surfaces are zero-congruent and conformal meshes with no meshing artifacts.

FE simulation setup

The used pipeline automatically sets up the FE problems based on two different scenarios; (1) uncontrolled tipping and (2) biting scenarios. It automatically generates FEM files of the uncontrolled tipping scenario for all patients and FEM files of the biting scenario for those whose scans were acquired in a natural biting position. Note that the utilized code for defining the boundary and loading conditions is scenario-specific, which requires to be adapted for other scenarios. The defined FE problem for each scenario is exported as an XML file including the tetrahedral meshes, types of elements, utilized material models and properties of each domain, as well as boundary and loading conditions.

In these scenarios, we use Tet4 elements for the teeth and bone with negligible deformations. Furthermore, to avoid the locking artifacts [110] that are common when linear tetrahedral elements are used to model large deformations, we apply a quadratic basis to the elements of the PDL layer, to consider Tet10 elements for the PDL domain. We prefer to use an explicit tetrahedral mesh to model the PDL layer [46,61,89] (instead of the cheaper option of using shell elements) as it can more faithfully capture shear, bending, and buckling of the membrane, and at the same time, it simplifies both meshing and simulation, as it does not require special handling for inserting shell elements in a tetrahedral mesh and coupling between the volumetric elastic model and its interaction with the shell. Further, providing a volumetric representation of the PDL layer allows future studies to explore the effects of utilizing visco-elastic-plastic material models for the PDL layer.

Material models and parameters In this study, the bone and teeth tissues deform negligibly under the applied forces. Therefore, we assume no distinctions between different structures of the bone (cortical and trabecular) and teeth (enamel, dentin, and pulp) [41,98,135]. Besides, the porous fibrous periodontal ligament tissue is assumed as a homogeneous structure [89]. We use the Neo-Hookean material model with Poisson's ratios of 0.3, 0.3, and 0.45, and Young's modulus values of 2000 MPa, 1500 MPa, and 68.9 MPa to describe the mechanical behavior of the tooth, PDL, and bone domains, respectively [16,17,41].

Note that the used simplex material models can be replaced with any complex constitutive models to properly mimic the anisotropic viscoelastic behavior of the PDL [38,89,98], or orthotropic characteristic of the bone. This can however increase the computational costs of the simulations.

Boundary conditions In the tipping scenario, depending on the type of the simulated jaw, a Dirichlet boundary condition is defined on all nodes located at the bottom of the mandible or top surface of the maxilla to fix nodes' displacements in all three directions. In the biting scenario, the same Dirichlet boundary condition is applied on the top nodes of the maxilla to fix them in all three directions. Besides, a similar Dirichlet boundary condition is used to restrict the movement of the mandible only in the anterior-posterior and medial-lateral directions with imposing no restrictions in the third direction.

Loading conditions In the tipping scenario, we apply a perpendicular force with a magnitude of 1 N at the center of each crown to mimic the uncontrolled tipping motion in the lingual direction. In the biting scenario, a pressure load of 200 N is applied to the bottom surface of the mandible to simulate the biting force.

Contact definition To have a perfect adhesion in the tooth-PDL and PDL-bone interfaces, we generate a single volumetric mesh by combining surface meshes of the shrunk teeth, PDL rim, and bone geometries using a union operation in fTetWild [48]. The nodes at the contacting interfaces are shared between the adjacent domains, thus guaranteeing a complete adhesion as well as conformal meshes at the contacting interfaces. Therefore, there will be no sliding, separation, or penetration at the tooth-PDL and PDL-bone contacting interfaces. Further details on the volumetric mesh generation can be found in Section 4.3.5.

Furthermore, in the both scenarios, any potential contacts between different teeth are modeled using the incremental potential contact formulation [62].

Technical details

Implicit shrinking approach The explicit representation of geometries only provides boundary information of them. This is while the implicit representation of geometries based on the signed distance function provides useful information about the interior and exterior of the shape as well as the outline/boundary of geometry. Therefore, we use boundary information obtained from the explicit representation to define the signed distance function/filed before evaluating it on the desired points in an R^3 space and shrinking the teeth. To do so, we sample the distance field in the R^3 space using a regular 3D grid in the bounding box of each tooth. A fine grid sampling size of 0.1 mm is used to be smaller than the minimum isotropic voxel size (0.15 mm) as presented in Table 4.2, to avoid the aliasing effect or spiky surfaces in the sampling process and have smooth geometries in the shrunk teeth.

Next, the signed distance values are obtained for each point of the grid considering the surface mesh of the tooth. Note that sampling using regular grids requires excessive memory for geometries with large dimensions, which is not the case here as the dimension of each tooth is relatively small. In general, for meshes with fine details that cover a larger space, it is suggested to use adaptive sampling approaches such as the octree-based methods [75], to densely sample voxels in specific regions near the boundary or regions with great details.

Alternative PDL modeling An alternative approach for generating FE models of the tooth-supporting complex can be using Delaunay-based volumetric meshing tools like TetGen. Still, one needs to assure mesh conformity or interface congruency on the surface meshes, and next, to enforce the explicit volumetric meshing algorithm to preserve the surface meshes [128]. Note that providing quality surface meshes with mesh conformity criteria per se is not trivial. Besides, even though the alternative explicit approach can provide quality surface meshes, it may not provide optimal quality for the tetrahedra due to the additional constraint applied to preserve the surface mesh on the boundary of the domain.

Advantages of implicit over explicit meshing algorithms The explicit volumetric mesh generation approaches such as the Delaunay-based algorithms with incremental local mesh operations generate tetrahedral meshes covering the domain interior and are highly faithful to the input mesh. This means that the algorithms cannot coarsen the triangles on the input surface meshes. Therefore, they cannot produce coarse quality tetrahedra on the boundary faces of the input mesh, indicating that the element size at the domain boundary depends on the dense and irregular/rugged surfaces exported from the segmentation step. Consequently, one needs to prepare an adaptive surface mesh with high-quality triangles before applying the Delaunay-based algorithms along with a sizing field function to create adaptive volumetric mesh both in the domain interior and its boundary. Furthermore, since the explicit meshing algorithms fail in generating volumetric meshes in the presence of any self-intersections, one needs to clean up the meshes before applying the Delaunay-based meshing algorithms to create quality and adaptive mesh.

In contrast, implicit volumetric meshing approaches like fTetWild impose no assumptions on the input mesh and can handle imperfect input meshes with self-intersection artifacts. They can also produce an adaptive mesh that provides coarse tetrahedra at the domain boundary, slightly deviating from the input surface mesh, based on a user-defined input parameter. In addition, fTetWild uses winding numbers along with surface meshes to generate tetrahedral meshes based on an implicit meshing approach. This enables us to use the constructive solid geometry (CSG) model for describing a domain with complex boundaries by combining several simpler domains using boolean operations [39]. This is while the explicit meshing tools cannot support CSG models [115].

Volumetric meshing The fTetWild algorithm uses the user-defined epsilon and ideal edge length parameters to control the output mesh's accuracy and size. The epsilon value indicates how much fTetWild can deviate from the input surface mesh for generating a quality volumetric mesh. Hence, using a smaller epsilon value preserves the input geometry's details at the cost of higher computational time. In contrast, larger values can provide less accurate meshes in less computational time. Moreover, smaller values of ideal edge length provide denser meshes, while larger values can produce coarser elements. Hence, these two parameters can control the output mesh size and its geometrical accuracy. In this work, the utilized values for epsilon and ideal edge length are obtained based on a grid-search method in the intervals $[10^{-6}, 10^{-3}]$ and $[0.005, 0.02]$, respectively. Note that the fTetWild multiplies these parameters by the length of the diagonal of the input meshes' bounding box. Hence, the parameters are sensitive to the size of the bounding box that includes all input meshes. In other words, they need to be adjusted according to the model's size; if, for instance, the model is a cut-out model with a much smaller bounding box dimension than the full jaw model.

4.4 Results and discussion

In this section, the generated models are assessed from different aspects, and the results are compared with the state-of-the-art. In Section 4.4.1, we measure the thickness of the generated PDL layers. In Section 4.4.2, different mesh properties such as mesh sizes and mesh qualities are evaluated for the developed models; the results are compared to the OpenMandible model. In Section 4.4.3,

TABLE 4.5: The thickness of the PDL layers generated using the utilized pipeline with the statistics in line with the literature [63]. Note that there is a significant difference between our model results and those of the OpenMandible.

Patient's	Mandibular jaw			Maxillary jaw		
ID	Minimum	Maximum	Average	Minimum	Maximum	Average
Patient 1	0.12316	0.23552	0.19530	-	-	-
Patient 2	0.14227	0.25042	0.19536	-	-	-
Patient 3	0.13779	0.33969	0.19379	0.08258	0.38502	0.20143
Patient 4	0.13779	0.21958	0.11962	0.14331	0.23754	0.19634
Patient 5	0.14537	0.24688	0.19770	0.11837	0.23631	0.19676
Patient 6	0.16350	0.24151	0.19737	0.14928	0.25741	0.19654
Patient 7	0.15258	0.25176	0.19527	-	-	-
Patient 8	0.13036	0.25292	0.20056	0.15210	0.32516	0.19745
Patient 9	0.13324	0.27437	0.19629	-	-	-
Patient 10	0.11951	0.23903	0.20100	-	-	-
Patient 11	0.14271	0.33307	0.19887	0.12834	0.25599	0.19465
Patient 12	0.11694	0.34803	0.20164	0.12070	0.31058	0.19219
Patient 13	0.12288	0.28818	0.20134	0.09648	0.26672	0.18296
Patient 14	0.12056	0.29998	0.19728	0.10014	0.29037	0.19222
Patient 15	0.13099	0.35793	0.20078	0.13277	0.34097	0.19148
Patient 16	0.12508	0.25914	0.19961	0.14156	0.30228	0.19535
Patient 17	0.13754	0.26163	0.19664	0.12427	0.28902	0.19610
Mean	0.13425	0.27645	0.19344	0.12416	0.29145	0.19446
± STD	± 0.0126	± 0.04360	± 0.01918	± 0.02193	± 0.044527	± 0.0045
OpenMandible	0.20576	1.93415	0.60772	-	-	-

FE simulation results of different patients are presented under identical tipping and biting scenarios.

4.4.1 Generated PDL properties

We assume an average thickness of 0.2 mm for the PDL layers according to the literature [90, 113] and assess the thicknesses of the generated PDLs across different patients models by computing the distances between the points located on the outer and inner surfaces of the PDL geometries. The thickness details of the generated PDLs can be seen in Table 4.5. As can be noticed from the table, the computed minimum, maximum, and average PDL thickness values are in line with those reported in the literature, i.e., 0.15, 0.3, and 0.2mm, respectively [63].

Likewise, we investigate the thicknesses for the PDLs from the OpenMandible dataset. As it can be seen in the last row of Table 4.5, the obtained thicknesses for OpenMandible are about two-three times the values reported in the literature. As the PDL thickness plays an essential role in exerting the applied load from teeth surfaces to the adjacent bone and teeth movements, it can be deduced that under identical scenarios and loading systems the OpenMandible

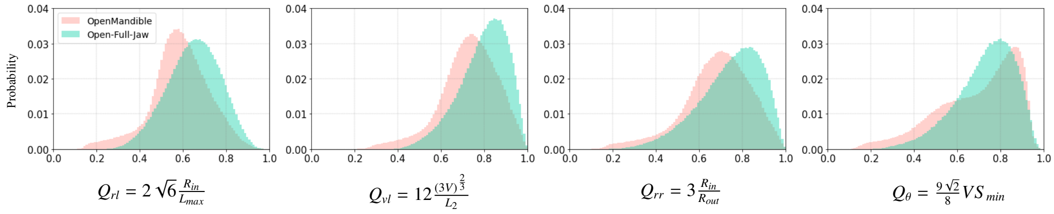

FIGURE 4.7: Comparison of the quality histograms of four different quality measurements used for the evaluation of the quality of the tetrahedra generated by OpenMandible and Open-Full-Jaw. **Left to right:** The radius-edge ratio Q_{rl}; The volume-edge ratio Q_{vl}; The radius ratio Q_{rr}; The angle measurement Q_{θ}. Note that L_{max}, R_{in}, and R_{out} denote the maximum edge length, the radius of the insphere, and radius of the circumsphere of a tetrahedron, respectively, and V and S_{min} represent the volume and minimum face area of the tetrahedron.

model cannot result in stress/strain values comparable with the ones obtained in this study.

4.4.2 Mesh properties

We evaluate the total number of elements and mesh qualities of the developed models and compare the mesh qualities of our model with those of the OpenMandible dataset. The maximum mesh deviation between the input and output meshes of ftetwild is then calculated to examine whether the meshing process alters the geometries negligibly.

Mesh sizes

We develop all computational meshes of our study on a machine with a 2.60 GHz processor and 16 GB of RAM, which takes around 40.78 ± 12.19 minutes per jaw. The details of the original dense meshes, the generated volumetric meshes, and their extracted surface meshes are summarized in Table 4.6. The pipeline produces conformal adaptive meshes from irregular dense meshes. The utilized adaptive meshing approach helps to reduce the total number of the elements, by producing coarser elements in regions far from the teeth while generating finer elements on root apexes, PDL layer, alveolar crest, or regions with fine details like thin walls of the maxilla.

Mesh quality analysis

The mesh quality required for an FE analysis can vary depending on the application and utilized numerical methods [114]. In general, a regular tetrahedron has the highest mesh quality in computational models, and the main guideline is to avoid using low-quality/badly-shaped tetrahedra, as they can affect the accuracy of the numerical methods.

The OpenMandible uses TetGen to obtain volumetric meshes from the manually generated conformal surface meshes. It sets the upper limit of the radius-edge ratio of to-be-generated tetrahedra to 1.5. This mesh quality constraint controls the ratio between the radius of the circumscribed sphere and the shortest edge of each tetrahedron, to prevent the production of low-quality/badly-shaped tetrahedra. In addition to this quality constraint, OpenMandible enforces TetGen to preserve the provided input surface meshes to have conformal volumetric meshes. Preserving the surface mesh is the only approach to produce conformal volumetric meshes when using explicit volumetric meshing approaches. This raises the question of whether TetGen can achieve the specified quality constraint value while enforcing another restriction to preserve the input surface mesh.

We quantitatively assess the quality of the generated volumetric meshes of this study and those of the OpenMandible. To be more specific, four different quality measurements presented in [114], i.e., the radius-edge ratio Q_{rl} [11], the volume-edge ratio Q_{vl} [69, 78], the radius ratio Q_{rr} [22, 40], and the angle measurement Q_θ [40], are used to evaluate the quality of the volumetric meshes. For a fair comparison, we compare the results from one of our patients to those of the OpenMandible study, as shown in Figure 4.7.

In a regular tetrahedron, the values of each utilized quality measurement correspond to one, indicating that an ideal high-quality mesh is expected to have a histogram peak at one. Therefore, the resulting distributions (normal or skewed normal) of all quality histograms show that our generated volumetric mesh has higher quality elements compared to OpenMandible. The proposed model also has narrower distributions with small discrepancies around their means. This holds even in the last case (Q_θ), where one of the peaks of the distribution (mode) for OpenMandible is closer to one. Moreover, the OpenMandible model sees two or more peaks in its distributions that can be modeled by mixed normal distributions.

Mesh deviation analysis

If one does not enforce the surface preservation criterion, the Delaunay-based volumetric meshing algorithms like TetGen include all points of the input surface mesh and a number of additional points. Hence, the generated volumetric meshes have boundary elements as fine as the input surface mesh. In contrast, fTetwild provides volumetric meshes as coarse as possible on the surface while preserving the input geometry. This algorithm slightly deviates from the input surface according to the user-defined maximal deviation (envelope) value. Therefore, to generate an accurate volumetric mesh, we must not deviate too much from the input surface mesh.

Accordingly, we quantitatively evaluate the deviation of final extracted surface meshes from the input surface meshes. We use Hausdorff distance as an error measurement between the input and extracted surface meshes from the generated volumetric meshes. The obtained distance values are presented in Table 4.7. As it can be seen, the maximum deviation of the meshes both in mandibular and maxillary jaws and their associated teeth is negligible with respect to the dimension of the entire jaw models.

TABLE 4.6: The total number of elements ($\times 10^3$) of the surface meshes (triangles) and volumetric meshes (tetrahedra). The number of elements is significantly reduced in the adaptive output surface meshes compared to that of the irregular dense input surface meshes.

Patient's ID	Mandibular jaw's mesh sizes									Maxillary jaw's mesh sizes								
	Input irregular mesh		Output surface mesh			Output volumetric mesh				Input mesh size		Output surface mesh			Output volumetric mesh			
	Teeth	Mandible	Teeth	PDLs	Mandible	Teeth	PDLs	Mandible	Total	Teeth	Maxilla	Teeth	PDLs	Maxilla	Teeth	PDLs	Maxilla	Total
Patient 1	198	478	59	60	75	178	87	252	517	-	-	-	-	-	-	-	-	-
Patient 2	531	1574	50	45	70	141	65	224	430	-	-	-	-	-	-	-	-	-
Patient 3	900	1576	82	77	96	243	111	315	669	948	1311	100	96	132	293	140	421	853
Patient 4	770	1592	94	108	106	294	155	338	788	824	1894	78	77	153	231	112	440	783
Patient 5	768	1553	77	88	98	227	127	326	681	851	2039	84	93	159	249	134	496	880
Patient 6	731	1406	78	82	91	233	119	312	664	904	2181	89	92	173	250	134	502	886
Patient 7	526	1556	51	49	73	142	71	236	448	-	-	-	-	-	-	-	-	-
Patient 8	625	2000	50	54	83	150	78	274	502	772	1921	75	70	157	221	101	469	791
Patient 9	869	2110	74	76	99	230	110	341	681	-	-	-	-	-	-	-	-	-
Patient 10	791	1867	69	71	91	202	103	301	606	-	-	-	-	-	-	-	-	-
Patient 11	708	2201	53	51	79	160	74	264	497	891	1531	91	85	135	260	124	416	799
Patient 12	233	629	57	60	82	163	87	261	511	232	636	67	61	133	203	87	399	689
Patient 13	188	469	54	50	78	163	72	252	487	190	1016	52	50	191	156	72	548	776
Patient 14	183	486	50	49	72	150	71	238	459	189	852	50	50	139	141	72	394	607
Patient 15	1016	1969	85	101	108	258	149	371	777	1032	2221	90	108	175	261	159	519	939
Patient 16	877	2958	61	69	97	194	99	311	605	851	2958	67	77	166	209	110	467	786
Patient 17	440	1045	69	80	94	210	116	305	630	447	577	91	93	126	273	135	378	787

TABLE 4.7: Hausdorff distances (HD) used as an error measurement to assess the deviation of the surface in the output mesh from the input mesh. The HD values indicate that the output surface meshes generated using our pipeline are close to the input surface meshes.

Patient's ID	Mandibular Jaw HD (mm)		Maxillary Jaw HD (mm)	
	Mandible	Mandibular Teeth	Maxilla	Maxillary Teeth
Patient 1	0.173	0.038	-	-
Patient 2	0.147	0.039	-	-
Patient 3	0.125	0.044	0.143	0.019
Patient 4	0.086	0.043	0.137	0.029
Patient 5	0.139	0.025	0.156	0.018
Patient 6	0.241	0.023	0.232	0.042
Patient 7	0.154	0.042	-	-
Patient 8	0.454	0.029	0.135	0.039
Patient 9	0.174	0.043	-	-
Patient 10	0.453	0.021	-	-
Patient 11	0.152	0.027	0.298	0.023
Patient 12	0.162	0.024	0.212	0.044
Patient 13	0.158	0.022	0.320	0.024
Patient 14	0.211	0.026	0.349	0.042
Patient 15	0.205	0.033	0.231	0.020
Patient 16	0.189	0.046	0.404	0.032
Patient 17	0.180	0.028	0.257	0.016
Mean ± STD	0.200 ± 0.102	0.032 ± 0.009	0.240 ± 0.089	0.029 ± 0.011

4.4.3 FEM verification

As the last part of our analyses, we assess the displacement and stress fields in the tipping and biting scenarios to ensure that the stress patterns are smooth and have no unrealistic stress concentrations. To do so, we run the simulations using the PolyFEM [109] FE solver. PolyFEM is an FE simulation toolkit that supports elastodynamic deformations with linear and non-linear material models. It provides an adaptive p-refinement that allows increasing the order of basis functions for specific domains while utilizing linear basis functions for the other domains. Hence, we use Tet10 elements for the PDL layer to increase the simulations' accuracy and avoid element locking issues [111]. Besides, PolyFEM uses the incremental potential contact formulation [62] for contact response and friction, which ensures valid, penetration-free meshes during the entire simulation. The contacts are automatically detected by proximity; hence, there is no need to specify contact surfaces, which significantly simplifies the scene setup.

The simulation results are visualized in ParaView [7]. Figure 4.8 shows the result of the biting scenario of a selected patient, including the resulting displacement and stress fields. Due to the deformation of the PDL layer under the applied biting load, the displacement fields can be seen both on the mandibular jaw and the posterior maxillary teeth (A). Besides, stress concentrations can be observed on the associated PDL layers, especially at root apexes and bifurcation regions indicated by arrows in (B).

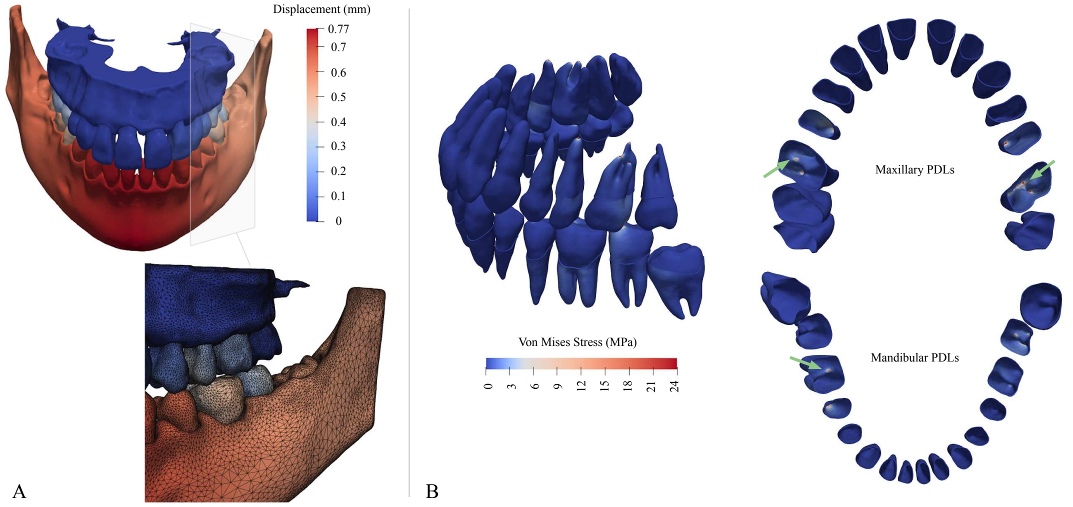

FIGURE 4.8: The obtained displacement (**A**) and stress (**B**) fields for Patient 17 under the biting scenario. Note that due to the deformation of the PDL layer caused by the exerted biting force from the contacting mandibular teeth, the displacement field is seen on the posterior maxillary teeth (**A**). Likewise, stress concentrations can be seen on the associated PDL layers, especially at the apexes and furcation regions, indicated by arrows in **B**.

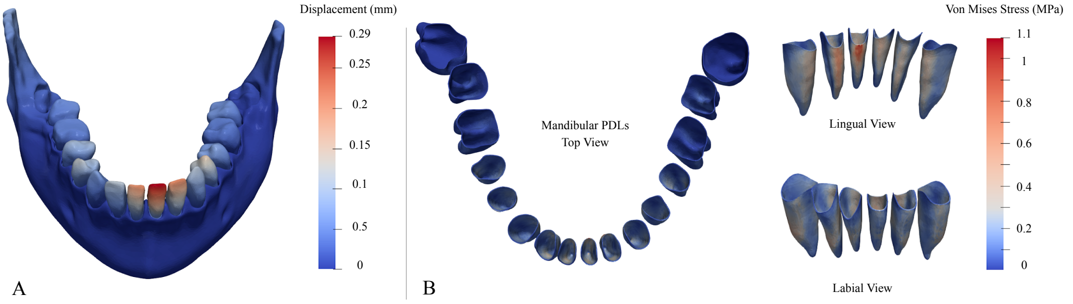

FIGURE 4.9: The obtained displacement (**A**) and stress (**B**) fields for the mandibular jaw of Patient 17 under the tipping scenario. Note that stress concentration is observed on the lingual side of anterior teeth due to the labiolingual tipping load.

Figure 4.9 illustrates the result of the auto-generated uncontrolled tipping scenario for the mandibular jaw of the same patient. As seen in [41], the anterior teeth have higher displacement fields than the posterior teeth under an identical load (A). Hence, higher stress concentrations can be seen on the lingual side of the PDLs associated with the anterior teeth (B). Additionally, simulation results of different patients in the tipping scenario are shown in Figure 4.10. As can be noticed, the stress values considerably change from one patient to another, indicating the importance of utilizing population models for multi-patient analysis.

It should be noted that although we have tested our models under two scenarios, the developed volumetric meshes can be used in various scenarios and different FE frameworks. Furthermore, the FE models can benefit from using more complex material models, boundary, and loading conditions. For example, the

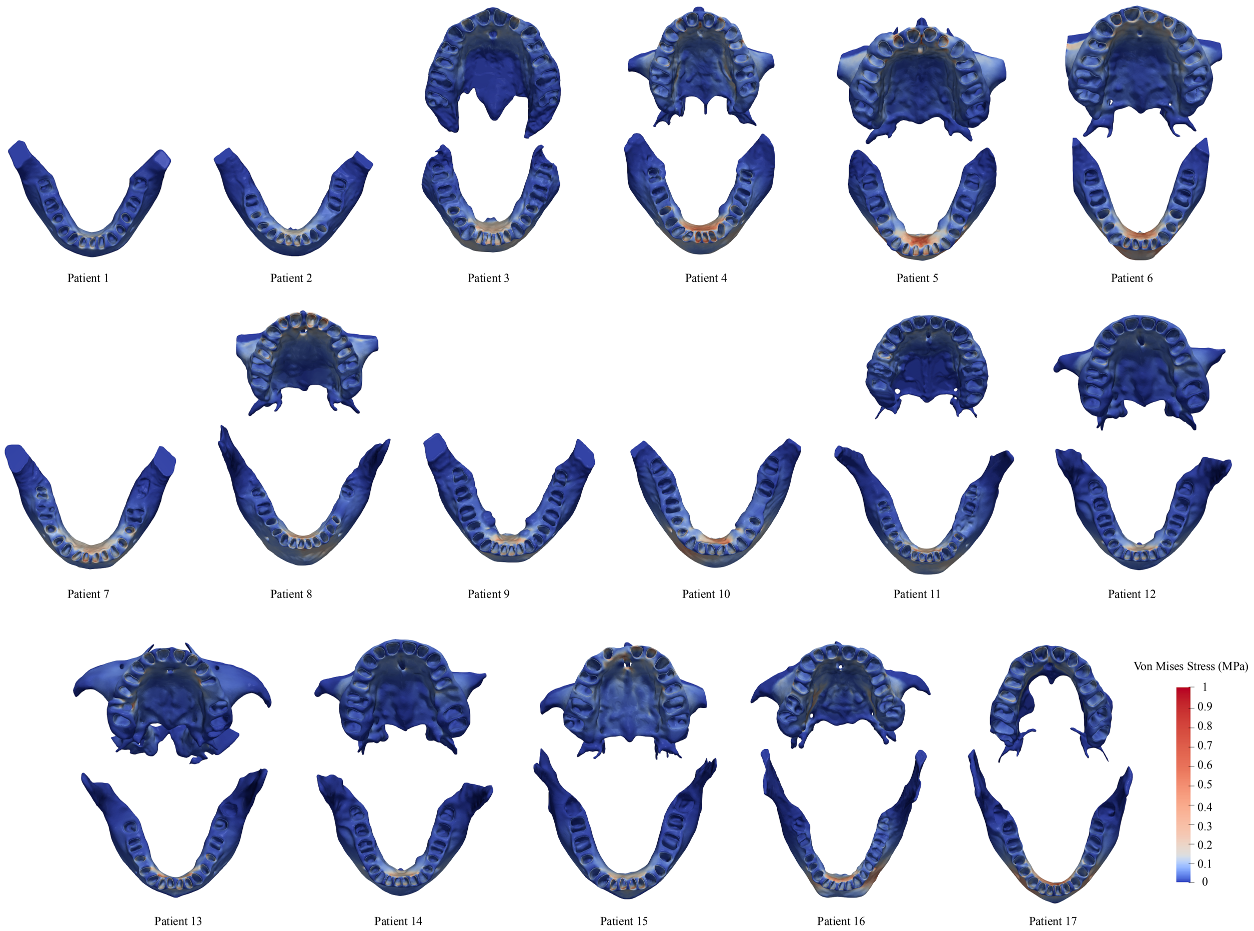

FIGURE 4.10: A comparison of stress distributions of all utilized jaws in the tipping scenario with identical load magnitudes. The stress fields are clipped within the range [0, 1] MPa to represent the changes better using the same color map. As can be noticed, the stress values and concentrations considerably vary across different patients, which indicates the importance of utilizing population models for multi-patient analysis and generalizability in computational modeling studies.

provided meshes can be integrated with outputs of other studies [90, 128] to consider masticatory muscles for more realistic biting scenarios.

4.5 General discussion

The utilized and conventional meshing approaches generate the volumetric meshes using reconstructed geometries based on accurately segmented scans. However, obtaining such an accurate segmentation is inherently time-consuming and labor-intensive and, in some cases, could be highly challenging due to the complexity of the problem or lack of high-resolution scans [134]. The template-based deformation techniques [64, 92] can be used to automatically reconstruct the 3D geometries by creating a template mesh and deforming it according to the new data samples. Still, deforming a template mesh using registration approaches or deep learning methods requires accurate spatial registration and high-quality volumetric meshes with no distorted elements.

Obtaining accurate spatial registration and high-quality volumetric meshes for the human jaw can be challenging, as there are large variations among geometries of different patients (Figure 4.2), such as geometrical differences in the bones and teeth, missing teeth, and topological changes in the number of roots, e.g., the mandibular and maxillary molars with two to four roots. Therefore, to include different types of variations in the data for a plausible deformation, one needs to have different templates covering missing teeth or various numbers of roots. This in turn is a time-consuming process and can increase the complexity of the model. On the other hand, large deformations in small volumes of teeth and roots can result in distorted elements, preventing us from generating high-quality meshes, especially in the PDL layers with thin structures that need to be modeled with fine volumetric elements.

The current study introduces the largest-ever dataset of patient-specific human jaws reconstructed from CBCT scans. We believe this unique clinically validated dataset would pave the way for future population studies in the field. More specifically, data augmentation techniques using machine learning [65, 94] can be applied to the Open-Full-Jaw dataset to expand its size and variability by generating plausible synthetic data. In addition, this would enable us to use deep learning methods, which require a large amount of data for training. Still, one needs to use a dataset with enough variations for sampling and assess the generated samples' validity.

4.6 Conclusion

In this work, we presented a large open-access dataset, called Open-Full-Jaw (`https://github.com/diku-dk/Open-Full-Jaw`), with patient-specific models of 17 human mandibles and maxillae. The dataset contains clinically validated segmented geometries shared as dense surface meshes and adaptive quality volumetric with conformal meshes in the contacting interfaces. It also includes the principal axes for each patient's teeth and the generated FEM files of the uncontrolled tipping and biting scenarios for all patients. Finally, we share the nearly-automated pipeline used for geometry processing, re-meshing, and generating volumetric meshes.

In addition, we evaluated the generated models and quantified them in terms of the mesh quality and accuracy of the models, and compared the results with the state-of-the-art. The obtained results indicate that the developed computational models are precise, considering the low error/distance from input surface meshes. Moreover, the quality of the volumetric elements evaluated based on different quality measurements imply that the generated volumetric meshes consist of quality elements suitable for the FEM of the human jaw. Hence, we believe the Open-Full-Jaw dataset can be used in various FE scenarios and a wide range of intra- and inter-patient analyses.

The shared repository includes all detailed information for reproducing the models of this study. In addition, the utilized pipeline allows other researchers in the field to generate quality volumetric meshes and FE model files directly using dense and irregular meshes with minimal human intervention. This will help other researchers easily extend their datasets without spending much time and effort on manually cleaning up the meshes and non-trivially producing conformal meshes. Furthermore, similar concepts as those used in this study to generate population models of the tooth-supporting complex can be adapted to other areas, such as pelvic girdles and hip joints [80].

Chapter 5

Summary and Future Work

This chapter summarizes the contributions of all the resulting publications presented in the previous chapters. In addition, it discusses possible future directions for the research carried out during this project. The summary is kept brief, as more detailed discussion and summaries are given in each chapter.

5.1 Summary

Accurate patient-specific computational modeling allows us to improve the efficiency of orthodontic treatment planning, e.g., in correcting malpositioned teeth or jaw. This requires developing accurate and reliable FEMs derived from patients' medical imaging and investigating the behavior of the human jaw and teeth under defined scenarios. For example, one can use the FEMs to better predict a patient's teeth movement under a physical load exerted from the orthodontic appliances, which leads to efficient and non-invasive treatment planning. Although a patient-specific FEM provides excellent and helpful information for a patient, deduced behavior of a single-patient analysis may not be suitable for answering clinical questions regarding a larger population due to ignoring the influence of geometrical variations across the population. Most studies focusing on the biomechanical behavior of the human jaw and tooth movement modeling are limited to a single-model analysis, which raises the question of whether their results can be generalized to a larger population. This is mainly because developing patient-specific FEMs of a population is highly time-consuming and labor-intensive, making the model generation pipeline and population analysis a non-trivial task.

In Chapter 1.3, we summarized some of the main challenges in tooth movement modeling using the FEM: (1) the lack of publicly-available high-resolution CBCT scans; (2) the highly challenging and time-consuming tooth-bone segmentation task with no publicly available dataset to be used for building complex models such as deep learning networks; (3) the errors produced by conventional discretization approaches resulting in numerical errors and instabilities; (4) the lack of publicly available research data including geometries and meshes; (5) the parameter tweaking requirement for FEM solver; last but not the least

(6) difficulties in analyzing multi-patient simulation results to get generalizable conclusions. In this thesis, we tackled most of these challenges by utilizing computer science skills and benefiting from international collaborations with clinical experts and researchers. Our contribution to addressing these challenges is summarized below.

In Chapter 2, we developed three detailed patient-specific FEMs of human mandibles using the conventional semi-automatic segmentation and mesh processing approaches as a contribution to the challenges of multi-patient analysis. Next, we examined intra- and inter-patient teeth movement variations under an identical scenario with different loading conditions. We then assessed the influence of geometrical variations on the tooth displacements across different patients' teeth. This was done by modeling the movement of each patient's tooth as a nonlinear function of both load and tooth size to provide a more generalized tooth movement prediction. Besides, In Chapter 3, we used the same models under more complex scenarios and loading systems to mimic different tooth movement types. Registration was used to align teeth geometries and the center of rotation trajectories, enabling us to define the loading conditions and perform a consistent inter-patient analysis. Both of the mentioned studies could benefit from more FEMs. However, this was not attainable due to the time-consuming and labor-intensive segmentation, geometry, and meshing procedures. Nevertheless, the developed meshes are made publicly available in "OpenJaw Dataset", to overcome the data availability challenges.

In Appendix A, we used a deep learning method developed based on a multi-planar U-Net architecture [95] to automate the hip area segmentation from CTs. We used an active learning-based strategy to fine-tune the network (trained on data with inferior/limited delineations) with a few accurate segmentations in an interactive way, to improve the segmentation accuracy of the model. A generalized loss function was used to enforce gaps in the required regions, such as regions where cartilages reside.

In Appendix B, we applied the same deep learning-based approach to automate the tooth-bone segmentations from CBCT scans. The prediction outcomes using the trained network were used as initial tooth-bone segmentations and manually refined to achieve the desired accuracy, clinically verified by the clinical experts. Based on our experience using the traditional semi-automated approaches, it could take up to 10 days to provide an accurate tooth-bone segmentation of a relatively low-resolution CBCT scan containing metal-filling artifacts. Utilizing such a deep learning-based approach for CBCT segmentation reduced the required manual refinements from several days to a few hours, making it feasible to extend our dataset.

The study in Chapter 4 attempted to cope with all the involved manual procedures in the geometry and mesh processing steps while avoiding any undesired gaps/penetrations in the contacting interfaces. Besides, it significantly contributed to the lack of publicly available research data. It suggests utilizing an FE solver that automatically detects the contacting surfaces and requires no parameter tweaking for contact definition.

More specifically, we developed a nearly automated pipeline for generating quality, conformal simulation-ready FEMs. The pipeline accepts the segmented geometries with irregular and dense surface meshes as input and applies a multi-domain meshing approach that outputs conformal volumetric meshes suitable for FE simulations. By applying the mentioned pipeline to the improved segmentation results of B, we introduced an open-access repository called "Open-Full-Jaw" in Chapter 4, composed of 29 patient-specific human mandibles and maxillae developed from 17 different CBCT scans.

For the reproducibility of our study, we employed open-source meshing tools to develop a nearly automated model generation pipeline that minimizes the required manual tasks and any potential biases in the model generation process caused by human intervention. The inputs to our pipeline (unprocessed reconstructed geometries) can be imported into any desired open-source or commercial meshing tools or FE frameworks to re-mesh and generate computational models. In addition, the pipeline allows other researchers to easily extend their datasets without spending much time manually cleaning up the meshes and non-trivially producing conformal meshes. This pipeline reduces the time needed for developing FE models using the conventional approach, which can take a few days to weeks, to less than an hour. Besides, it can significantly help with the reproducibility of other studies in the future.

Finally, in collaboration with other researchers, we showed that a pipeline with similar concepts to those presented in Chapter 4 could be applied to the pelvic girdles and hip joints to eliminate most of the manual procedures in the FE model generation pipeline. This resulted in a paper presented in Appendix C, where the segmentation results of Appendix A were improved and used as inputs to a multi-material meshing tool to provide a dataset of 11 subject-specific models of the hip joint area, including the bones and cartilages.

5.2 Future work

Now that we know how to efficiently create FEMs of a population, it opens up a new field of research focusing on population studies of human jaws and tooth movements. This would require tackling multi-patient analysis on a larger scale; for example, how should one formulate clinically interesting questions to learn from simulation results? How should one deal with the massive simulation output? Can this be useful to deduce interesting results with confidence in general trends to improve the treatment plans in orthodontic clinics?

Our clinically-validated open-access dataset of the human jaws and the shared pipeline for generating them lays a foundation for future studies focusing on finding correlations between the patient-specific features and tooth movement variations in large cohorts. This requires a suitable formulation of the clinical hypothesis and numerous simulations across the population. Data analysis methods such as advanced machine learning techniques can then be applied to the processed simulation results to find fine-grained conclusions such as clinically interesting trajectories, similarities, or dissimilarities across the population.

For example, the generated FEMs can provide many simulation results to train nonparametric models to achieve more accurate tooth movement predictions. In addition, one can explore meaningful and clinically interesting representations obtained from complex models, e.g., deep learning, trained based on the simulation results.

The current study can help clinicians quickly and efficiently generate reproducible patient-specific FEMs for their patients with minimal human intervention in geometry reconstruction and model generation. This, in turn, allows for conducting potential clinical studies for teeth movement validation by comparing the predicted results with clinically measured values. In addition, one could utilize the initial tooth movement and the predicted stress/strain in the tooth-supporting complex to mimic long-term tooth movement for cost- and time-efficient treatment plans, resulting in societal and clinical impacts.

From the clinical point of view, patient-specific FEMs could be used as safety monitoring tools in cases where the designed treatment plan can lead to root resorption due to excessive stress or fenestration in regions with a narrower bone thickness. Besides, from the educational point of view, one can utilize the developed FEMs of this work as a digital typodont for dentistry or orthodontic students to provide better visualization and understanding of how the physical forces can lead to the mentioned diseases.

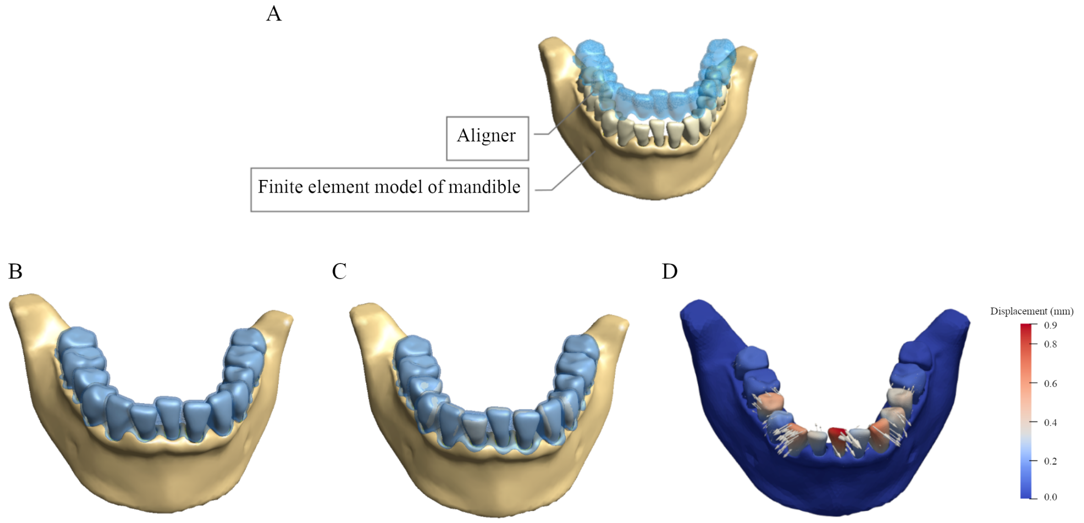

Figure 5.1: **A:** Modeling transparent-aligner treatments using the FE models of the Open-Full-Jaw dataset. **B:** A *retainer* model perfectly fits the patient's teeth to keep them in the current position. **C:** An *aligner* model designed to reach the desired target position of the teeth. As can be noticed, there are some disagreements in the current position of the teeth and the designed aligner illustrated as bright shades in **C**. Such disagreements in teeth positions result in loads exerted from the aligner surface to the teeth pushing them towards the planned positions. **D:** The displacement fields of FE results, and the displacement arrows that indicate the direction and magnitude of the teeth displacements.

Last but not least, as an ongoing project, we use the same FEMs obtained in Chapter 4 to design and develop transparent-aligner models to reach the desired target position of the teeth, as shown in Figure 5.1. This project aims to study the influence of the aligners' shapes and that of associated auxiliary tools on effectively and accurately moving the teeth to planned positions. With the gained experience in generating large-scale FEMs of human jaws and by adapting the pipeline presented in Chapter 4 with some geometry processing methods suitable for the task, we hope to develop various aligner models for each patient. The effectiveness of each aligner type can then be examined based on results from different patients.

Bibliography

[1] 3Shape Trios Intraoral Scanner. https://www.3shape.com/en/scanners/trios

[2] Autodesk Meshmixer. http://www.meshmixer.com/

[3] FEBio Software Suite. https://febio.org/

[4] Virtual Population. https://itis.swiss/virtual-population/, [Online; accessed December 26, 2021]

[5] WIAS-Software, TetGen. http://wias-berlin.de/software/index.jsp?id=TetGen&lang=1

[6] OpenJaw Dataset. https://erda.ku.dk/archives/97cd65fe80e83356f618bb9fbc7d5980/published-archive.html (2021)

[7] Ahrens, J., Geveci, B., Law, C.: Paraview: An end-user tool for large data visualization. The visualization handbook **717**(8) (2005)

[8] Arbelaez, M.L., Garcia, S.M.V., Lopez, J.P., Avila, D., Munevar, J.C., Pauwels, A.: Effect of bisphosphonates on orthodontic tooth movement in osteoporotic patients: A review. Journal of the World Federation of Orthodontists **7**(2), 49–55 (2018)

[9] Arnold, D.N., Logg, A., Schlager, M., Narayanan, H.: FEMTable. https://www-users.cse.umn.edu/~arnold/femtable/ (2022)

[10] Ausiello, P., Gloria, A., Maietta, S., Watts, D.C., Martorelli, M.: Stress distributions for hybrid composite endodontic post designs with and without a ferrule: Fea study. Polymers **12**(8), 1836 (2020)

[11] Baker, T.J.: Element quality in tetrahedral meshes. In: 7th International Conference on Finite Element Methods in Flow Problems. p. 1018 (1989)

[12] Baron, M., Hudson, M., Dagenais, M., Macdonald, D., Gyger, G., El Sayegh, T., Pope, J., Fontaine, A., Masetto, A., Matthews, D., et al.: Relationship between disease characteristics and oral radiologic findings in systemic sclerosis: results from a canadian oral health study. Arthritis care & research **68**(5), 673–680 (2016)

[13] Barone, S., Paoli, A., Paolo, N., Razionale, A.V., Giannese, M.: Mechanical and geometrical properties assessment of thermoplastic materials for biomedical application. In: Advances on Mechanics, Design Engineering and Manufacturing, pp. 437–446. Springer (2017)

[14] Bayome, M., Park, J.H., Kook, Y.A.: New three-dimensional cephalometric analyses among adults with a skeletal class i pattern and normal occlusion. The Korean Journal of Orthodontics **43**(2), 62–73 (2013)

[15] Beek, M., Koolstra, J., Van Ruijven, L., Van Eijden, T.: Three-dimensional finite element analysis of the human temporomandibular joint disc. Journal of biomechanics **33**(3), 307–316 (2000)

[16] Benaissa, A., Merdji, A., Bendjaballah, M.Z., Ngan, P., Mukdadi, O.M.: Stress influence on orthodontic system components under simulated treatment loadings. Computer Methods and Programs in Biomedicine **195**, 105569 (2020)

[17] Benazzi, S., Nguyen, H.N., Kullmer, O., Hublin, J.J.: Unravelling the functional biomechanics of dental features and tooth wear. PLoS One **8**(7), e69990 (2013)

[18] Besl, P.J., McKay, N.D.: A method for registration of 3-D shapes. IEEE Transactions on Pattern Analysis and Machine Intelligence **14**(2), 239–256 (1992)

[19] Boryor, A., Hohmann, A., Geiger, M., Wolfram, U., Sander, C., Sander, F.G.: A downloadable meshed human canine tooth model with pdl and bone for finite element simulations. Dental Materials **25**(9), e57–e62 (2009)

[20] Buikstra, J.E.: Standards for data collection from human skeletal remains. Arkansas archaeological survey research series **44** (1994)

[21] Burstone, C.J.: The biomechanics of tooth movement. Vistas in Orthodontics pp. 197–213 (1962)

[22] Caendish, J.C., Field, D.A., Frey, W.H.: An approach to automatic three-dimensional finite element mesh generation. International Journal for Numerical Methods in Engineering **21**(2), 329–347 (1985)

[23] Cattaneo, P.M., Cornelis, M.A.: Orthodontic tooth movement studied by finite element analysis: an update. what can we learn from these simulations? Current Osteoporosis Reports pp. 1–7 (2021)

[24] Cattaneo, P.M., Dalstra, M., Melsen, B.: Moment-to-force ratio, center of rotation, and force level: A finite element study predicting their interdependency for simulated orthodontic loading regimens. American Journal of Orthodontics and Dentofacial Orthopedics **133**(5), 681–689 (2008)

[25] Cattaneo, P., Dalstra, M., Melsen, B.: The finite element method: A tool to study orthodontic tooth movement. Journal of Dental Research **84**(5), 428–433 (2005)

[26] Cervino, G., Fiorillo, L., Arzukanyan, A.V., Spagnuolo, G., Campagna, P., Cicciù, M.: Application of bioengineering devices for stress evaluation in dentistry: the last 10 years fem parametric analysis of outcomes and current trends. Minerva Stomatologica **69**(1), 55–62 (2020)

[27] Chen, J., Li, W., Swain, M.V., Darendeliler, M.A., Li, Q.: A periodontal ligament driven remodeling algorithm for orthodontic tooth movement. Journal of Biomechanics **47**(7), 1689–1695 (2014)

[28] Chen, Y., Medioni, G.: Object modelling by registration of multiple range images. Image and Vision Computing **10**(3), 145–155 (1992)

[29] Christiansen, R.L., Burstone, C.J.: Centers of rotation within the periodontal space. American Journal of Orthodontics **55**(4), 353–369 (1969)

[30] Clark, K., Vendt, B., Smith, K., Freymann, J., Kirby, J., Koppel, P., Moore, S., Phillips, S., Maffitt, D., Pringle, M., et al.: The cancer imaging archive (TCIA): maintaining and operating a public information repository. Journal of Digital Imaging **26**(6), 1045–1057 (2013)

[31] Connolly, B., Wang, C.: Segmented CT pelvis scans with annotated anatomical landmarks (2019), `doi:10.23698/aida/ctpel`

[32] Ding, X., Liao, S.H., Zhu, X.H., Wang, H.M.: Influence of orthotropy on biomechanics of peri-implant bone in complete mandible model with full dentition. BioMed research international **2014** (2014)

[33] Dorow, C., Krstin, N., Sander, F.G.: Determination of the mechanical properties of the periodontal ligament in a uniaxial tensional experiment. Journal of Orofacial Orthopedics/Fortschritte der Kieferorthopädie **64**(2), 100–107 (2003)

[34] Dorow, C., Schneider, J., Sander, F.G.: Finite element simulation of in vivo tooth mobility in comparison with experimental results. Journal of Mechanics in Medicine and Biology **3**(01), 79–94 (2003)

[35] Dreischarf, M., Zander, T., Shirazi-Adl, A., Puttlitz, C., Adam, C., Chen, C., Goel, V., Kiapour, A., Kim, Y., Labus, K., et al.: Comparison of eight published static finite element models of the intact lumbar spine: predictive power of models improves when combined together. Journal of biomechanics **47**(8), 1757–1766 (2014)

[36] Ernstbrunner, L., Werthel, J., Hatta, T., Thoreson, A., Resch, H., An, K., Moroder, P.: Biomechanical analysis of the effect of congruence, depth and radius on the stability ratio of a simplistic 'ball-and-socket'joint model. Bone & joint research **5**(10), 453–460 (2016)

[37] Fedorov, A., Beichel, R., Kalpathy-Cramer, J., Finet, J., Fillion-Robin, J.C., Pujol, S., Bauer, C., Jennings, D., Fennessy, F., Sonka, M., et al.: 3D Slicer as an image computing platform for the quantitative imaging network. Magnetic Resonance Imaging **30**(9), 1323–1341 (2012)

[38] Fill, T.S., Toogood, R.W., Major, P.W., Carey, J.P.: Analytically determined mechanical properties of, and models for the periodontal ligament: critical review of literature. Journal of Biomechanics **45**(1), 9–16 (2012)

[39] Foley, J.D., Van, F.D., Van Dam, A., Feiner, S.K., Hughes, J.F., Hughes, J.: Computer graphics: principles and practice, vol. 12110. Addison-Wesley Professional (1996)

[40] Freitag, L.A., Ollivier-Gooch, C.: Tetrahedral mesh improvement using swapping and smoothing. International Journal for Numerical Methods in Engineering **40**(21), 3979–4002 (1997)

[41] Gholamalizadeh, T., Darkner, S., Cattaneo, P.M., Søndergaard, P., Erleben, K.: Mandibular teeth movement variations in tipping scenario: A finite element study on several patients. In: Computational Biomechanics for Medicine, pp. 31–43. Springer (2021)

[42] Gholamalizadeh, T., Darkner, S., Søndergaard, P.L., Erleben, K.: A multi-patient analysis of the center of rotation trajectories using finite element models of the human mandible. Plos one **16**(11), e0259794 (2021)

[43] Gholamalizadeh, T., Moshfeghifar, F., Ferguson, Z., Schneider, T., Panozzo, D., Darkner, S., Makaremi, M., Chan, F., Søndergaard, P.L., Erleben, K.: Open-Full-Jaw: An open-access dataset and pipeline for finite element models of human jaw. Computer Methods and Programs in Biomedicine p. 107009 (2022), `https://github.com/diku-dk/Open-Full-Jaw`

[44] Gosselin, M.C., Neufeld, E., Moser, H., Huber, E., Farcito, S., Gerber, L., Jedensjö, M., Hilber, I., Di Gennaro, F., Lloyd, B., et al.: Development of a new generation of high-resolution anatomical models for medical device evaluation: the virtual population 3.0. Physics in Medicine & Biology **59**(18), 5287 (2014)

[45] Hamanaka, R., Yamaoka, S., Anh, T.N., Tominaga, J.y., Koga, Y., Yoshida, N.: Numeric simulation model for long-term orthodontic tooth movement with contact boundary conditions using the finite element method. American Journal of Orthodontics and Dentofacial Orthopedics **152**(5), 601–612 (2017)

[46] Hohmann, A., Kober, C., Young, P., Dorow, C., Geiger, M., Boryor, A., Sander, F.M., Sander, C., Sander, F.G.: Influence of different modeling strategies for the periodontal ligament on finite element simulation results. American Journal of Orthodontics and Dentofacial Orthopedics **139**(6), 775–783 (2011)

[47] Hu, Y., Schneider, T., Wang, B., Zorin, D., Panozzo, D.: Fast tetrahedral meshing in the wild. ACM Trans. Graph. **39**(4), 117–1 (2020)

[48] Hu, Y., Schneider, T., Wang, B., Zorin, D., Panozzo, D.: Fast tetrahedral meshing in the wild. ACM Trans. Graph. **39**(4) (Jul 2020)

[49] Hu, Y., Zhou, Q., Gao, X., Jacobson, A., Zorin, D., Panozzo, D.: Tetrahedral meshing in the wild. ACM Trans. Graph. **37**(4), 60–1 (2018)

[50] Huang, H.L., Tsai, M.T., Yang, S.G., Su, K.C., Shen, Y.W., Hsu, J.T.: Mandible integrity and material properties of the periodontal ligament during orthodontic tooth movement: A finite-element study. Applied Sciences **10**(8), 2980 (2020)

[51] Jacobson, A., Kavan, L., Sorkine, O.: Robust inside-outside segmentation using generalized winding numbers. ACM Trans. Graph. **32**(4) (2013)

[52] Jacobson, A., Panozzo, D., et al.: libigl: A simple C++ geometry processing library. `https://libigl.github.io/` (2018)

[53] Jones, M., Hickman, J., Middleton, J., Knox, J., Volp, C.: A validated finite element method study of orthodontic tooth movement in the human subject. Journal of Orthodontics **28**(1), 29–38 (2001)

[54] Kawamura, J., Park, J.H., Kojima, Y., Kook, Y.A., Kyung, H.M., Chae, J.M.: Biomechanical analysis for total mesialization of the mandibular dentition: A finite element study. Orthodontics & craniofacial research **22**(4), 329–336 (2019)

[55] Kawamura, J., Park, J.H., Tamaya, N., Oh, J.H., Chae, J.M.: Biomechanical analysis of the maxillary molar intrusion: A finite element study. American Journal of Orthodontics and Dentofacial Orthopedics (2022)

[56] Kawarizadeh, A., Bourauel, C., Zhang, D., Götz, W., Jäger, A.: Correlation of stress and strain profiles and the distribution of osteoclastic cells induced by orthodontic loading in rat. European Journal of Oral Sciences **112**(2), 140–147 (2004)

[57] Keilig, L., Drolshagen, M., Tran, K., Hasan, I., Reimann, S., Deschner, J., Brinkmann, K., Krause, R., Favino, M., Bourauel, C.: In vivo measurements and numerical analysis of the biomechanical characteristics of the human periodontal ligament. Annals of Anatomy-Anatomischer Anzeiger **206**, 80–88 (2016)

[58] Kluess, D.: Finite element analysis in orthopaedic biomechanics. In: Finite element analysis. Citeseer (2010)

[59] Komatsu, K.: Mechanical strength and viscoelastic response of the periodontal ligament in relation to structure. Journal of Dental Biomechanics **2010** (2010)

[60] Lavorgna, L., Cervino, G., Fiorillo, L., Di Leo, G., Troiano, G., Ortensi, M., Galantucci, L., Cicciù, M.: Reliability of a virtual prosthodontic project realized through a 2D and 3D photographic acquisition: An experimental study on the accuracy of different digital systems. International Journal of Environmental Research and Public Health **16**(24), 5139 (2019)

[61] Lee, J.S., Choi, H.I., Lee, H., Ahn, S.J., Noh, G.: Biomechanical effect of mandibular advancement device with different protrusion positions for treatment of obstructive sleep apnoea on tooth and facial bone: A finite element study. Journal of oral rehabilitation **45**(12), 948–958 (2018)

[62] Li, M., Ferguson, Z., Schneider, T., Langlois, T., Zorin, D., Panozzo, D., Jiang, C., Kaufman, D.M.: Incremental potential contact: Intersection- and inversion-free large deformation dynamics. ACM Trans. Graph. (SIGGRAPH) **39**(4) (2020)

[63] Li, Y., Jacox, L.A., Little, S.H., Ko, C.C.: Orthodontic tooth movement: The biology and clinical implications. The Kaohsiung Journal of Medical Sciences **34**(4), 207–214 (2018)

[64] Liang, L., Kong, F., Martin, C., Pham, T., Wang, Q., Duncan, J., Sun, W.: Machine learning based 3D geometry reconstruction and modeling of aortic valve deformation using 3D computed tomography images. International journal for numerical methods in biomedical engineering **33**(5), e2827 (2017)

[65] Liang, L., Liu, M., Martin, C., Elefteriades, J.A., Sun, W.: A machine learning approach to investigate the relationship between shape features and numerically predicted risk of ascending aortic aneurysm. Biomechanics and modeling in mechanobiology **16**(5), 1519–1533 (2017)

[66] Liang, W., Rong, Q., Lin, J., Xu, B.: Torque control of the maxillary incisors in lingual and labial orthodontics: A 3-dimensional finite element analysis. American Journal of Orthodontics and Dentofacial Orthopedics **135**(3), 316–322 (2009)

[67] Liao, Z., Chen, J., Li, W., Darendeliler, M.A., Swain, M., Li, Q.: Biomechanical investigation into the role of the periodontal ligament in optimising orthodontic force: a finite element case study. Archives of Oral Biology **66**, 98–107 (2016)

[68] Likitmongkolsakul, U., Smithmaitrie, P., Samruajbenjakun, B., Aksornmuang, J.: Development and validation of 3D finite element models for prediction of orthodontic tooth movement. International Journal of Dentistry **2018** (2018)

[69] Liu, A., Joe, B.: Relationship between tetrahedron shape measures. BIT Numerical Mathematics **34**(2), 268–287 (1994)

[70] Logan, D.L.: A first course in the finite element method. Cengage Learning (2016)

[71] Lorensen, W.E., Cline, H.E.: Marching cubes: A high resolution 3d surface construction algorithm. ACM siggraph computer graphics **21**(4), 163–169 (1987)

[72] Maas, S., Rawlins, D., Weiss, J., Ateshian, G.: FEBio 2.8 user manual (2018)

[73] Maas, S.A., Ellis, B.J., Ateshian, G.A., Weiss, J.A.: FEBio: finite elements for biomechanics. Journal of Biomechanical Engineering **134**(1) (2012)

[74] McCormack, S.W., Witzel, U., Watson, P.J., Fagan, M.J., Gröning, F.: The biomechanical function of periodontal ligament fibres in orthodontic tooth movement. Plos One **9**(7), e102387 (2014)

[75] Meagher, D.: Geometric modeling using octree encoding. Computer graphics and image processing **19**(2), 129–147 (1982)

[76] Melsen, B., Cattaneo, P.M., Dalstra, M., Kraft, D.C.: The importance of force levels in relation to tooth movement. In: Seminars in Orthodontics. vol. 13, pp. 220–233. Elsevier (2007)

[77] Meyer, B.N., Chen, J., Katona, T.R.: Does the center of resistance depend on the direction of tooth movement? American Journal of Orthodontics and Dentofacial Orthopedics **137**(3), 354–361 (2010)

[78] Misztal, M.K., Erleben, K., Bargteil, A., Fursund, J., Christensen, B.B., Bærentzen, J.A., Bridson, R.: Multiphase flow of immiscible fluids on unstructured moving meshes. IEEE Transactions on Visualization and Computer Graphics **20**(1), 4–16 (2013)

[79] Mortazavi, H., Baharvand, M.: Review of common conditions associated with periodontal ligament widening. Imaging science in dentistry **46**(4), 229–237 (2016)

[80] Moshfeghifar, F., Gholamalizadeh, T., Ferguson, Z., Schneider, T., Nielsen, M.B., Panozzo, D., Darkner, S., Erleben, K.: Libhip: An open-access hip joint model repository suitable for finite element method simulation. submitted to Computer Methods and Programs in Biomedicine (March 2022)

[81] Moshfeghifar, F., Nielsen, M.K., Tascón-Vidarte, J.D., Darkner, S., Erleben, K.: A direct geometry processing cartilage generation method using segmented bone models from datasets with poor cartilage visibility. arXiv preprint arXiv:2203.10667 (2022)

[82] Myronenko, A., Song, X.: Point set registration: Coherent point drift. IEEE Transactions on Pattern Analysis and Machine Intelligence **32**(12), 2262–2275 (2010)

[83] Nanci, A., Bosshardt, D.D.: Structure of periodontal tissues in health and disease. Periodontology 2000 **40**(1), 11–28 (2006)

[84] Natali, A.N., Carniel, E.L., Pavan, P.G., Sander, F.G., Dorow, C., Geiger, M.: A visco-hyperelastic-damage constitutive model for the analysis of the biomechanical response of the periodontal ligament. Journal of Biomechanical Engineering **130**(3) (2008)

[85] Nyashin, Y., Nyashin, M., Osipenko, M., Lokhov, V., Dubinin, A., Rammerstorfer, F., Zhurov, A.: Centre of resistance and centre of rotation of a

tooth: experimental determination, computer simulation and the effect of tissue nonlinearity. Computer Methods in Biomechanics and Biomedical Engineering **19**(3), 229–239 (2016)

[86] Oenning, A.C., Freire, A.R., Rossi, A.C., Prado, F.B., Caria, P.H.F., Correr-Sobrinho, L., Haiter-Neto, F.: Resorptive potential of impacted mandibular third molars: 3d simulation by finite element analysis. Clinical oral investigations **22**(9), 3195–3203 (2018)

[87] Oh, M.B., Mo, S.S., Hwang, C.J., Chung, C., Kang, J.M., Lee, K.J.: The 3-dimensional zone of the center of resistance of the mandibular posterior teeth segment. American Journal of Orthodontics and Dentofacial Orthopedics **156**(3), 365–374 (2019)

[88] OpenStax College, Anatomy & Physiology, Connexions Web site: 2409 tooth.jpg, available under the CC BY 3.0 license. (2013), `https://commons.wikimedia.org/wiki/File:2409_Tooth.jpg`, [Online; accessed July 1, 2022]

[89] Ortún-Terrazas, J., Cegoñino, J., Santana-Penín, U., Santana-Mora, U., del Palomar, A.P.: Approach towards the porous fibrous structure of the periodontal ligament using micro-computerized tomography and finite element analysis. Journal of the Mechanical Behavior of Biomedical Materials **79**, 135–149 (2018)

[90] Ortún-Terrazas, J., Cegoñino, J., Del Palomar, A.P.: In silico study of cuspid'periodontal ligament damage under parafunctional and traumatic conditions of whole-mouth occlusions. a patient-specific evaluation. Computer methods and programs in biomedicine **184**, 105107 (2020)

[91] Osher, S., Sethian, J.A.: Fronts propagating with curvature-dependent speed: Algorithms based on hamilton-jacobi formulations. Journal of computational physics **79**(1), 12–49 (1988)

[92] Pak, D.H., Liu, M., Kim, T., Liang, L., McKay, R., Sun, W., Duncan, J.S.: Distortion energy for deep learning-based volumetric finite element mesh generation for aortic valves. In: International Conference on Medical Image Computing and Computer-Assisted Intervention. pp. 485–494. Springer (2021)

[93] Park, M., Na, Y., Park, M., Ahn, J.: Biomechanical analysis of distalization of mandibular molars by placing a mini-plate: a finite element study. The Korean Journal of Orthodontics **47**(5), 289–297 (2017)

[94] Pascoletti, G., Aldieri, A., Terzini, M., Bhattacharya, P., Calì, M., Zanetti, E.M.: Stochastic PCA-based bone models from inverse transform sampling: Proof of concept for mandibles and proximal femurs. Applied Sciences **11**(11), 5204 (2021)

[95] Perslev, M., Dam, E.B., Pai, A., Igel, C.: One network to segment them all: A general, lightweight system for accurate 3d medical image segmentation. In: International Conference on Medical Image Computing and Computer-Assisted Intervention. pp. 30–38. Springer (2019)

[96] Pinter, C., Lasso, A., Fichtinger, G.: Polymorph segmentation representation for medical image computing. Computer methods and programs in biomedicine **171**, 19–26 (2019)

[97] Provatidis, C.G.: An analytical model for stress analysis of a tooth in translation. International Journal of Engineering Science **39**(12), 1361–1381 (2001)

[98] Qian, L., Todo, M., Morita, Y., Matsushita, Y., Koyano, K.: Deformation analysis of the periodontium considering the viscoelasticity of the periodontal ligament. Dental Materials **25**(10), 1285–1292 (2009)

[99] Roda-Casanova, V., Zubizarreta-Macho, Á., Sanchez-Marin, F., Alonso Ezpeleta, Ó., Albaladejo Martínez, A., Galparsoro Catalán, A.: Computerized generation and finite element stress analysis of endodontic rotary files. Applied Sciences **11**(10), 4329 (2021)

[100] Sambataro, S., Cervino, G., Fiorillo, L., Cicciù, M.: Upper first premolar positioning evaluation for the stability of the dental occlusion: Anatomical considerations. Journal of Craniofacial Surgery **29**(5), 1366–1369 (2018)

[101] Sanctuary, C.S., Wiskott, H.A., Justiz, J., Botsis, J., Belser, U.C.: In vitro time-dependent response of periodontal ligament to mechanical loading. Journal of Applied Physiology **99**(6), 2369–2378 (2005)

[102] Sarrafpour, B., Swain, M., Li, Q., Zoellner, H.: Tooth eruption results from bone remodelling driven by bite forces sensed by soft tissue dental follicles: a finite element analysis. PLoS One **8**(3), e58803 (2013)

[103] Savignano, R., Valentino, R., Razionale, A., Michelotti, A., Barone, S., D'Antò, V.: Biomechanical effects of different auxiliary-aligner designs for the extrusion of an upper central incisor: a finite element analysis. Journal of Healthcare Engineering **2019** (2019)

[104] Savignano, R., Viecilli, R.F., Oyoyo, U.: Three-dimensional nonlinear prediction of tooth movement from the force system and root morphology. The Angle Orthodontist **90**(6), 811–822 (2020)

[105] Savignano, R., Viecilli, R.F., Paoli, A., Razionale, A.V., Barone, S.: Nonlinear dependency of tooth movement on force system directions. American Journal of Orthodontics and Dentofacial Orthopedics **149**(6), 838–846 (2016)

[106] Schmidt, F., Geiger, M.E., Jäger, R., Lapatki, B.G.: Comparison of methods to determine the centre of resistance of teeth. Computer Methods in Biomechanics and Biomedical Engineering **19**(15), 1673–1682 (2016)

[107] Schmidt, R., Singh, K.: Meshmixer: an interface for rapid mesh composition. In: ACM SIGGRAPH 2010 Talks. p. 6. ACM (2010)

[108] Schneider, J., Geiger, M., Sander, F.G.: Numerical experiments on long-time orthodontic tooth movement. American Journal of Orthodontics and Dentofacial Orthopedics **121**(3), 257–265 (2002)

[109] Schneider, T., Dumas, J., Gao, X., Zorin, D., Panozzo, D.: Polyfem. `https://polyfem.github.io/` (2019)

[110] Schneider, T., Hu, Y., Dumas, J., Gao, X., Panozzo, D., Zorin, D.: Decoupling simulation accuracy from mesh quality. ACM Trans. Graph. **37**(6) (dec 2018)

[111] Schneider, T., Hu, Y., Dumas, J., Gao, X., Panozzo, D., Zorin, D.: Decoupling simulation accuracy from mesh quality. ACM Transactions on Graphics **37**(6) (10 2018)

[112] Schneider, T., Hu, Y., Gao, X., Dumas, J., Zorin, D., Panozzo, D.: A large scale comparison of tetrahedral and hexahedral elements for finite element analysis. arXiv preprint arXiv:1903.09332 (2019)

[113] Seo, J.H., Eghan-Acquah, E., Kim, M.S., Lee, J.H., Jeong, Y.H., Jung, T.G., Hong, M., Kim, W.H., Kim, B., Lee, S.J.: Comparative analysis of stress in the periodontal ligament and center of rotation in the tooth after orthodontic treatment depending on clear aligner thickness—finite element analysis study. Materials **14**(2), 324 (2021)

[114] Shewchuk, J.R.: What is a good linear finite element? Interpolation, conditioning, anisotropy, and quality measures. University of California at Berkeley **73**, 137 (2002)

[115] Si, H.: Tetgen, a delaunay-based quality tetrahedral mesh generator. ACM Transactions on Mathematical Software (TOMS) **41**(2), 1–36 (2015)

[116] Sia, S.S., Koga, Y., Yoshida, N.: Determining the center of resistance of maxillary anterior teeth subjected to retraction forces in sliding mechanics: an in vivo study. The Angle Orthodontist **77**(6), 999–1003 (2007)

[117] Sia, S., Shibazaki, T., Koga, Y., Yoshida, N.: Experimental determination of optimal force system required for control of anterior tooth movement in sliding mechanics. American Journal of Orthodontics and Dentofacial Orthopedics **135**(1), 36–41 (2009)

[118] Smith, R.J., Burstone, C.J.: Mechanics of tooth movement. American Journal of Orthodontics **85**(4), 294–307 (1984)

[119] Soille, P.: Morphological image analysis: principles and applications. Springer Science & Business Media (2013)

[120] Tanne, K., Nagataki, T., Inoue, Y., Sakuda, M., Burstone, C.J.: Patterns of initial tooth displacements associated with various root lengths and alveolar bone heights. American Journal of Orthodontics and Dentofacial Orthopedics **100**(1), 66–71 (1991)

[121] Taubin, G., Zhang, T., Golub, G.: Optimal surface smoothing as filter design. In: European Conference on Computer Vision. pp. 283–292. Springer (1996)

[122] Tunis, T.S., Sarig, R., Cohen, H., Medlej, B., Peled, N., May, H.: Sex estimation using computed tomography of the mandible. International journal of legal medicine **131**(6), 1691–1700 (2017)

[123] Uhlir, R., Mayo, V., Lin, P.H., Chen, S., Lee, Y.T., Hershey, G., Lin, F.C., Ko, C.C.: Biomechanical characterization of the periodontal ligament: Orthodontic tooth movement. The Angle Orthodontist **87**(2), 183–192 (2016)

[124] Vallabh, R., Zhang, J., Fernandez, J., Dimitroulis, G., Ackland, D.C.: The morphology of the human mandible: A computational modelling study. Biomechanics & Modeling in Mechanobiology **19**(4) (2020)

[125] Van Schepdael, A., Geris, L., Vander Sloten, J.: Analytical determination of stress patterns in the periodontal ligament during orthodontic tooth movement. Medical Engineering & Physics **35**(3), 403–410 (2013)

[126] Viecilli, R.F., Budiman, A., Burstone, C.J.: Axes of resistance for tooth movement: does the center of resistance exist in 3-dimensional space? American Journal of Orthodontics and Dentofacial Orthopedics **143**(2), 163–172 (2013)

[127] Villanueva, E.Á., Garmendia, A.M., Torres, G., Sánchez-Mejorada, G., Gómez-Valdés, J.A.: Gender assessment using the mandible in the mexican population. Spanish Journal of Legal Medicine **43**(4), 146–154 (2017)

[128] Vukicevic, A.M., Zelic, K., Milasinovic, D., Sarrami-Foroushani, A., Jovicic, G., Milovanovic, P., Djuric, M., Filipovic, N., Frangi, A.F.: Openmandible: An open-source framework for highly realistic numerical modelling of lower mandible physiology. Dental Materials **37**(4), 612–624 (2021)

[129] Wang, C., Connolly, B., de Oliveira Lopes, P.F., Frangi, A.F., Smedby, Ö.: Pelvis segmentation using multi-pass u-net and iterative shape estimation. In: International Workshop on Computational Methods and Clinical Applications in Musculoskeletal Imaging. pp. 49–57. Springer (2018)

[130] White, S.C., Pharoah, M.J.: Oral radiology-E-Book: Principles and interpretation. Elsevier Health Sciences (2014)

[131] Xu, H., Barbic, J.: Signed distance fields for polygon soup meshes. In: Graphics Interface. pp. 35–41 (2014)

[132] Yoshida, N., Jost-Brinkmann, P.G., Koga, Y., Mimaki, N., Kobayashi, K.: Experimental evaluation of initial tooth displacement, center of resistance, and center of rotation under the influence of an orthodontic force. American Journal of Orthodontics and Dentofacial Orthopedics **120**(2), 190–197 (2001)

[133] Yoshida, N., Koga, Y., Peng, C.L., Tanaka, E., Kobayashi, K.: In vivo measurement of the elastic modulus of the human periodontal ligament. Medical Engineering & Physics **23**(8), 567–572 (2001)

[134] Zheng, Z., Yan, H., Setzer, F.C., Shi, K.J., Mupparapu, M., Li, J.: Anatomically constrained deep learning for automating dental cbct segmentation and lesion detection. IEEE Transactions on Automation Science and Engineering **18**(2), 603–614 (2020)

[135] Ziegler, A., Keilig, L., Kawarizadeh, A., Jäger, A., Bourauel, C.: Numerical simulation of the biomechanical behaviour of multi-rooted teeth. The European Journal of Orthodontics **27**(4), 333–339 (2005)

[136] Żmudzki, J., Chladek, W.: Stress present in bone surrounding dental implants in FEM model experiments. Journal of Achievements in Materials and Manufacturing Engineering **27**(1), 71–74 (2008)

Appendix A

Segmentation of Hip Joints using U-Net with Transfer Learning

---

This appendix presents our work in the article titled "Auto-segmentation of hip joints using MultiPlanar UNet with transfer learning". The authors of this paper are listed as

- Peidi Xu, Faezeh Moshfeghifar, **Torkan Gholamalizadeh**, Kenny Erleben, and Sune Darkner. "Auto-segmentation of hip joints using MultiPlanar UNet with transfer learning" in Medical Image Learning with Noisy and Limited Data, MICCAI Workshop, 2022.

This work aimed to employ deep learning methods to speed up the geometry reconstruction process by pre-training a U-Net model on a publicly available dataset using inaccurate segmentations. An interactive learning strategy is then used to fine-tune the network using a few anatomically accurate annotated data. This paper addresses the large-scale geometry reconstruction challenge in developing FE models for human hip areas.

The developed network using the limited number of accurate segmentations and the weighted loss used to enforce the gap between the bones help to provide an accurate approximation of bones' boundaries. Considering such gaps between different bones (where the cartilages reside) leads to anatomically accurate hip-joint segmentations, requiring minimal manual modifications for FEM development.

It should be noted that the publicly available segmented CT scans of the hip area and the high-resolution scans considering the dimensions of the anatomical structures make the hip segmentation task relatively easy compared to the tooth-bone segmentation of the CBCT scans.

Appendix B

Tooth and Bone Segmentation using U-Net with Transfer Learning

---

This appendix presents our work in the article titled “Tooth and Bone Segmentation using MultiPlanar U-Net with Transfer Learning”. The authors of this paper are listed as

- Peidi Xu, **Torkan Gholamalizadeh**, Faezeh Moshfeghifar, Kenny Erleben, and Sune Darkner. “Tooth and Bone Segmentation using MultiPlanar U-Net with Transfer Learning” to be submitted to Medical Image Computing and Computer Assisted Intervention (MICCAI), 2023.

We successfully use similar transfer learning strategies mentioned in Appendix A for automatically segmenting teeth-bone from CBCT scans of different patients. This can tackle the large-scale geometry reconstruction problem for segmenting many human jaw models from CBCT scans.

We benefit from the segmentation network in two different phases. First, for tooth-bone segmentation, ignoring the PDL layer’s existence and training/fine-tuning the MultiPlanar U-Net to segment the teeth-bone in both jaws. Even though the predicted labels of the network for new scans were promising, some manual modifications were needed to enhance the tooth-bone delineations before using them as input geometries to the pipeline mentioned in Chapter 4. Second, for PDL gap generation, using the same weighted loss and network fine-tuning mentioned in Appendix A to improve tooth-bone segmentations by imposing the gaps between the teeth and bone where PDL resides.

Furthermore, task-specific data augmentation was used to expand the training data with high variations, and a marker-based watershed segmentation approach was applied to the U-Net outputs to better separate teeth, especially when it is challenging to detect boundaries in the presence of metal artifacts. The results show that the proposed method can detail crucial features such as the gap between teeth-bone interfaces and the interproximal regions of the teeth.

In this work, I helped prepare the manually segmented training data, correct the automatic segmentation results during the interactive learning step, and provide data for examining proper preprocessing techniques, e.g., to handle various resolutions. We also tried augmentation strategies to increase the training samples and make the network robust to variations.

Appendix C

LibHip: An Open-Access Hip Joint Model Repository suitable for Finite Element Method Simulation

---

This appendix presents our work in the article titled “LibHip: An Open-Access Hip Joint Model Repository suitable for Finite Element Method Simulation”. The authors of this paper are listed as

- Faezeh Moshfeghifar, **Torkan Gholamalizadeh**, Zachary Ferguson, Teseo Schneider, Michael Bachmann Nielsen, Daniele Panozzo, Sune Darkner, and Kenny Erleben. “LibHip: An Open-Access Hip Joint Model Repository suitable for Finite Element Method Simulation” Submitted to Computer Methods and Programs in Biomedicine, 2022.

This work provides a repository of multiple subject-specific hip joint FE models. First, we utilize the outputs of Appendix A and improve the reconstructed bone geometries. Next, the surface mesh of each bone’s corresponding cartilage is generated using curvature information of the contacting bone geometries. Finally, unified meshes of the hip pairs and the pelvic girdle are developed using the meshing tools presented in Chapter 4.

The work provides 11 patient-specific FE models of the human hip area, including the sacrum, the paired hip bones, the paired proximal femurs, and the cartilages of each associated joint. This is one of the largest model repositories of the human hip area, considering the number of subjects and regions of interest. All models are clinically verified, and the high-quality discretizations are shown to be accurate and suitable for simulation purposes.